GRANT IN-18-CR

VIRGINIA TECH

187802
P-249

TITLE: SURFACE CHARACTERIZATION OF LDEF MATERIALS

TYPE: FINAL TECHNICAL REPORT

PRINCIPAL INVESTIGATOR: J. P. WIGHTMAN

PERIOD COVERED: SEPTEMBER 18, 1990 - OCTOBER 1, 1993

GRANTEES INSTITUTION: VIRGINIA POLYTECHNIC INSTITUTE AND STATE UNIVERSITY

GRANT NUMBER: NAG-1-1186

VIRGINIA TECH
CHEMISTRY DEPARTMENT
BLACKSBURG, VA 24061

(703) 231-6604

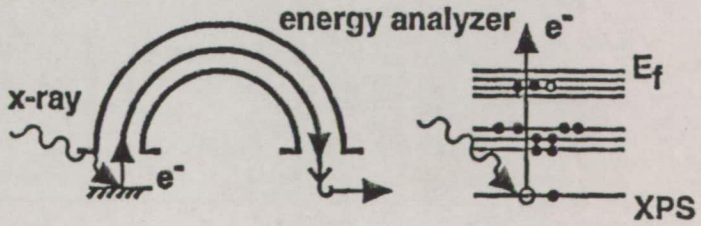

FINAL TECHNICAL REPORT

SURFACE CHARACTERIZATION OF LDEF MATERIALS

HOLLY LITTLE GRAMMER
J. P. WIGHTMAN

PREPARED FOR

NASA-LANGLEY RESEARCH CENTER
DR. P. R. YOUNG
MAIL STOP 226
HAMPTON, VIRGINIA 23665

FROM

CHEMISTRY DEPARTMENT
VIRGINIA POLYTECHNIC INSTITUTE AND STATE UNIVERSITY
BLACKSBURG, VIRGINIA 24061-0212

OCTOBER 1993

SURFACE CHARACTERIZATION OF LDEF MATERIALS*

by

Holly L. Grammer

Committee Chairman: Dr. James P. Wightman

Chemistry

(ABSTRACT)

The NASA Long Duration Exposure Facility (LDEF), a passive experimental satellite, was placed into low-Earth orbit by the Shuttle Challenger in April 1984. The LDEF spent an unprecedented 69 months in space. The flight and recovery of the LDEF has provided a wealth of information on the long-term space environmental effects of a variety of materials exposed to the low-Earth orbit environment.

Surface characterization of LDEF materials included polymers, composites, thermal control paints, and aluminum. X-ray photoelectron spectroscopy (XPS), Auger electron spectroscopy (AES), scanning electron microscopy (SEM), and contact angle analysis were used to document changes in both the surface composition and surface chemistry of these materials. Detailed XPS analysis of the polymer systems, such as Kapton®, polyimide polysiloxane copolymers, and fluorinated

* This final technical report is based wholly on the M.S. thesis of Holly Little Grammer in Chemistry (1993).

ethylene propylene thermal blankets on the backside of the LDEF revealed significant changes in both the surface composition and surface chemistry as a result of exposure to the low-Earth orbit environment. Polymer systems such as Kapton®, polyimide polysiloxane copolymers, and polysulfone showed a common trend of decreasing carbon content and increasing oxygen content with respect to the control sample.

Carbon 1s curve fit XPS analysis of the composite samples, in conjunction with SEM photomicrographs, revealed significant ablation of the polymer matrix resin to expose the carbon fibers of the composite during exposure to the space environment.

Surface characterization of anodized aluminum tray clamps, which were located at regular intervals over the entire LDEF frame, has provided the first results to evaluate the extent of contamination with respect to position on the LDEF. The XPS results clearly showed that the amount and state of both silicon and fluorine contamination were directly dependent upon the position of the tray clamp on the LDEF.

Table of Contents

List of Tables

List of Figures

I. Introduction

The Long Duration Exposure Facility (LDEF) was designed and fabricated by both NASA's Office of Aeronautics and Space Technology and the Langley Research Center in the late 1970's [1]. The LDEF, a passive satellite, was designed to evaluate the durability/resistance of both science and technology experiments exposed to the low-Earth orbit space environment. An in-orbit photograph of the LDEF is shown in Figure 1.1. The LDEF was designed to facilitate the determination of directional effects of the space environmental parameters. These parameters include atomic oxygen, solar radiation, micro-meteoroids and debris. The effects of the low-Earth orbit environment on LDEF experiments were ascertained by post-flight laboratory investigations.

The cylindrical LDEF was an aluminum 6061-T6 structure with the cylindrical cross section of a 12-sided regular polygon [2]. The LDEF was 914.14 m (30 ft) in length and 426.7 m (14 ft) in diameter. The LDEF contained 86 experimental bays which housed 57 different experiments. These 57 different experiments encompassed the fields of electronics & optics, heat pipes & thermal systems, materials & coatings, science, and power & propulsion.

The LDEF was deployed by the Shuttle Challenger on April

LDEF IN ORBIT

FIGURE 1.1: PHOTOGRAPH OF LDEF IN ORBIT.

7, 1984, during the STS-41C mission. The LDEF was deployed at an altitude of approximately 257 nautical miles. The original LDEF mission was scheduled for retrieval by the Shuttle Challenger in early 1985 after a 10-month to 1-year mission. The loss of the Challenger in 1985 and subsequent rescheduling problems delayed the LDEF retrieval. The LDEF was retrieved by the Shuttle Columbia on January 12, 1990, during the STS-32 mission. The LDEF was thus retrieved nearly 69 months after deployment in 1984. This was a truly unique scientific opportunity since no materials had ever been recovered from space after such a length of time. After 32,422 orbits around the Earth, the LDEF's altitude had declined to approximately 179 nautical miles.

Four Special Investigation Groups (SIGs) were established in January of 1989 to evaluate the effects of the low-Earth orbit space environment on the LDEF's experiments. The SIGs were established to evaluate the effects of ionizing radiation, meteoroid/debris, environment, and contamination on systems and materials.

The flight and recovery of the LDEF have provided a wealth of information on the long-term space environmental effects of a variety of materials exposed to the low-Earth orbit environment. The space environmental parameters determined by the LDEF provides a data baseline unparalleled in the history of space environmental research [3].

The primary materials from the LDEF of interest in this study were the anodized aluminum tray clamps containing two thermal control paints. These tray clamps were located over the entire LDEF frame. Therefore, these materials provide a complete picture of the effects induced by the low-Earth orbit space environment on these three materials. Surface analysis provides a piece to the overall picture of the effects of atomic oxygen, ultraviolet radiation and contamination on materials aboard the LDEF.

The first objective of this work was the post-flight surface analysis LDEF materials including polymers, composites, thermal control paints and aluminum. The second objective was the correlation of observed surface chemical properties such as surface composition and surface chemistry with the low-Earth orbit exposure conditions.

II. Literature Review

The major areas reviewed in this chapter include the following: design and fabrication of the LDEF, experiments on the LDEF and, elements and conditions of the low-Earth orbit environment. An understanding of these areas is essential to ascertain the exposure conditions of materials with respect to the LDEF and the low-Earth orbit environment. Also reviewed in this chapter is the LDEF science team which consists of four special investigation groups which were established to evaluate the low-Earth orbit environment. The effects of the low-Earth orbit environment on materials exposed on previous missions will be reviewed.

A. Design/Fabrication of LDEF

The LDEF was developed by both NASA's Office of Aeronautics and Space Technology and the Langley Research Center [1]. The LDEF was designed and fabricated at the Langley Research Center in the late 1970's [1]. The LDEF as a passive satellite was designed to evaluate the durability/ resistance of materials and experiments exposed to the low-Earth orbit space environment.

1. Structure

The LDEF was an aluminum 6061-T6 structure with the cylindrical cross section of a 12-sided regular polygon [2] and weighed 3632 kg (8000 lbs). LDEF dimensions were 914.4 m x 426.7 m (30 ft x 14 ft) in diameter. The aluminum 6061-T6 center ring frame and end frames were of welded and bolted construction [1]. The longerons, the fore and aft framing, were bolted to both frames. The intercostal, crosspieces between the main rings, were bolted to the longerons. Lateral support was secured by a keel fitting on the center ring frame [1].

A schematic diagram of the LDEF frame is shown in Figure 2.1 [2]. The LDEF frame was divided by the experimental bays labelled A through F which correspond to the twelve rows labelled 1 through 12. The Earth and space ends were labelled G and H, respectively.

The LDEF contained a total of 86 experimental bays. The circumference of the frame contained 6 bays per row for a total of 72 bays. The Earth and space oriented ends contained 6 and 8 bays, respectively. A photograph of an experimental tray is shown in Figure 2.2. Typical experimental tray dimensions were 0.86 m x 1.27 m (34 in x 50 in). Experimental tray depths were 0.8, 0.2 and 0.3 m (3, 6 and 12 in). The experimental bays housed experiments weighing 82 to 91 kg (180 to 200 lbs).

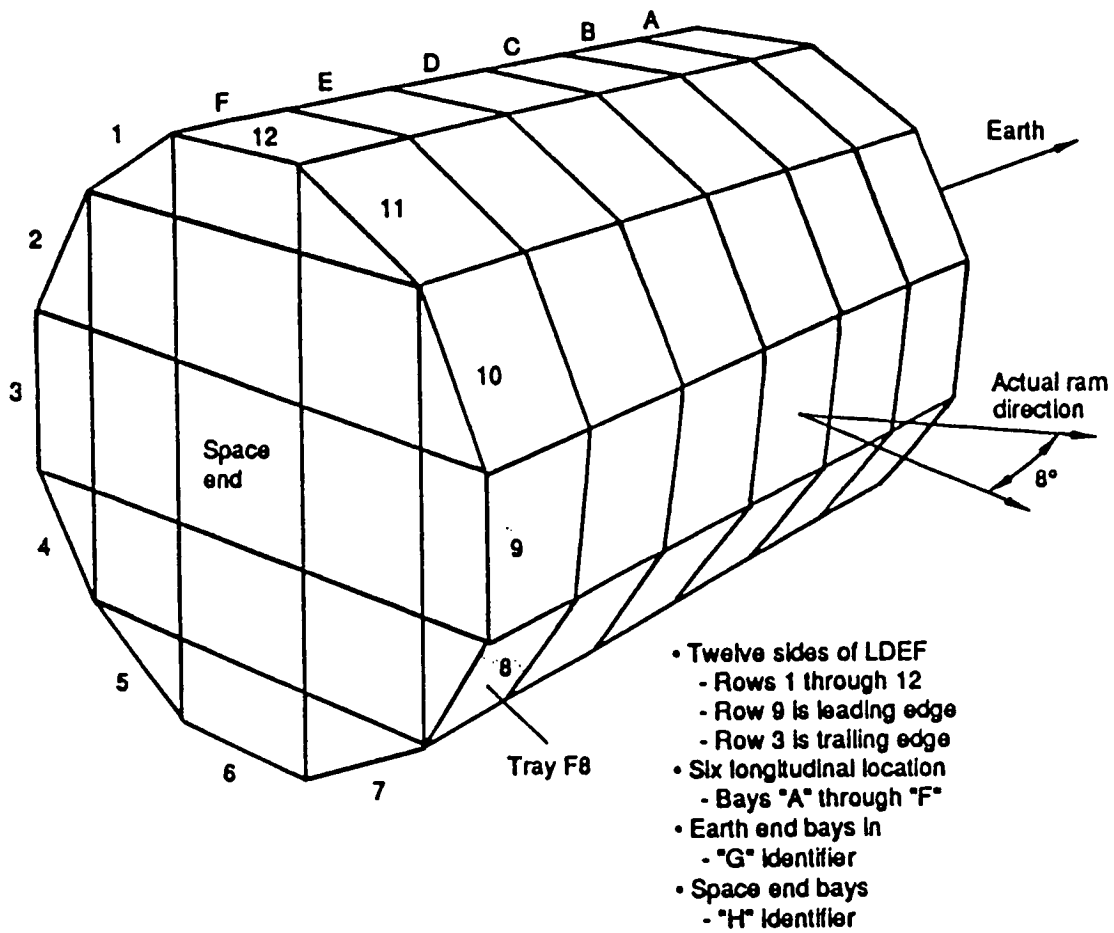

FIGURE 2.1: SCHEMATIC DIAGRAM OF LDEF FRAME [2].

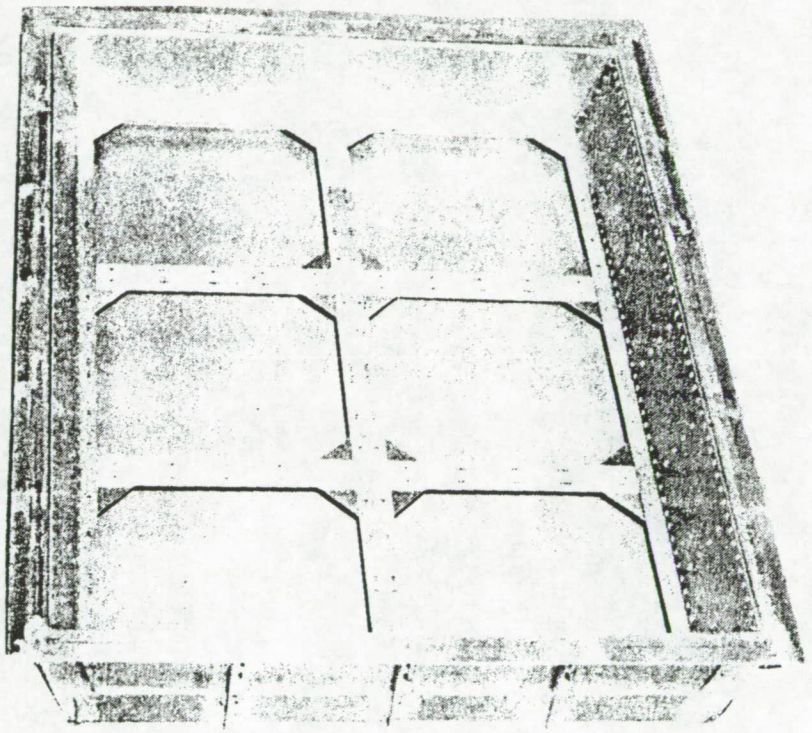

FIGURE 2.2: PHOTOGRAPH OF A TYPICAL DEINTEGRATED LDEF EXPERIMENTAL TRAY.

The 86 experimental trays were secured to the periphery of the LDEF structure by tray clamps which were located over the entire LDEF frame. Over four hundred tray clamps were used to secure the experimental trays. Approximately two hundred tray clamps contained Chemglaze® A276 white and Chemglaze® black thermal control paints. Figure 2.3 is a photograph of an integrated experimental tray which was located on Bay D, Row 9 of the LDEF frame. Figure 2.3 also shows the two types of tray clamps which were used to secure the experimental bay. Fully integrated, with experiments, the LDEF weighed 9716 kg (21,400 lbs).

2. Experiments

The 86 experimental bays housed 57 different experiments. Experiments were categorized as follows: electronics & optics, heat pipes & thermal systems, materials & coatings, science, power & propulsion [1]. The 57 experiments involved investigators from the United States and nine other countries. Specific experiments included exposure effects of the low-Earth orbit environment on polymers, fiber optics, infrared detectors, and solid rocket materials [1]. Additional experiments were designed to study the ability to grow crystals during long exposure to low gravity [1]. Experiments were designed to provide information on the performance and endurance of advanced and conventional solar cells [1].

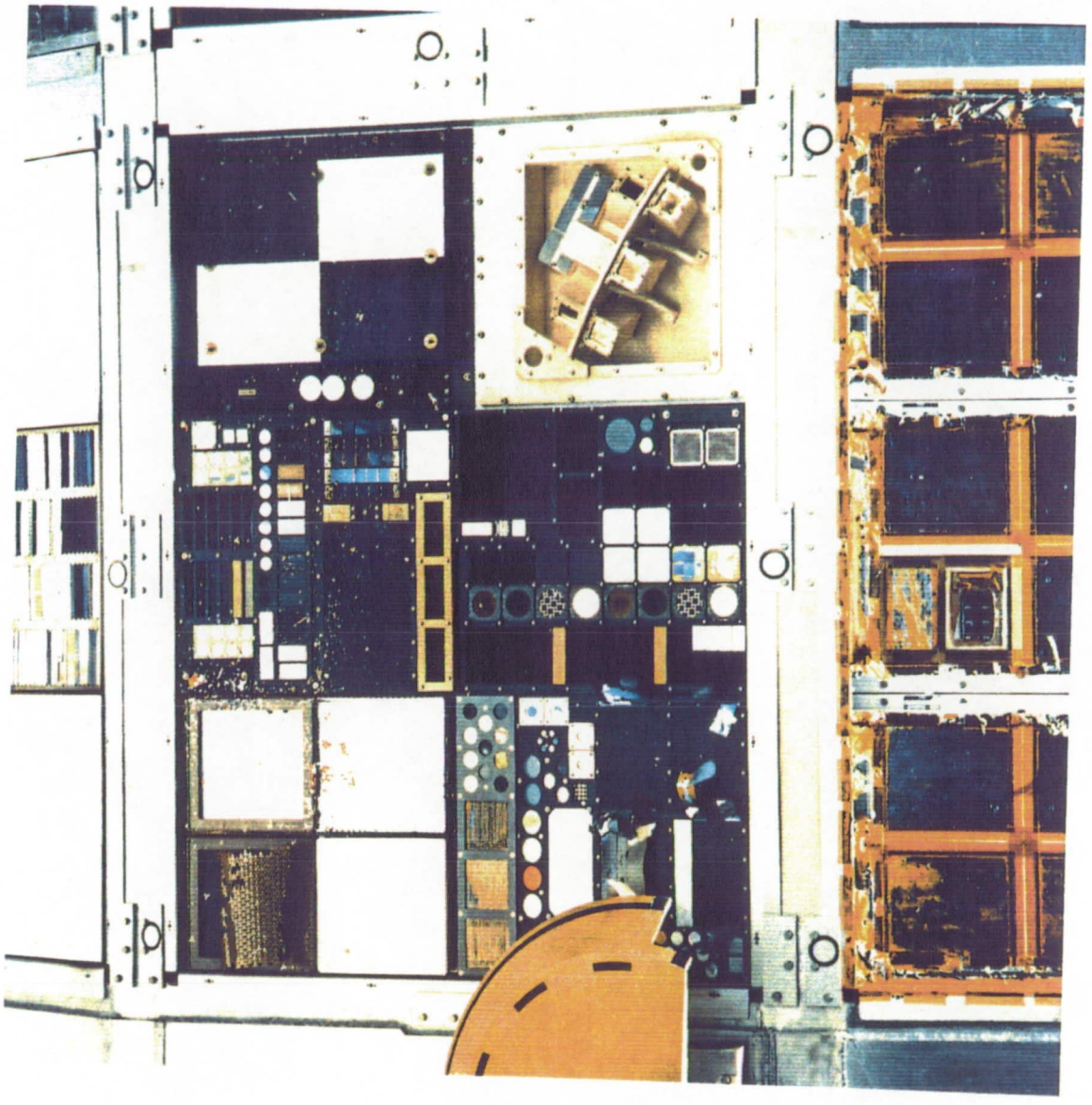

FIGURE 2.3: PHOTOGRAPH OF INTERGRATED EXPERIMENTAL TRAY - D9.

Figure 2.4 illustrates the distribution of materials across the LDEF external surface [2].

A high visibility experiment, which involved grade schools around the United States, was the SEEDS experiments or Space-Exposed Experiment Developed for Students [1]. The objective of this experiment was to involve a large number of students to generate national interest in science and related disciplines [1]. The experiment was designed to evaluate the survivability of approximately 11 to 12 million tomato seeds stored in the space environment under sealed conditions [1].

Table 2.1 is a complete list of experiments flown on the LDEF [2]. Figure 2.5 is a flat representation of the LDEF frame [1]. Figure 2.5 also includes the experimental numbers corresponding to the experiments. These experiments are detailed in *The Long Duration Exposure Facility Mission 1 Experiments* [1]. Figure 2.6 is an in-orbit retrieval photograph of the LDEF structure showing several experimental trays.

3. Flight Orbit Orientation

The LDEF was a passive satellite with no central power or data systems [1]. No telemetry data was sent to Earth during the mission. The LDEF was engineered to maintain a 3-axis gravity-gradient stabilized attitude [1]. This design allowed the orbit orientation to be constant while orbiting the Earth.

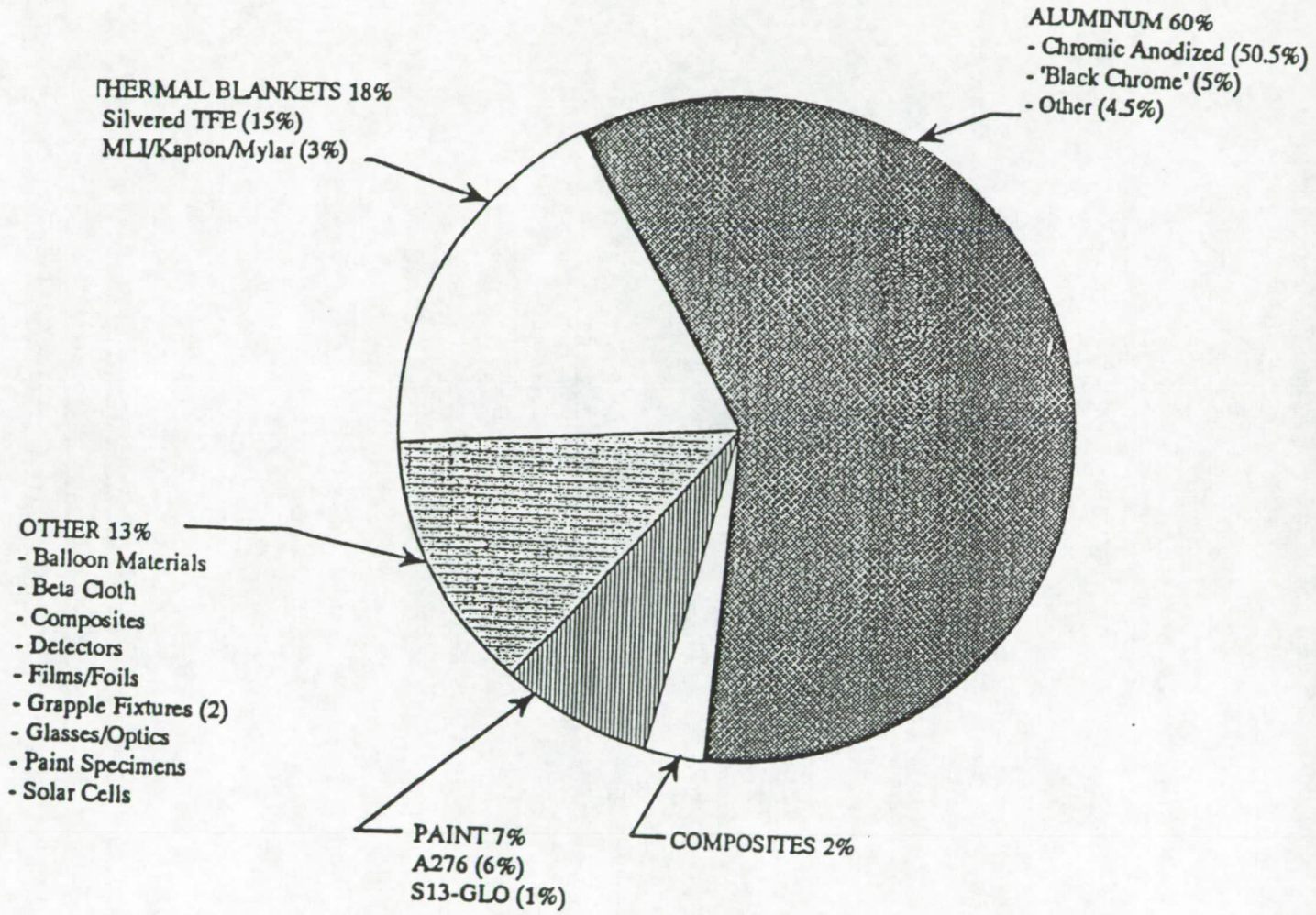

FIGURE 2.4: MATERIAL DISTRIBUTION ON LDEF [2].

TABLE 2.1: LIST OF EXPERIMENTS FLOWN ON LDEF [2].

ELECTRONICS & OPTICS

- Holographic Data Storage Crystals
- Infrared Multilayer Filters
- Pyroelectric Infrared Detectors
- Metal Film and Multilayers
- Vacuum-Deposited Optical Coatings
- Ruled and Holographic Gratings
- Optical Fibers and Components
- Earth Radiation Budget Experiment Components
- Solar Radiation On Glasses
- Quartz Crystal Oscillators
- Active Optical System Components
- Fiber Optic Data Transmission
- Fiber Optics Systems
- Space Environments Effects

HEAT PIPES & THERMAL SYSTEM

- Variable Conductance Heat Pipe
- Low-Temperature Heat Pipe
- Transverse Flat-Plate Heat Pipe
- Thermal Measurements

MATERIALS & COATINGS

- Crystal Growth
- Radar Phased-Array Antenna
- Atomic Oxygen Outgassing
- Atomic Oxygen Interaction
- High-Toughness Graphite Epoxy
- Composite Materials For Space Structures
- Epoxy Matrix Composites
- Composite Materials
- Graphite-Polymide and Graphite-Epoxy
- Polymer Matrix Composites
- Spacecraft Materials
- Balloon Materials Degradation
- Thermal Control Surfaces
- Textured and Coated Surfaces
- Metallic Materials Under Ultravacuum

SCIENCE

- Interstellar Gas
- Ultra-Heavy Cosmic Ray Nuclei
- Heavy Ions
- Trapped-Proton Energy Spectrum
- Heavy Cosmic Ray Nuclei
- Linear Energy Transfer Spectrum
- Microabrasion Package
- Meteoroid Impact Craters
- Dust Debris Collection
- Chemistry Of Micrometeoroids
- Measurements of Micrometeoroids
- Interplanetary Dust
- Space Debris Impact
- Meteoroid Damage to Spacecraft
- Biostack
- Seeds In Space
- Student Seeds Experiment

POWER & PROPULSION

- High Voltage Drainage
- Solar Array Materials
- Advanced Photovoltaics
- Coatings and Solar Celols
- Solid Rocket Materials

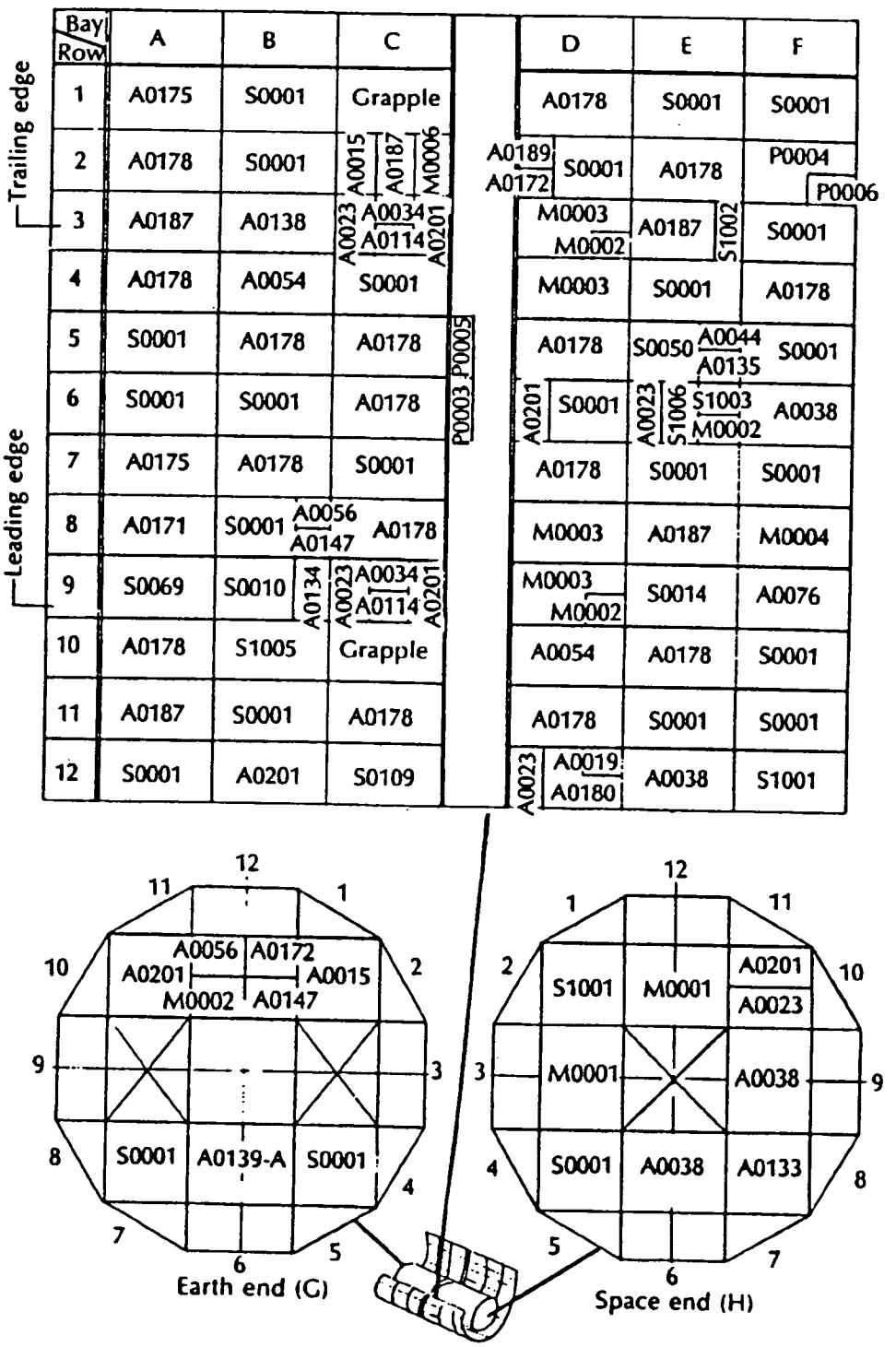

FIGURE 2.5: FLAT REPRESENTATION OF LDEF FRAME [1].

FIGURE 2.6: PHOTOGRAPH OF LDEF DURING RECOVERY.

The constant orientation of the LDEF was due to mass loading and a viscous magnetic damper located on the interior of the space end [1].

A schematic diagram of the LDEF's flight orbit orientation is shown in Figure 2.7. The orbit orientation was designed so that one end, the space end (H), was always pointed towards deep space, as labelled in Figure 2.7. The opposite end of the LDEF, or the Earth end (G), was always pointed toward the Earth. As labelled in Figure 2.7, Row 9 of the LDEF was designated as the leading edge of the LDEF. The leading edge was oriented perpendicular to the direction of travel or ram direction, as shown by the red arrows in Figure 2.7. Row 3, not labelled in Figure 2.7, was designated as the trailing edge of the LDEF. The leading edge is considered to be the front of the LDEF, whereas, the trailing edge is considered to the back of the LDEF.

4. Launch/Retrieval

The LDEF was deployed by the Shuttle Challenger on April 7, 1984 during STS-41C mission. The LDEF was deployed at 257 nautical miles in a nearly circular orbit with a 28.4° degree inclination [2]. The orientation of the LDEF remained constant throughout the mission. As a result of one rotation around the long axis, the degree of inclination was offset from the original 28.4°. Row 9 or the leading edge was

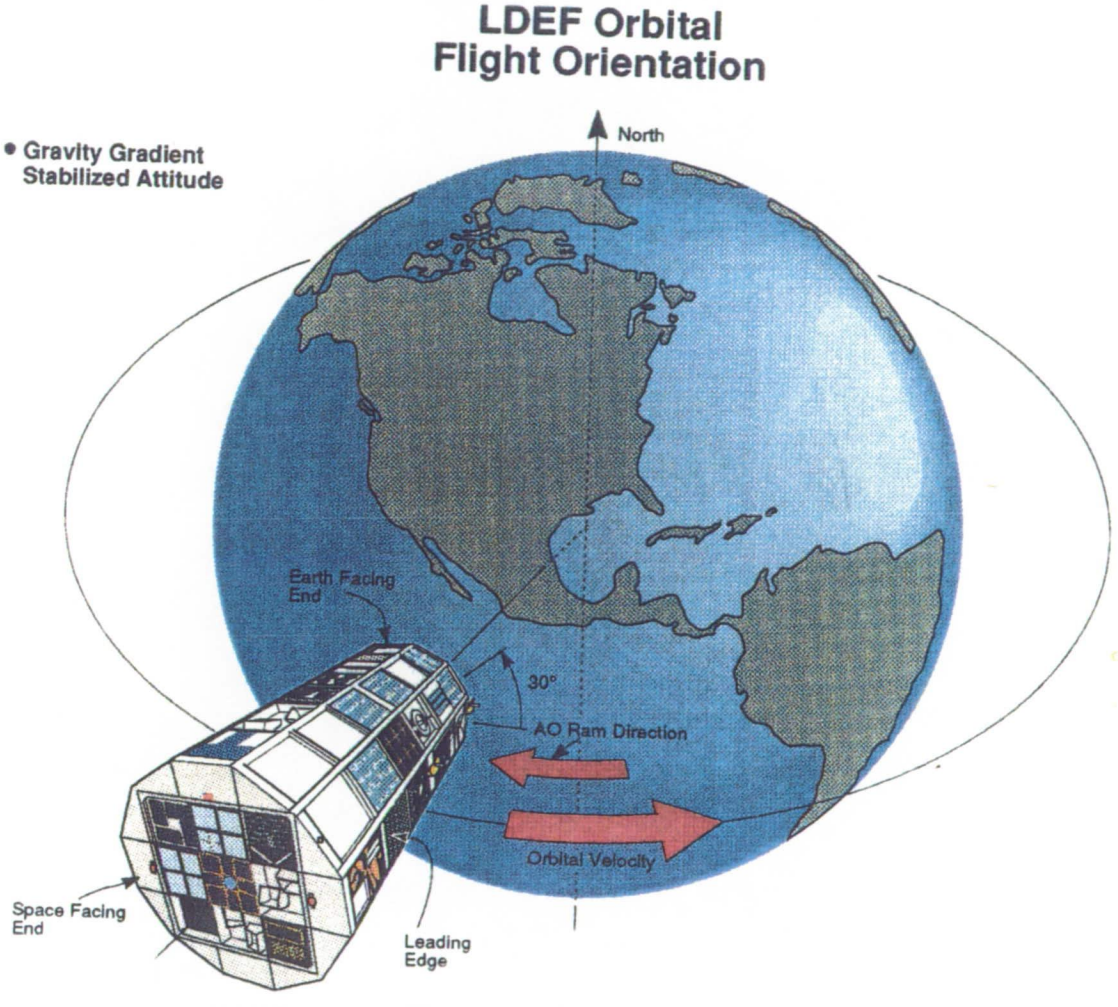

FIGURE 2.7: SCHEMATIC DIAGRAM OF LDEF'S ORBITAL FLIGHT ORIENTATION.

thereby offset 8 degrees from the ram direction as a result of this rotation [2].

The original LDEF mission was scheduled for retrieval by the Shuttle Challenger in early 1985 after a 10-month to 1-year mission. Due to the loss of the Challenger in 1985 and subsequent rescheduling problems, the LDEF was not retrieved by the Shuttle Columbia until January 12, 1990 during the STS-32 mission. The LDEF was retrieved nearly 69 months after deployment in 1984. After 32,422 orbits, (741,928,837 miles), in the low-Earth orbit, the LDEF's altitude had declined to 179 nautical miles. Figure 2.8 illustrates the LDEF's altitude versus exposure time [2]. As shown in Figure 2.8, the LDEF orbit was fairly stable for the first 48 months of the mission but the altitude began to significantly decay in the last 21 months.

B. Elements/Conditions of the Low-Earth Orbit Environment

As a result of the detailed measurements of many sophisticated, in situ satellite platforms, an understanding of the low-Earth orbit environment had grown rapidly throughout the 1970's [4]. Knowledge of the elements and conditions of the low-Earth orbit environment is essential in understanding the effects of the space environment on materials.

The low-Earth orbit environment contains neutral atoms,

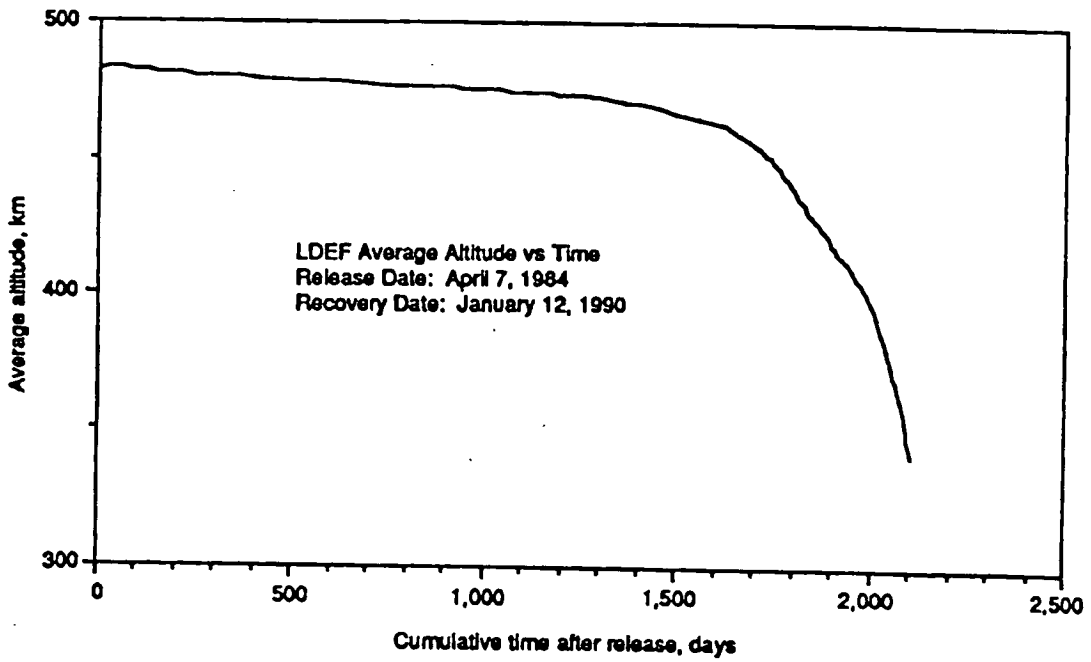

FIGURE 2.8: LDEF'S ALTITUDE VS EXPOSURE TIME [2].

plasmas, magnetic fields, radiation, and particulates [4,5]. The constituents, densities, and energies of the natural orbital environment vary with local time, seasonal solar activity, and position (attitude, latitude and longitude) [5]. The constituents of the natural low-Earth orbit environment such as plasmas and particles are modified as a result of the presence and activities of space systems [6]. Therefore, the space system environment or local space environment may be considerably different than the natural space environment [7]. The major areas of the low-Earth orbit space environment discussed will be the atmospheric chemical regimes, atomic oxygen, ultraviolet radiation, thermal cycling, meteoroids and space debris, and contamination.

1. Atmospheric Chemical Regimes

The altitude of the low-Earth orbit space environment is generally defined between 300 to 500 km. The atmospheric chemical regime from 0 to 2,500 km is shown in Figure 2.9 [5]. The major constituents are molecular nitrogen (N_2), relative weight per molecule of 28; molecular oxygen (O_2), 32; atomic oxygen (O), 16; argon (Ar), 40; helium (He), 4; and atomic hydrogen (H), 1 [5].

The pressure of the low-Earth orbit environment is 10^{-6} to 10^{-7} torr. This high vacuum environment is believed to have facilitated the outgassing of a large number of materials

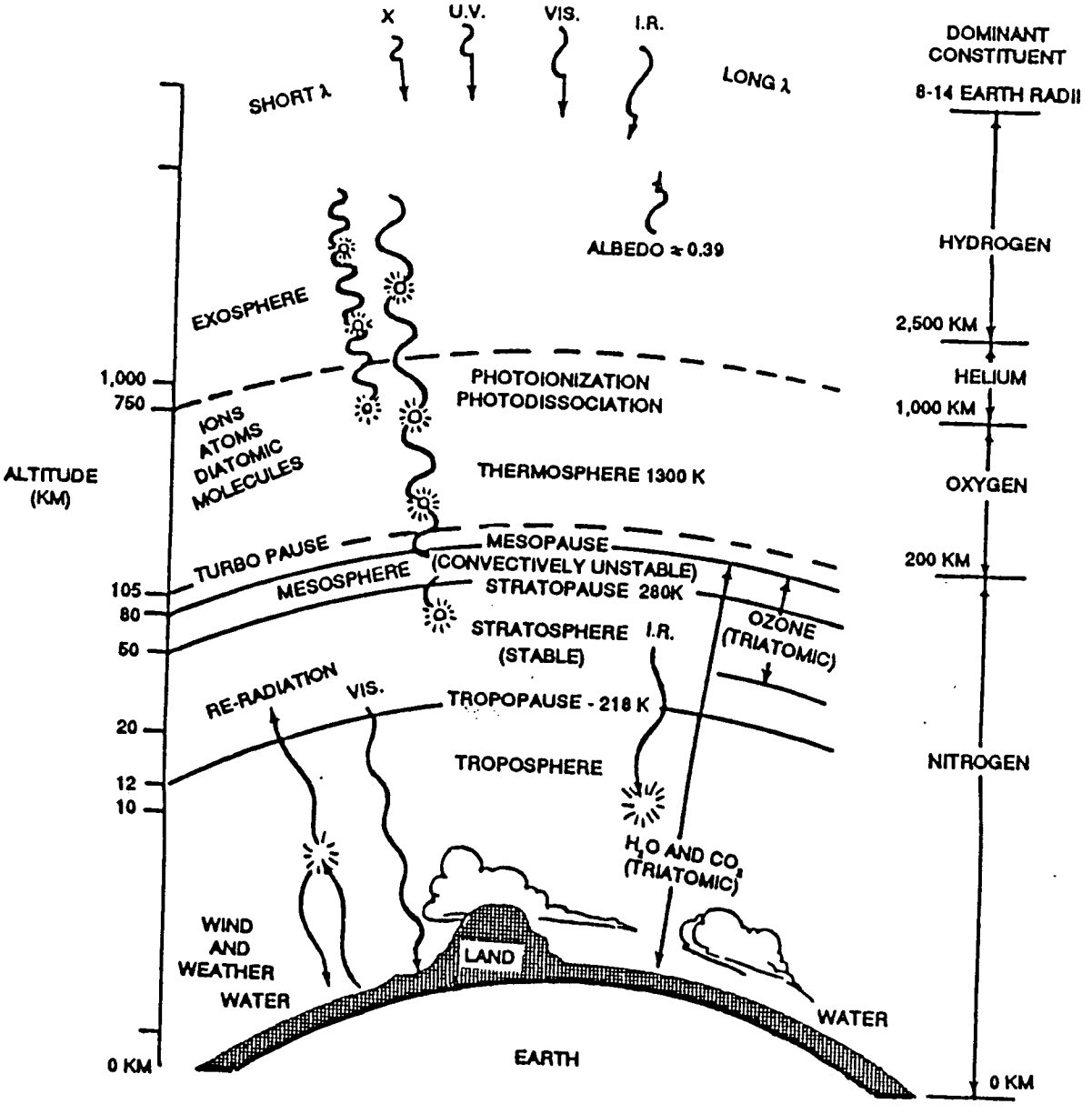

FIGURE 2.9: SCHEMATIC DIAGRAM OF THE LOW-EARTH ORBIT CHEMICAL REGIMES [5].

aboard the LDEF.

2. Atomic Oxygen

Atomic oxygen is the most abundant constituent in the low-Earth orbit environment [5]. At altitudes of 300 to 500 km the atmosphere consists of 80% atomic oxygen and 20% molecular nitrogen [5]. Atomic oxygen is formed when solar ultraviolet light dissociates oxygen molecules as shown below:

$$O_2 + h\nu \text{ --------> } 2O \qquad (2.1)$$

The center of the atmospheric regime, the thermosphere, is heated by atomic oxygen, which absorbs extreme ultraviolet radiation with wavelengths of 100 to 200 nm [5].

The calculated orbital speed of the LDEF was 7.690 km s^{-1}. The resultant energy of atomic oxygen colliding with the LDEF was approximately 4-5 eV [2]. The collisional energy of atomic oxygen generates chemical and/or physical changes on the surface of materials [8,9,10,11].

Atomic oxygen fluence was calculated for all rows and end bays of the LDEF [12]. Fluence (F) was calculated by the following equation:

$$F = f*t \qquad (2.2)$$

where the flux (f) is the number density times orbital velocity and t is the exposure time. Figure 2.10 illustrates the calculated atomic oxygen fluence for the LDEF [13]. The

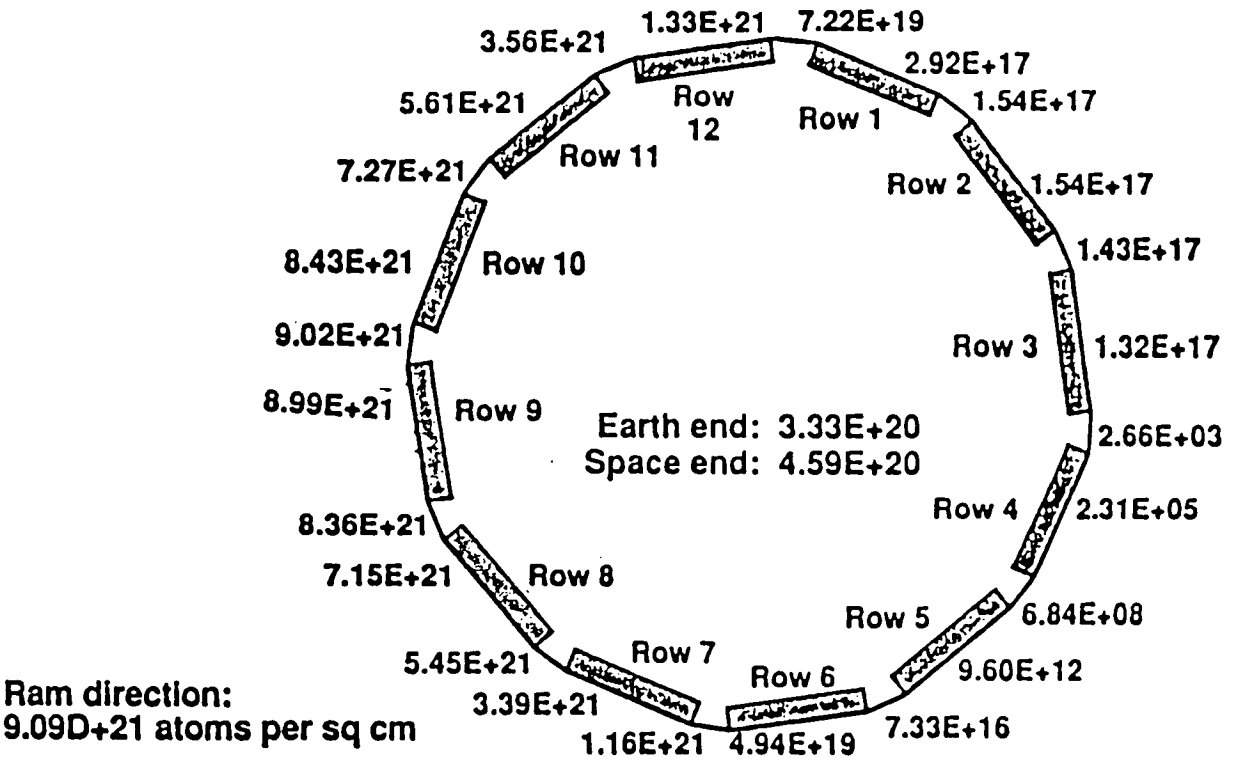

Atomic oxygen fluences at end of mission for all row, longeron, and end bay locations including the fluence received during the retrieval attitude excursion.

FIGURE 2.10: CALCULATED ATOMIC OXYGEN FLUENCE FOR ALL ROW AND END BAYS OF LDEF [13].

analytical model incorporated the effects of thermal molecular velocity, atmospheric temperature, number density, spacecraft velocity, incidence angle, and atmospheric rotation during the 69 month mission [13].

As a result of both increasing solar activity and decaying orbit altitude [2], approximately 54% of the total atomic oxygen fluence was accrued during the last 6 months of the LDEF mission.

3. Ultraviolet Radiation

Ultraviolet radiation is one component of solar radiation. Calculated cumulative equivalent sun hours for each tray location on the LDEF are shown in Figure 2.11 [14,15]. Cumulative equivalent sun hours (SH) are the sum of the Earth reflected radiation and direct solar exposure. The Earth reflected radiation or the Earth albedo is the sunlight reflected from clouds, water and terrain. The Earth albedo value was based on the Nimbus 7 earth radiation data set [16]. Cumulative equivalent sun hours were based on calculations from form factor reported in the Solar Illumination Data Package [17]. Solar fluence (SF) can be calculated by the following equation:

$$SF = SH * (492.48 \text{ Joule cm}^{-2} \text{ hr}^{-1}) \qquad (2.3)$$

The earth end received 72% of its exposure from the Earth reflected radiation and 28% from direct solar radiation [2].

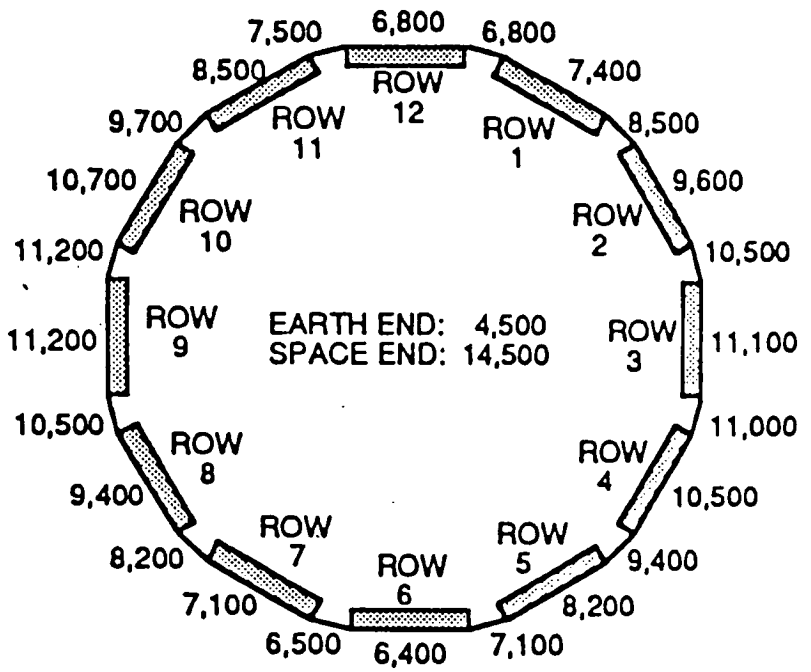

FIGURE 2.11: CALCULATED CUMULATIVE EQUIVALENT SUN HOURS FOR ALL ROW AND END BAYS OF LDEF [14,15].

Rows 1 through 12 received only 9% to 12% Earth reflected radiation [2]. The space end received no Earth reflected radiation.

4. Thermal Cycling

The LDEF orbited the Earth approximately 34,000 times. The average thermal cycling temperatures for the entire LDEF mission were [± 293 K] to [243 K to 463 K] (±20° F) to (-30° F to 190° F) [18]. These temperatures were determined by Greene who was the principal investigator of LDEF experiment "LDEF Thermal Measurements Systems" [1]. The thermal measurement systems consisted of six copper-constantan thermocouples, two thermistor reference measurements, and a 7.5 V battery. This experiment was also interfaced with the "Low-Temperature Heat Pipe Experiment Package" [1].

5. Meteoroids and Space Debris

Meteoroids are naturally occurring small interplanetary particles. These particles may be composed of sodium, magnesium, sulfur, calcium and iron [19]. Meteoroids are pulled into the Earth's atmosphere as a result of the Earth's gravitational field. As these materials enter the atmosphere, they may strike spacecraft systems.

Space debris is defined as man-made material left in space as a result of previous space activity [20]. This

debris ranges in size from microscopic fragments to large spent rocket motors [20]. A model of the man-made orbit debris is currently used in the design of spacecraft in the low-Earth orbit environment [21].

The LDEF Meteoroid and Debris Special Investigation Group estimated that approximately 36,000 particles bombarded the LDEF. The diameter of these impacts ranged from approximately 0.1 mm to 2.0 mm.

6. Contamination

Extensive contamination of all materials aboard the LDEF has been reported [22-30]. Figure 2.12 is a photograph of the trailing edge of the deintegrated LDEF structure. The extensive contamination is apparent by the brown discoloration of the LDEF frame. The origin of this contamination is believed to be the result of outgassing followed by the redeposition of materials aboard the LDEF [23,24,25]. The origin of the extensive contamination present on LDEF materials as a result of the low-Earth orbit space environment and/or pre- and post-flight handling of the LDEF is difficult to ascertain.

The contamination history of the LDEF, as determined by the Boeing Defense and Space Group, is shown in Figure 2.13 [30]. Figure 2.13 provides a model for the possible locations where contamination may have accrued throughout integration,

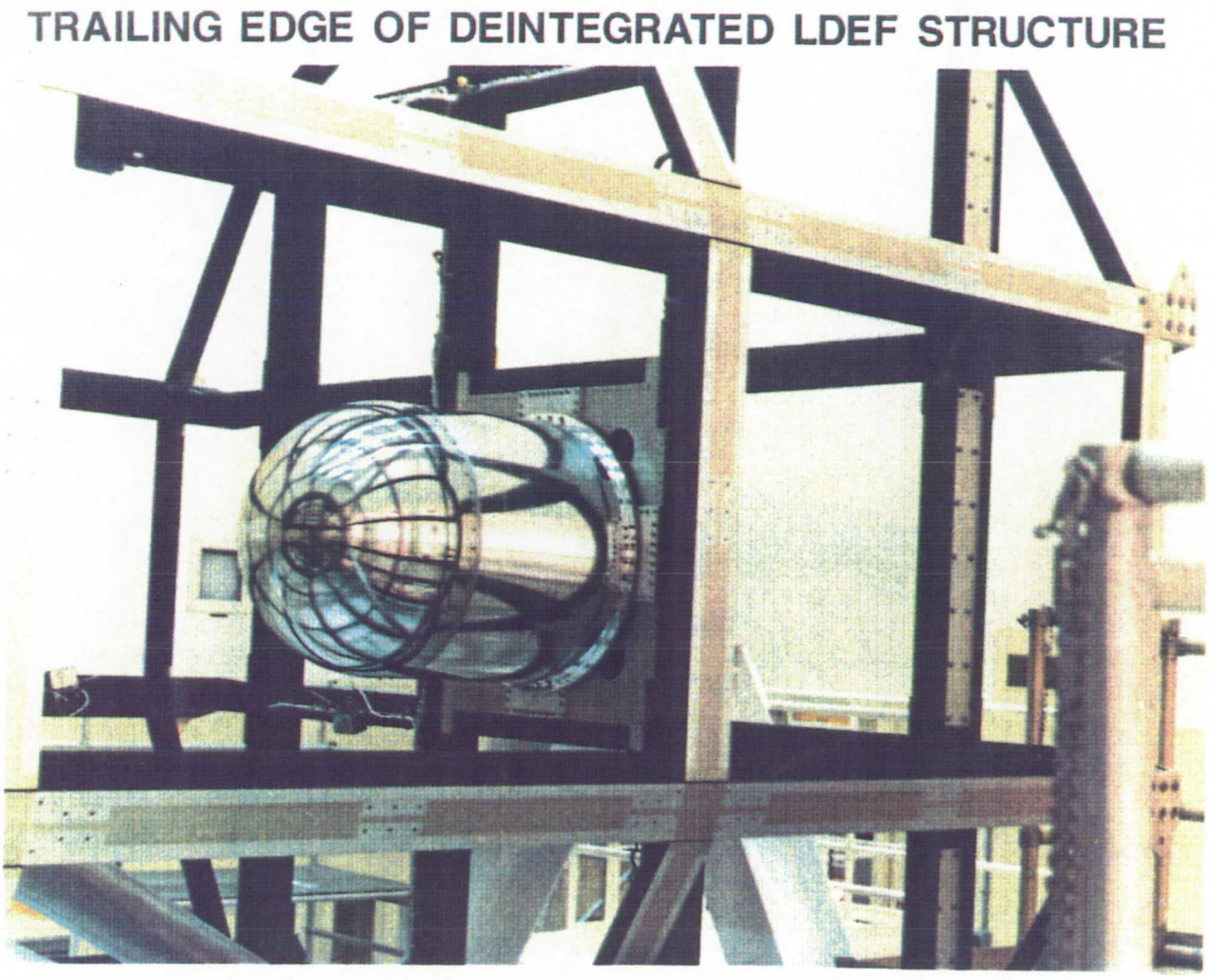

FIGURE 2.12: PHOTOGRAPH OF TRAILING EDGE OF DEINTEGRATED LDEF STRUCTURE.

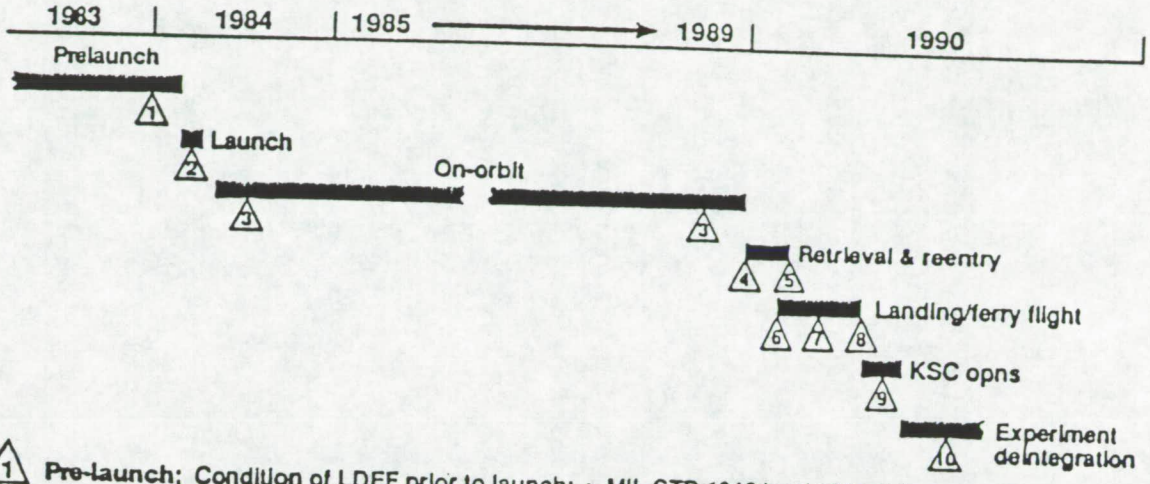

1. **Pre-launch;** Condition of LDEF prior to launch: > MIL STD 1246 level 1000 C for some trays.
2. **Launch;** During launch particulate contaminants are redistributed and Shuttle Bay Debris is added.
3. **On-orbit;** Contaminants are modified and new contaminants are generated in the orbital environment.
4. **Retrieval;** Grappling jars particles and films free, some may have relocated.
5. **Re-entry;** During reentry particles and molecular contaminants relocate or are created.
6. **Landing;** The Shuttle is exposed the Edwards Environment, accumulation of natural dusts.
7. **Ferry flight;** High humidity conditions, high velocity flow, thermal and pressure stresses occur.
8. **Ferry flight;** HEPA filter fibers appear on tape lifts after exposure to new filter.
9. **KSC Ground operations;** Ground operations prior to SAEF 2 include many manipulations of LDEF in complex environment.
10. **De-integration;** SAEF 2 exposure

FIGURE 2.13: SCHEMATIC DIAGRAM OF CONTAMINATION HISTORY FOR LDEF [30].

flight, and deintegration procedures of the LDEF. During all phases of preparation, position 1, the LDEF collected a large amount of contaminants [30]. The basic contamination requirement was Visible Clean Level II which was used during the integration of the LDEF [30]. As a result of the Visible Clean Level II requirement, a large number of the experimental trays were handled without the use of protective gloves [30]. During the launch of the LDEF, position 2, contaminants from the payload bay of the Shuttle Columbia also accumulated [30]. As a result of the low-Earth orbit space environment, position 3, hydrocarbon and silicon components, paints, adhesives and contaminant films outgassed into the local LDEF environment [30]. During the retrieval, the LDEF was sprayed with an aerosol of fine droplets of hydrocarbon-containing material [30]. Contaminants from the payload bay of the Shuttle Columbia, position 4, were also accrued during retrieval. The LDEF was removed from the payload bay of the Shuttle Columbia, position 5, at the Kennedy Space Center. The LDEF was subsequently transported to the SAEF-2 clean room, position 6. The deintegration of the LDEF was performed in the SAEF-2 clean room.

C. LDEF Science Team

NASA's Office of Aeronautics and Space Technology and the LDEF Science Office oversee the coordination of all LDEF

experiments, supporting data, and, data generated by the Special Investigation Groups (SIGs) [31]. The LDEF Science Office is located at the NASA Langley Research Center within the Materials Division [31].

1. Special Investigation Groups (SIGs)

Four special investigation groups (SIGs) were established in January of 1989 to evaluate the low-Earth orbit space environment. The SIGs were established to evaluate ionizing radiation, meteoroid/debris, environmental effects on systems and materials. Data/results generated by the SIGs will be used for future development and design of spacecraft systems. The SIGs have established four databases from the data/results obtained from each group. The four SIGs are discussed below.

a. Ionizing Radiation SIG

The Ionizing Radiation Special Investigation Group was established to evaluate the radiation dose, particle fluences, linear energy transfer spectra, and radioactivity upon retrieval of the LDEF [32]. Radiation measurements were obtained to evaluate the dosimetry and astrophysics of the low-Earth orbit environment [32].

b. Meteoroid & Debris SIG

The Meteoroid & Debris Special Investigation Group was

established to ascertain the number and location of meteoroid/debris impacts present on the LDEF. This group also had responsibility for the development of a new model of the near-Earth meteoroid environment. This new model includes directionality, speed distribution, density, gravitational focus, spatial density, and size distribution of meteoroids.

c. Systems SIG

The Systems Special Investigation Group was established to investigate the four major engineering disciplines represented by LDEF hardware. The four disciplines are electrical, mechanical, thermal, and optical systems. The Systems SIG includes members from eight NASA centers, the European Space Agency, the Department of Defense and the domestic commercial sector [33].

d. Environmental Effects on Materials SIG

The Material Special Investigation Group was established to investigate the long-term space environmental effects on the LDEF structure and materials experiments. The materials experiments also included materials which were not originally planned to be test specimens. For example, the tray clamps, which were used to secure the experimental bays to the periphery of the LDEF frame, were given to the MSIG upon deintegration of the LDEF. These materials were not a part of

the original LDEF Mission I experiments. The MSIG was also established to integrate the results of the investigations with data generated by the principal investigators of the LDEF experiments.

The MSIG includes approximately 25 experts in the fields of atomic oxygen, radiation, and contamination. The MSIG also includes researchers in the fields of chemical, mechanical, and physical characterization of spacecraft materials. These members represent technical laboratories, universities, and organizations throughout Canada, Europe, and the United States.

The data/results generated from the SIGs have provided a wealth of information on the condition/components of the low-Earth orbit environment as well as the long term space environmental effects on engineering systems and materials [34]. The data/results have also provided the first model to evaluated the synergistic effect of atomic oxygen and ultraviolet radiation on spacecraft materials subjected to long term low-Earth orbit exposures [34].

D. Previous Exposure of Materials

Several Space Shuttle flights throughout the 1980's contained materials experiments located on the periphery of Shuttle spacecraft [35]. Approximately 300 different materials were evaluated from STS-5, STS-8 and STS-41G [35-

38]. The materials experiments aboard the Shuttles were designed to evaluate the extent of interaction of materials with atomic oxygen. The materials consisted of polymers such as Kapton®, Teflon®, silicones, polysiloxane/polyimide copolymers, graphite/epoxy composites, thermal control paints, and metals. A description of the flight experiments can be found in references [36,37,38].

1. Space Shuttle Flights

Space Shuttle flight STS-5 was launched in November 1982. The materials experiments were exposed to the near-Earth orbit environment at approximately 222 km for 44 hours [36]. Space Shuttle flight STS-8 was launched in September 1983. The materials experiments were exposed for 41.75 hours at approximately 222 km [37]. Space Shuttle flight STS-41-G was launched in October 1984. The materials experiments were exposed for 38 hours at approximately 225 km [38].

The extent of atomic oxygen interaction with materials was determined by post flight measurements. Atomic oxygen fluences were calculated using the model of the thermosphere [6]. Reaction efficiency or the susceptibility of materials to atomic oxygen attack was represented as the volume or mass of material lost per incident oxygen atom [35]. These experiments provided only a limited understanding of the kinetics and mechanistic interaction with atomic oxygen. As

a result of flight altitudes, possible synergistic effects present in the space environment could not be evaluated.

The interaction of atomic oxygen with many organic materials produced a characteristic surface damage morphology [35-38]. The surface damage morphology is frequently referred to as "carpet" morphology [35-38]. Polymeric materials containing hydrocarbon bonds, diamond, and graphite have reactivities on the order of 10^{-23} cm^3/atom [6]. Silicone materials react with atomic oxygen to form a protective surface oxide layer, SiO_x. This protective layer prevents further attack of atomic oxygen. Pure fluorocarbon polymers show very low reactivities to atomic oxygen. The reaction efficiency is less than 0.05×10^{23} cm^3/atom. Polymers that contain both carbon-fluorine and carbon-carbon bonds, such as fluorinated ethylene propylene (FEP), also show very low reactivities towards atomic oxygen. The reaction efficiency is also less than 0.05×10^{23} cm^3/atom.

2. Solar Maximum Mission (SMM)

The Solar Maximum Mission (SMM) was launched in February 1990, in a nearly circular orbit at approximately 491-574 km [35]. The SMM spent 50 months in the low-Earth orbit environment. Materials analyses were performed on materials retrieved from the Solar Max thermal control system [35]. The materials analyzed were aluminized Kapton®, Mylar®, silvered

Teflon®, and Dacron® [35]. The primary tools used in the analyses of the materials were optical and scanning electron microscopy/energy dispersive spectroscopy. The appearance of the aluminized Kapton® after 50 months in the low-Earth orbit environment was dull when compared to the shiny appearance of the control. The change in appearance was attributed to surface degradation/erosion, thereby creating the dull appearance [35]. Infrared spectroscopy revealed surface erosion/degradation, however, the actual polymer structure had not changed. Thickness measurements indicated the Kapton® mass loss ranged from 0.54 to 31.4% [35].

Significant surface morphology damage was observed for silvered Teflon samples. The damaged surface morphology has been described as having a "bristle-like" reaction pattern [35], whereas, the surface morphology of the control samples is smooth in appearance. The results obtained for Teflon® and FEP from the STS Missions suggested that both polymers were inert to atomic oxygen.

III. Experimental

A. Materials

The materials analyzed in this study were received from Dr. Philip R. Young of the NASA Langley Research Center (Hampton, Virginia). The primary materials of interest in this study were chromic acid anodized 6061-T6 aluminum alloy tray clamps. Some of the clamps contained Chemglaze® A276 white and Chemglaze® Z306 black thermal control paints. The tray clamps were given to the Materials Special Investigation Group (MSIG) during the deintegration of the LDEF at the NASA-Kennedy Space Center. The polymer and composite samples were provided by Wayne S. Slemp, also at the NASA Langley Research Center, who was principal investigator of LDEF experiment A0134 "Space Exposure of Composite Materials for Large Space Structures" [1]. This materials experiment was located on Row 9 (leading edge), Tray B of the LDEF (see Figure 2.5). The fluorinated ethylene propylene (FEP) samples came from various thermal blanket specimens made available to the MSIG. A 6061-T6 aluminum sample with a meteoroid impact was provided by Dr. Donald H. Humes, also at the NASA Langley Research Center, who was principal investigator of LDEF experiment S0001 "Space Debris Impact Experiment" [1]. This materials experiment was located on Row 3 (trailing edge), Tray F of the LDEF.

As a result of the large number, as well as the different types of materials analyzed, the materials section is divided into the following four sections: 1) tray clamps, 2) polymers, 3) composites, and 4) aluminum sample with meteoroid impact.

1. Tray Clamps

Over four hundred chromic acid anodized 6061-T6 aluminum alloy tray clamps were designed to secure the eighty-six experimental bays to the LDEF frame. Thus tray clamps were located over the entire LDEF frame. Approximately 200 chromic acid anodized 6061-T6 aluminum alloy tray clamps contained Chemglaze® A276 white and Chemglaze® Z306 black thermal control paints. A photograph of two flight Chemglaze® white-on-black tray clamps is shown in Figure 3.1. The right tray clamp, shown in Figure 3.1, is representative of tray clamps taken from the leading edge of the LDEF. The left tray clamp, shown in Figure 3.1, is representative of tray clamps taken from the trailing edge of the LDEF. Figure 3.1 clearly illustrates the effects of the low-Earth orbit environment on the two thermal control paints.

The fifteen (fourteen flight and one control) tray clamps investigated in this study contained both paints. The control clamp sample was stored in a Fluoroware® H22-603 container for the duration of the LDEF flight. During the deintegration of

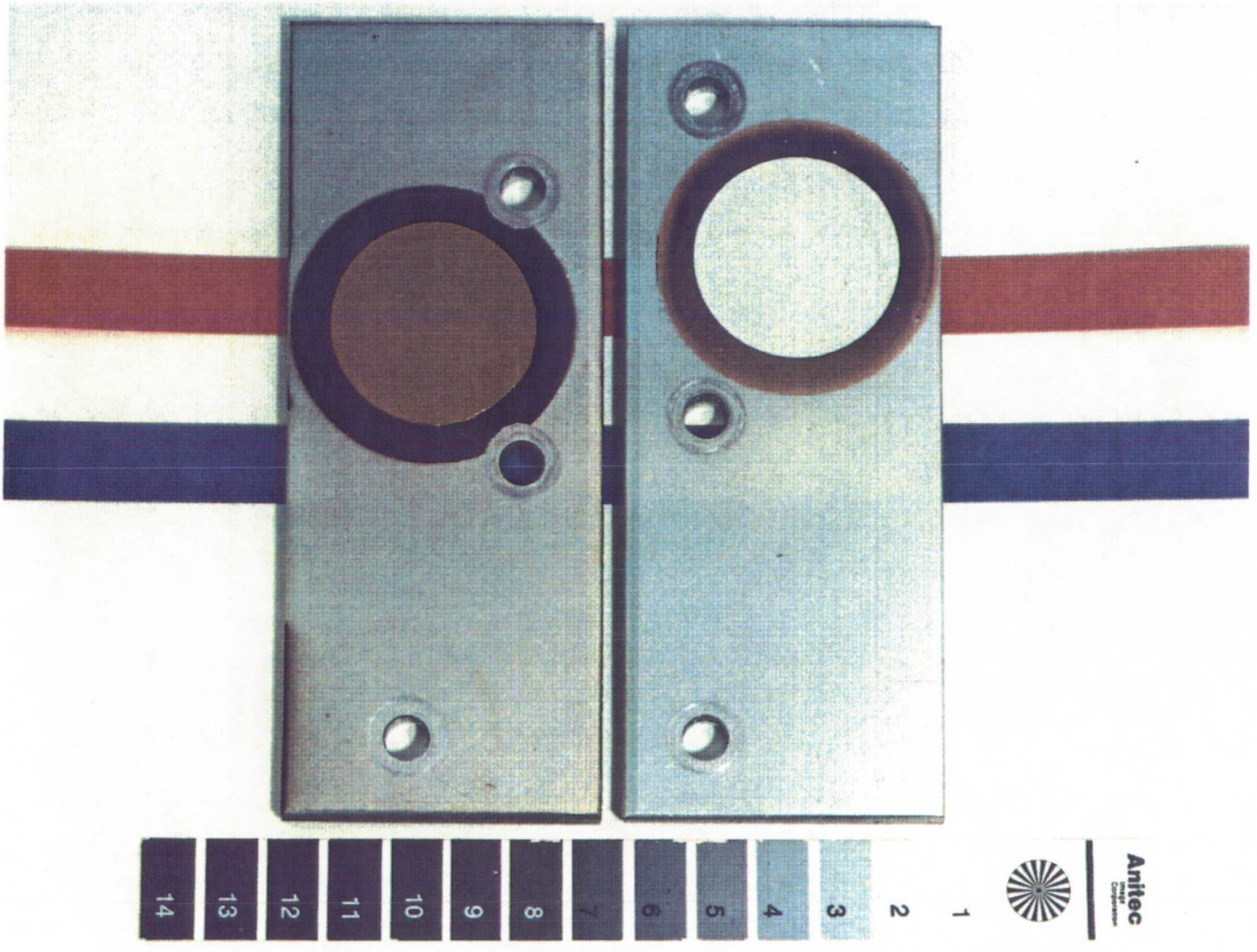

FIGURE 3.1: PHOTOGRAPH OF TWO BLACK-ON-WHITE LDEF TRAY CLAMPS - LEFT: TRAILING EDGE, RIGHT: LEADING EDGE.

the LDEF, the flight samples were placed in labelled Fluoroware® H22-603 containers corresponding to the Tray and Row in which the tray clamp was removed. The fourteen flight samples represent the twelve sides, earth and space end of the LDEF. Table 3.1 lists the location by Tray and Row of the fourteen flight tray clamps.

The 6061 aluminum alloy is commonly used in the fabrication of heavy-duty structures. The chemical composition by weight of the alloy is 1.00% magnesium, 0.60% silicon, 0.20% chromium, and 0.27% copper [39].

"A variable thermal control coating", modified chromic acid anodization, was developed by Duckett and Gilland of the NASA Langley Research Center [40]. The modified chromic acid anodization was designed to meet the needs for spacecraft thermal control [40]. The controlling variables for this coating were thermal emittance (ϵ_T) with a range of 0.10 to 0.72 and solar absorptance (α_S) with a range of 0.2 to 0.4 [40]. This thermal control coating, in contrast to sulfuric acid anodization, conversion coating (alodine), or dielectric films, allows a selected thermal emittance and solar absorptance to be obtained on the same piece of aluminum with a specified range [40].

The Chemglaze® A276 white and Chemglaze® Z306 black thermal control paints were produced by the Lord Corporation, Industrial Coatings Division (Erie, Pennsylvania). The

TABLE 3.1: TRAY CLAMP POSITION ON LDEF.

TRAY CLAMP	TRAY	ROW
F1	F	1
F2	F	2
E3	E	3-trailing edge
B4	B	4
B5	B	5
C6	C	6
D7	D	7
A8	A	8
D9	D	9-leading edge
A10	A	10
E11	E	11
D12	D	12
G6	G-earth end	
H9	H-space end	

Chemglaze® A276 and Z306 are both polyurethane-based paints. The pigment in the A276 white paint is titanium dioxide (TiO_2). Chemglaze® 9924 wash primer-part A and part B, used during the fabrication of the tray clamps, was also produced by the Lord Corporation, Industrial Coatings Division.

Following production of the anodic thermal control coating, the aluminum tray clamp was coated with the Chemglaze® 9924 wash primer-part A. A 4 cm diameter disk of Chemglaze® Z306 black paint was applied to each aluminum clamp. The clamp was subsequently coated with Chemglaze® 9924 wash primer-part B. A separate 3 cm diameter aluminum foil disk was coated with Chemglaze® A276 white paint. This aluminum foil disk containing the white paint was then adhesively bonded to the center of the 4 cm Z306 black paint disk. The fabrication steps of the tray clamps, outlined above, are shown in Figure 3.2.

2. Polymers

The several types of polymers analyzed in this study were obtained from commercial sources, synthesized at the NASA Langley Research Center, or synthesized through a grant agreement [41]. Control samples were obtained from the original batch of polymers used for flight specimens. Most of the polymers analyzed in this study, except the fluoropolymers, were located on Tray B, Row 9 of the LDEF.

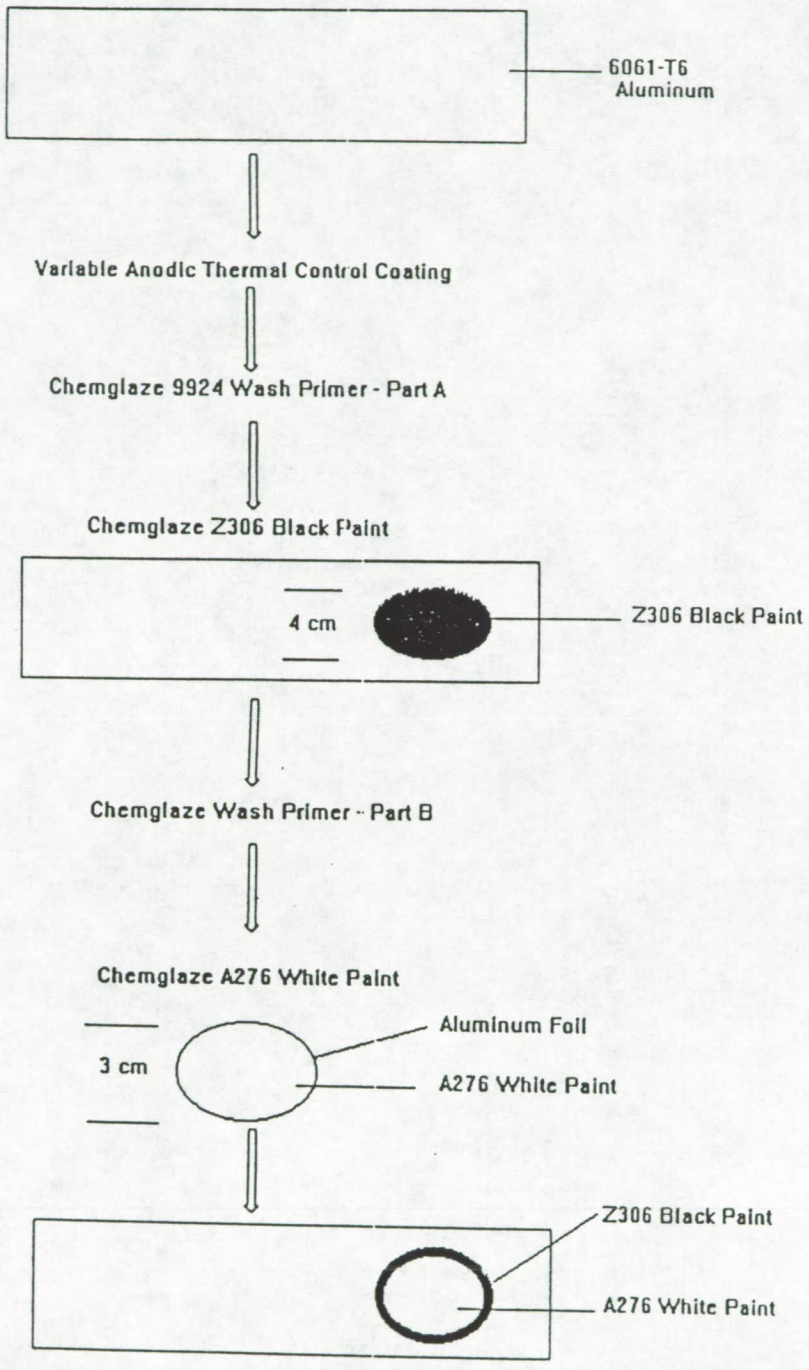

FIGURE 3.2: SCHEMATIC DIAGRAM OF FABRICATION STEPS OF LDEF TRAY CLAMPS.

The polymers are subdivided into the following groups: a) fluoropolymers, b) polyimides, c) polysulfones and d) polyimide polysiloxane copolymers.

a) Fluoropolymers

Silvered fluorinated ethylene propylene (FEP) is a light-weight thermal control material. These thin silvered-FEP films are ideal thermal control materials because the silver provides high solar reflectance while the transparent FEP produces high infrared emittance [42]. A schematic representation of the silvered-FEP material is shown in Figure 3.3 [42].

FEP films, manufactured by DuPont, were produced by the copolymerization of tetrafluoroethylene and perfluoropropylene in an approximately 6:1 mole ratio [43]. The chemical structure of FEP is shown in Figure 3.4. Several control and flight FEP samples were analyzed in this study. Table 3.2 lists the position, by Tray and Row, of the flight samples. All flight samples were exposed for 69-months.

b) Polyimides

Poly (N,N'-p,p"-oxydiphenylene-pyromellitimide) is a well characterized aromatic polyimide. This polyimide in film form is more commonly known as Kapton® and was obtained from a commercial source [41]. The chemical structure of Kapton is shown in Figure 3.5. A control and 10-month flight sample

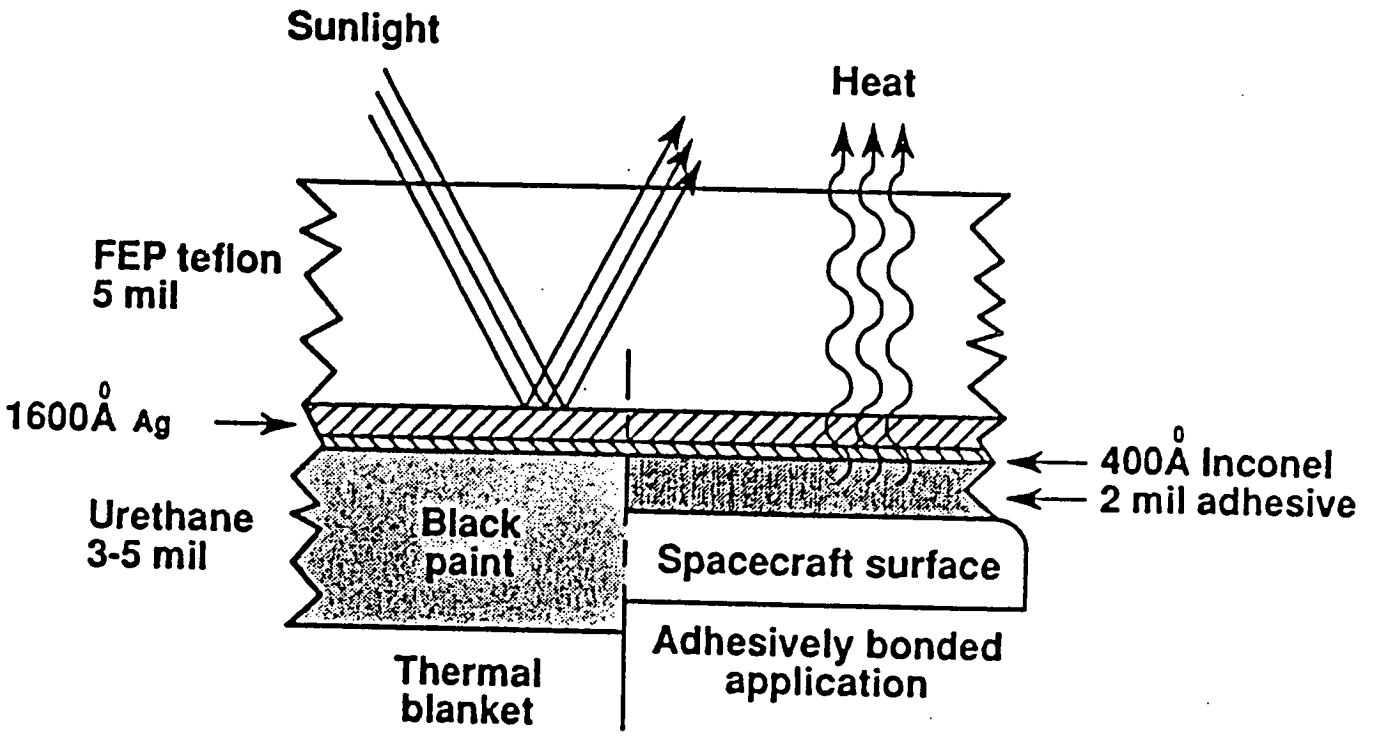

FIGURE 3.3: SCHEMATIC PICTURE OF SILVERED FLUORINATED ETHYLENE PROPYLENE (FEP) THERMAL BLANKETS [42].

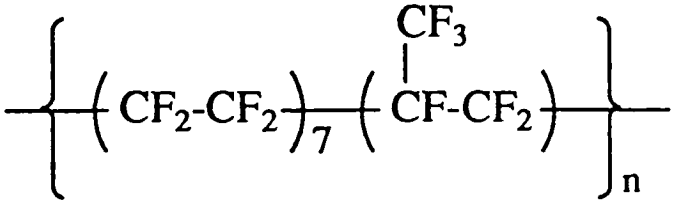

FIGURE 3.4: CHEMICAL STRUCTURE OF FLUORINATED ETHYLENE PROPYLENE (FEP).

TABLE 3.2: LOCATION, TRAY AND ROW, OF FEP FLIGHT SAMPLES.

FEP SAMPLE	TRAY	ROW
F2	F	2
C5	C	5
C8	C	8
B9	B	9

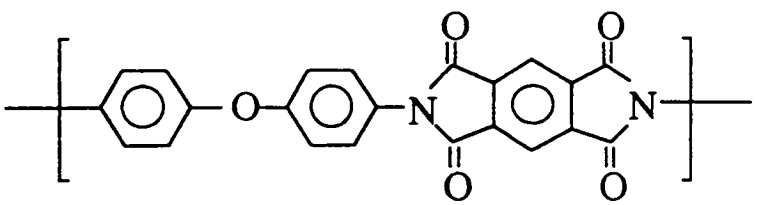

FIGURE 3.5: CHEMICAL STRUCTURE OF KAPTON®.

were both analyzed in this study.

c) Polysulfones

Udel P1700 polysulfone films were fabricated at the NASA Langley Research Center. The films were made from dried resin pellets by applying pressure to a mold that was heated to 250-300°C [44]. This pressure remained constant for one hour before cooling. The chemical structure of polysulfone is shown in Figure 3.6. A control and 10-month flight sample were both analyzed in this study.

d) Polyimide-polysiloxane copolymers

Two polyimide-polysiloxane (PIPSX) copolymers, (PIPSX-6 and BJPIPSX-11), were analyzed in this study. These copolymers were synthesized by personnel at Virginia Tech [45]. The chemical structure of the copolymer is shown in Figure 3.7. Both copolymers were exposed for 10-months. A control and one flight sample were analyzed for the two sets of copolymers.

3. Composites

Two types of carbon fiber reinforced polymer matrix composites were analyzed in this study. All flight samples were located on Tray B, Row 9 of the LDEF. The flight samples were cut from larger panels processed at the NASA Langley Research Center using prepreg manufacturer's specifications [44]. Control samples were cut from the same panel as the

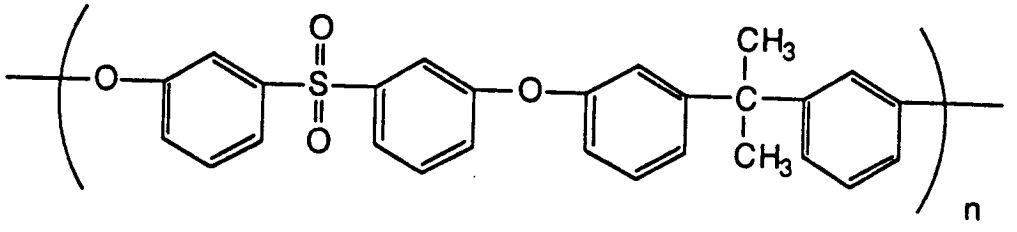

FIGURE 3.6: CHEMICAL STRUCTURE OF POLYSULFONE.

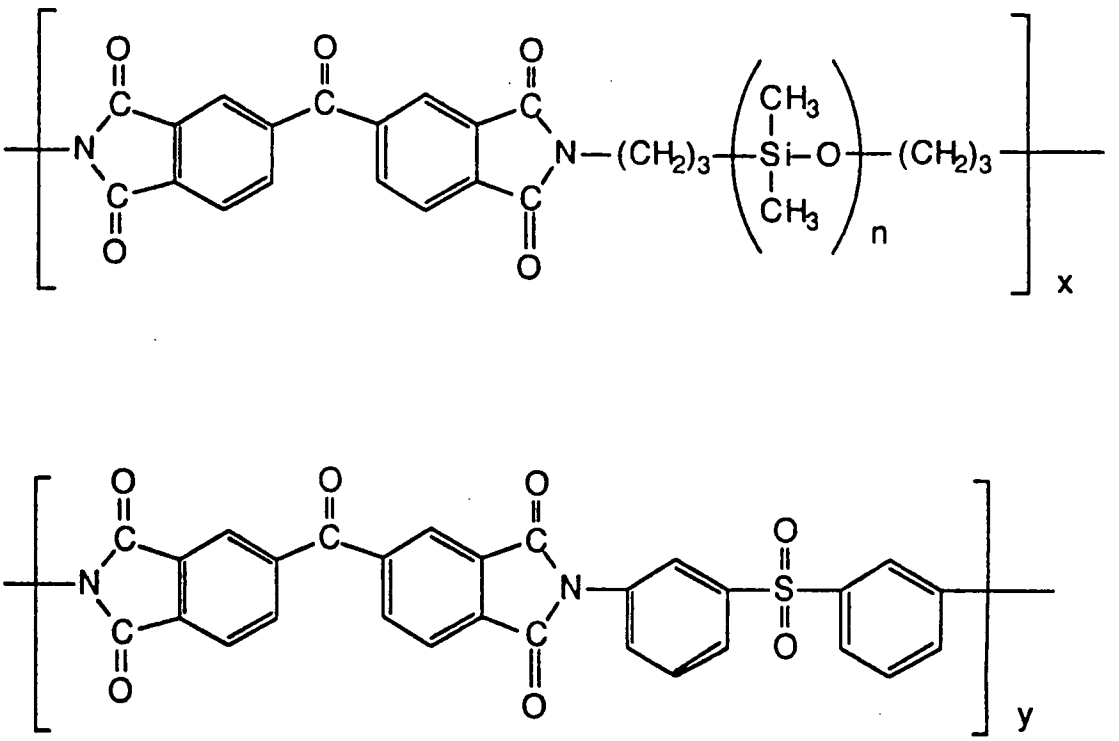

FIGURE 3.7: CHEMICAL STRUCTURE OF POLYIMIDE POLYSILOXANE (PIPSX) COPOLYMER.

flight specimen. The control sample remained at the NASA Langley Research Center in a low humidity environment [44]. This section will be subdivided into two groups corresponding to the type of polymer used as the matrix resin, namely, epoxy and polysulfone.

a) Epoxy

An epoxy matrix composite, 934/T300, was investigated in this study. The epoxy resin in 934/T300 was produced by Fiberite Corporation. The T300 carbon fibers used in both composites were produced by Union Carbide Corporation. A control and 69-month flight sample were investigated.

b) Polysulfone

P1700/C6000 is a carbon fiber reinforced polysulfone composite. The P1700 polysulfone resin was produced by Union Carbide Corporation. The C6000 carbon fibers were produced by the Celanese Corporation. A control and two flight samples exposed for 10 and 69 months were investigated in this study.

4. Aluminum Sample with Meteoroid Impact

A 2 cm diameter 6061-T6 aluminum disk containing a meteoroid impact was provided by Dr. Donald H. Humes, of the NASA Langley Research Center. The sample was located on Tray F, Row 3 of the LDEF. The meteoroid impact was approximately 2 mm in diameter.

B. Sample Preparation

Extreme care was used when preparing the samples for the various surface characterization techniques. Lint free nylon white gloves from Fisher Scientific Company were used to prevent sample contamination. The gloves, prior to use, were washed in solvent grade hexane, also obtained by Fisher Scientific, to remove any silicon contamination. The gloves were then subsequently washed with soap and water and allowed to dry. Scotch Magic Tape®, a pressure sensitive adhesive, made by the 3M Company (St. Paul, Minnesota) was used to secure samples for XPS, SEM and AES analysis. Samples for SEM and AES analysis were sputtered for approximately two to three minutes with gold to reduce charging and destruction of the surface by the electron beam.

Preparation of the polymers and composites for XPS and SEM analysis required cutting of the sample utilizing an acetone wiped pair of scissors or an Exacto-knife. Typical sample dimensions were 13 mm x 13 mm.

The size of the sample tray clamps, 12.7 cm x 5.1 cm x 1 cm, required cutting prior to any surface analysis. The samples were cut manually with a hacksaw to prevent sample heating or contamination of the surface when cutting. Prior to cutting the hacksaw blade was grit blasted to remove the blue paint coating on the surface. The blade was subsequently washed with acetone.

Several cuts were made for the various surface characterization techniques. The cutting procedure of the tray clamps for XPS analysis is shown in Figure 3.8. A 13 mm x 13 mm sample was cut to encompass the anodized aluminum, Chemglaze® A276 white and Chemglaze® Z306 black paints. The sample was first placed in a vise with the exposed side face down to prevent contamination of the exposed surface while cutting. The first cut was made in the y-direction through the middle of the white-on-black Chemglaze® paints. Subsequent cutting was performed on the smaller piece of the tray clamp. The second cut was made in the x-direction through the middle of the white-on-black Chemglaze® paints. As shown in Figure 3.8, XPS analysis was performed on the three portions of the cut tray clamp.

Additional cutting was required for a second XPS analysis of the aluminum as well as AES, SEM, and contact angle analysis. The cutting procedures are shown in Figure 3.9. These cuts were made on the larger piece of the tray clamp from the initial cutting for XPS analysis. The first cut was made in the y direction through the anodized aluminum. Subsequent cutting was performed on the small piece of the tray clamp. Smaller pieces of aluminum were randomly cut from this piece for AES, SEM, contact angle, and XPS analysis.

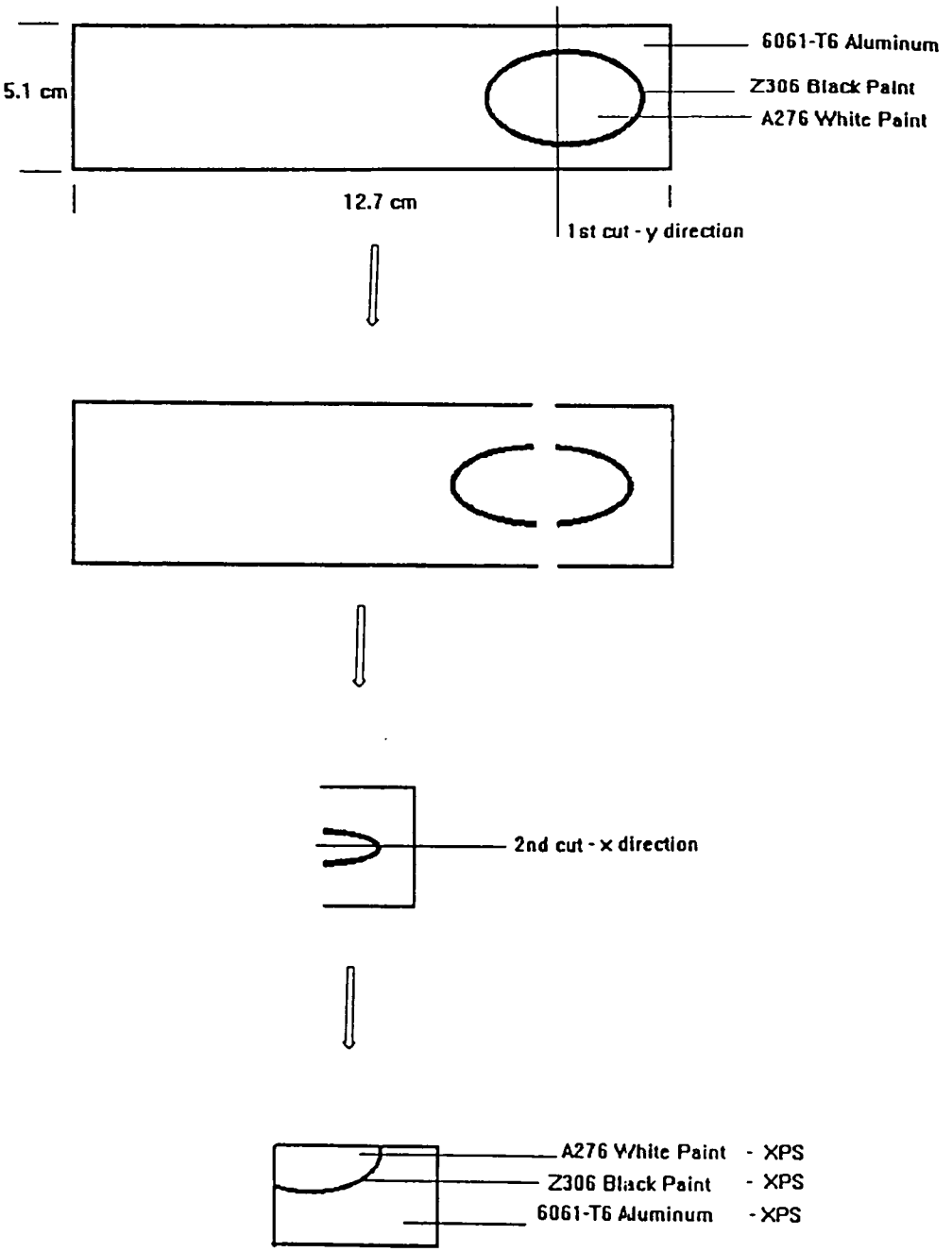

FIGURE 3.8: CUTTING PROCEDURE OF TRAY CLAMPS FOR XPS ANALYSIS.

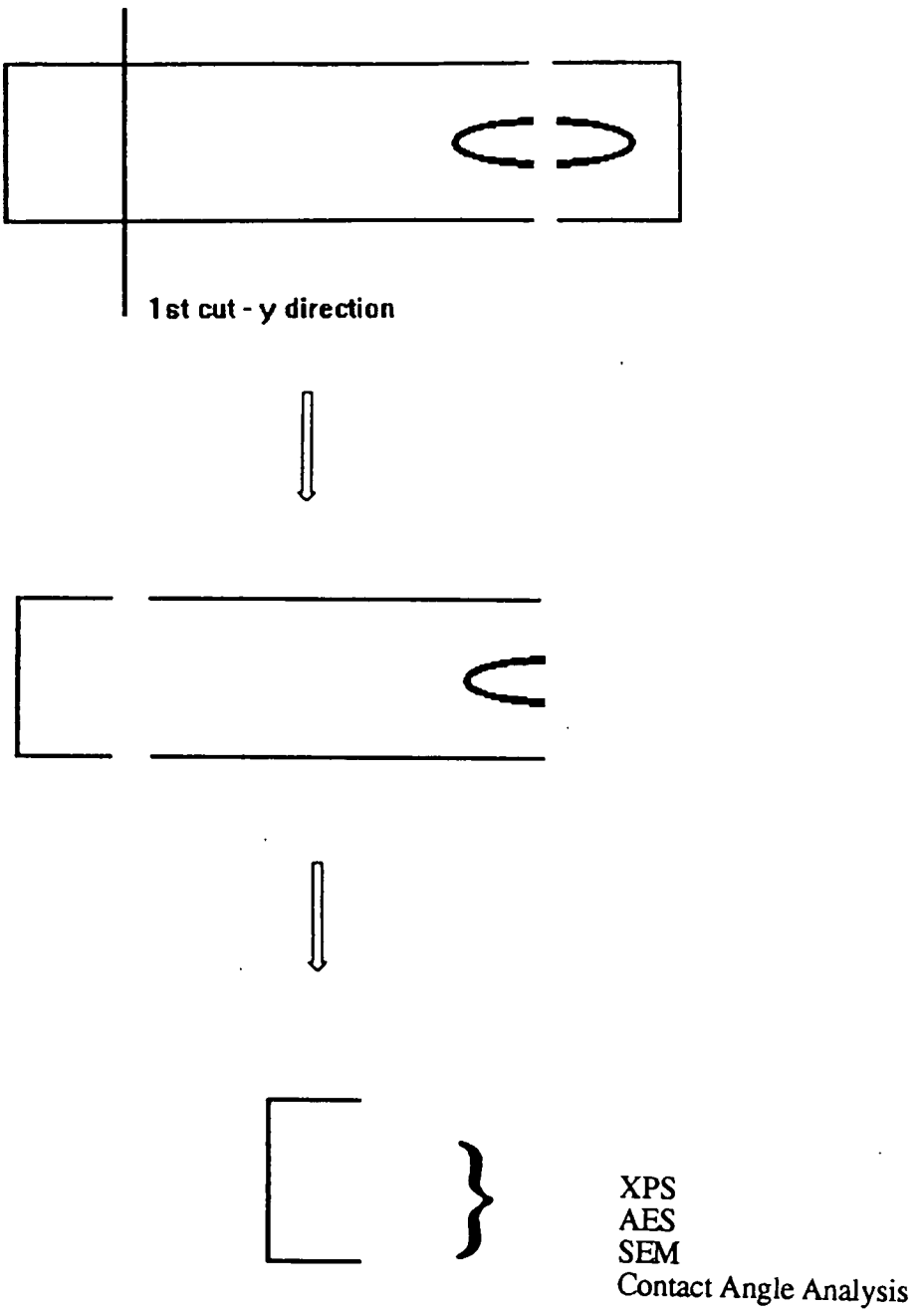

FIGURE 3.9: CUTTING PROCEDURE OF TRAY CLAMPS FOR SECOND XPS ANALYSIS, AES, SEM, AND CONTACT ANGLE ANALYSIS.

C. X-ray Photoelectron Spectroscopy (XPS)

In this study, x-ray photoelectron spectroscopy (XPS) was the primary surface tool used to characterize the changes in surface composition which occurred as a result of exposure to the low-Earth orbit environment. XPS is a powerful and well established technique for investigating the chemical nature of surfaces [46-49]. XPS was ideal for this study due to the non-destructive nature of the analysis.

Figure 3.10 is a simplified schematic diagram of the process that gives rise to XPS. As shown in Figure 3.10, the sample was irradiated with achromatic x-rays. The absorption of the x-rays induces the ejection of core level photoelectrons from within the top 5 nm of the sample surface with some fraction of the x-ray energy. The binding energy (B.E.) is characteristic of the photoejected electron of a specific energy level of a particular atom and can be calculated by the following equation:

$$B.E. = h\nu - KE - \phi \qquad (3.1)$$

where $h\nu$ is the x-ray energy, KE is the kinetic energy of the ejected photoelectron, and ϕ is the spectrometer work function. The spectrometer work function is dependent upon the sample as well as the spectrometer [50].

Shake-up satellite peaks may also be observed in XPS when studying aromatic polymers [51,52]. These peaks are observed when an electron moves from an occupied to an unoccupied

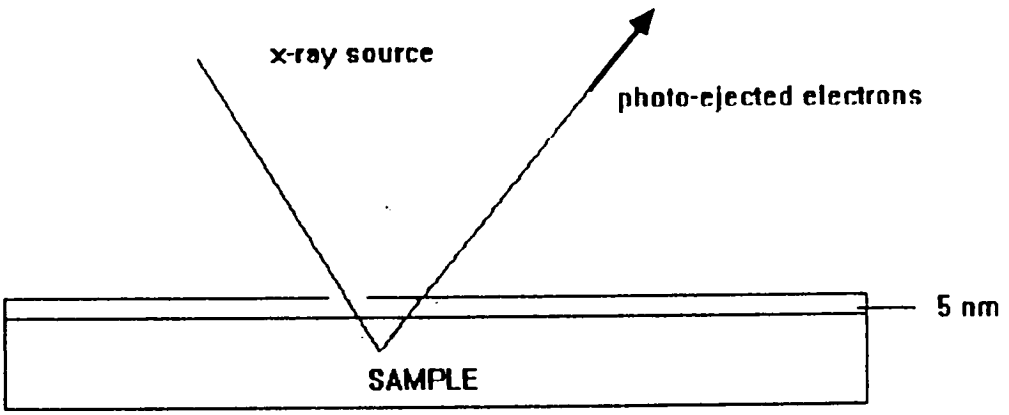

FIGURE 3.10: SCHEMATIC DIAGRAM OF X-RAY PHOTOELECTRON SPECTROSCOPY (XPS) PROCESS.

energy level. This transition results in a fractional loss of energy with respect to the total core photoelectron and thus shake-up satellite peaks are observed at a higher binding energy relative to the main photopeak [52]. The binding energy of an element, as calculated by equation 3.1, provides information about the chemical environment or bonding state. A commonly used technique in XPS analysis utilizing known binding energies is curve fitting. Curve fitting is based on the principle of chemical shifts. A decrease in electron density around a central atom results in an increase in binding energy for that atom. Changes in electron density can be attributed to changes in oxidation state as well as substituent changes. Shifts in binding energy provide information about the type of chemical functionality or chemical environment present on the surface.

Curve fitting was carried out by use of PHI software, version 3.0. All photopeaks were fitted with Gaussian curves. The peak positions, which are indicative of the type of chemical functionality present, were determined by the use of known literature values [53-55]. The various peak positions were held at a constant value and were referenced to the C1s photopeak characteristic of hydrocarbon species at 285.0 eV. The full width at half maximum (FWHM) for the C1s photopeaks was held constant at 1.70 eV.

Atomic concentrations were determined by the use of the

PHI software, version 3.0. Atomic concentration is directly proportional to the area under the photopeak. The PHI software, version 3.0 determines the atomic concentrations by the following equation:

$$AP_x = (I_x/S_xT_x)/\Sigma_{i=1}^{n}(I_x/S_xT_x) \qquad (3.2)$$

where AP is the atomic percent, I is the area of the photopeak, S is the sensitivity factor, T is the total acquisition time for each data point and n is total number of photopeaks. All atomic concentrations are statistically rounded and are reported to the tenth decimal point.

XPS analysis was performed on a Perkin-Elmer PHI series 5400 spectrometer with a Magnesium Kα achromatic X-ray source (1253.6 eV), operating at 15 keV and 400 watts with an emission current of 30 mA. The spectrometer was calibrated to the 4f7/2 photopeak of gold.

D. Auger Electron Spectroscopy (AES)

Auger electron spectroscopy (AES) - depth profiling was used to determine the oxide thickness of the 6061-T6 aluminum. Depth profiling involves the determination of the elemental composition of a surface as it is being etched or sputtered away by a beam of argon ions [49,56]. Figure 3.11 shows schematically how the process is carried out [56]. A highly

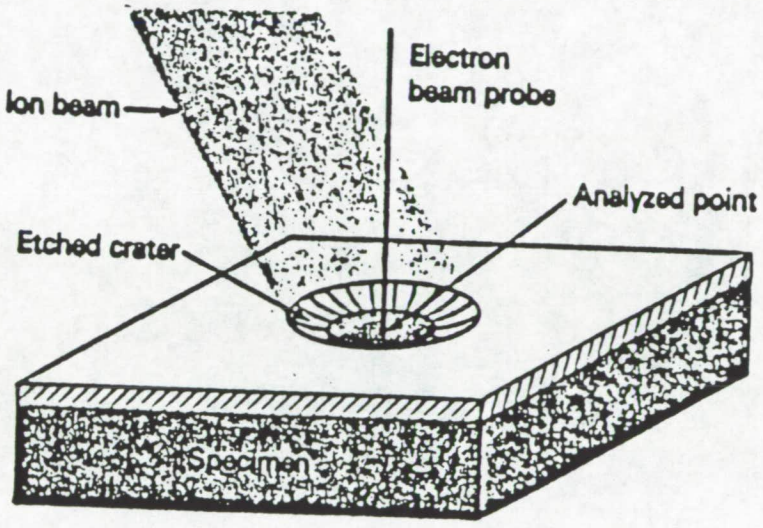

FIGURE 3.11: SCHEMATIC PICTURE OF AUGER DEPTH PROFILING [56].

focused electron beam called an Auger microprobe and an argon beam are operated simultaneously. Oxide thickness (τ) can be calculated by the following equation:

$$\tau = t * R \qquad (3.3)$$

where t is the sputter time and R is the sputter rate. A standard sputter rate of 300 Å/min, obtained for tantalum oxide (Ta_2O_5), was used as a reference. The sputter time was arbitrarily taken at the point at which the aluminum and oxygen atomic concentration signals crossed.

AES was performed on a Perkin-Elmer PHI 610 scanning Auger microprobe with an electron beam voltage of 5 kV and a beam current of 0.05 A. An argon ion beam current of 0.2 A was used for Auger depth profiling. In this study, the aluminum oxide thickness was determined for both the exposed and protected sides of the fifteen tray clamps. The protected side of the tray clamp corresponds to the side which was against the LDEF frame. All samples were sputtered for approximately two to three minutes with gold to reduce charging and destruction of the surface by the electron beam.

E. Scanning Electron Microscopy (SEM)

Scanning electron microscopy (SEM) is a widely used technique to obtain a microscopic image of the sample's surface topography. Images are obtained by a focused electron beam which is rastered over the surface. The electron beam

induces the ejection of secondary electrons, Auger electrons and backscattered electrons from the top 5 to 10 nm of the material. The image results from the detection of the secondary electrons emitted from the sample. The secondary electrons detected are displayed as an image on a cathode ray tube. Surface topography was examined using an International Scientific Instrument SX-40 scanning electron microscope operating at a beam voltage of approximately 20kV. All samples were sputtered for approximately two to three minutes with gold to reduce charging and destruction of the surface by the electron beam.

F. Contact Angle Analysis

Contact angle measurements were used to evaluate the wettability of the 6061-T6 aluminum tray clamp surface. Aluminum oxide has a high surface energy and therefore, a near zero contact angle would be expected for a clean surface [57]. Contact angle analysis was performed using a Rame-Hart 100-00 115 NRL goniometer equipped with a video monitor. 5 1 drops of deionized distilled water were placed on the aluminum surface with a microliter syringe. Immediate advancing contact angles were measured on the left and right hand side of three separate drops.

G. Plasma Treatment

Plasma treatments of FEP samples were carried out in a March Instruments Plasmod® unit. The operating parameters were 13.56 MHz and 50 watts. Plasma treatment times were 5 and 10 minutes. Experiments were carried out to evaluate the changes in the surface chemistry of a control and two flight (C5 and C8) FEP samples following exposure to an oxygen plasma. XPS was used to characterize changes in the surface of the samples following plasma treatment.

IV. Results and Discussion

A. Surface Characterization of Polymers

The surface analysis of the polymers described in the Experimental chapter is discussed in this section. XPS was the primary surface tool used to characterize the changes induced in polymer surfaces as the result of exposure to the low-Earth orbit environment. The XPS results are reported as binding energy in eV and surface concentration in atomic percent. The XPS results are divided into two sections. The atomic composition results first and then the results from the curve fit analysis. These results will be used to evaluate the effects of the low-Earth orbit environment on the surface chemical properties of polymers.

1. Kapton®

a. Atomic Composition

The XPS atomic concentrations measured for the control and B9 flight samples are listed in Table 4.1. The flight sample was located on the leading edge, (Tray B, Row 9), of the LDEF for 10 months. The theoretical atomic composition of Kapton®, as shown in Figure 3.5, is 75.9% carbon, 17.2% oxygen, and 6.9% nitrogen. The atomic composition of the control sample, determined by XPS, is 82.9% carbon, 12.1%

TABLE 4.1: XPS ANALYSIS OF KAPTON® CONTROL AND 10 MONTH FLIGHT SAMPLE.

CONTROL

PHOTOPEAK	BINDING ENERGY(eV)	ATOMIC CONC(%)	X/C RATIO
C 1s	285.0	82.9	--
O 1s	532.2	12.1	0.15
N 1s	400.5	5.0	0.06

10 MONTH

PHOTOPEAK	BINDING ENERGY(eV)	ATOMIC CONC(%)	X/C RATIO
C 1s	285.0	71.9	--
O 1s	532.3	20.5	0.28
N 1s	400.3	6.6	0.09
Si 2p	104.0	1.0	0.01

oxygen, and 5.0% nitrogen. The atomic composition of the control sample is in fair agreement with the theoretical composition.

XPS analysis of the flight sample, as illustrated in Table 4.1, revealed carbon, oxygen, nitrogen and silicon. The atomic composition of the flight sample is 71.9% carbon, 20.5% oxygen, 6.6% nitrogen and 1.0% silicon. Changes in the atomic composition were observed for the flight sample with respect to the control. The carbon content of the flight sample decreased 13%, whereas the oxygen content increased 69%. The nitrogen content also increased 32% with respect to the control sample. This trend of decreasing/increasing carbon, oxygen and nitrogen contents for the control and flight samples is shown in Figure 4.1.

A small amount of silicon was detected on the flight sample. The fact that silicon was not present on the control sample suggests that silicon was deposited during the LDEF mission. Nearly 90 kg (200 lbs) of silicon-containing materials were aboard the LDEF [1]. Extensive silicon contamination of all materials aboard the LDEF has been reported [22-30]. The source of the silicon contamination is believed to be the result of outgassing/re-deposition or surface migration of silicon-containing materials. Reaction of silicon-containing material with atomic oxygen has been reported to yield an inorganic or silicate type of material

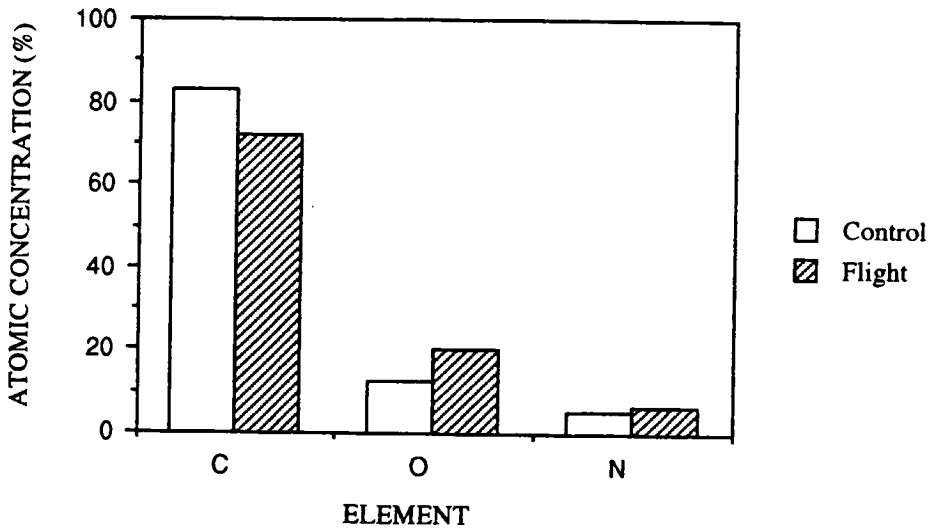

FIGURE 4.1: COMPARISON OF ATOMIC CONCENTRATIONS OF CARBON, OXYGEN, AND NITROGEN FOR KAPTON® CONTROL AND 10 MONTH FLIGHT SAMPLE.

[22-30]. The binding energy of silicon, at 104.0 eV, present on the flight sample, corresponds to inorganic silicon or an SiO_x type of material. Thus, the silicon contamination on the Kapton® film located at B9 was converted from organic silicon (binding energy 102 eV) to an inorganic silicon material.

The O/C atomic concentration ratio for the control and flight sample showed an 87% increase. The N/C ratio for the control and flight sample increased 50%. The increase in both atomic concentration ratios suggests that the surface chemistry of Kapton® was significantly changed. The XPS results for the flight sample indicate an increase in the overall oxygen and nitrogen contents and a decrease in the carbon content. The increase in the oxygen content may correspond to an incorporation of oxygen functionality on the surface as a result of exposure to the low-Earth orbit environment. The decrease in carbon content observed may correlate to erosion and/or degradation of the carbon backbone by atomic oxygen.

Hemminger has reported XPS results for various polymers and composites which were flown on the LDEF [58]. The XPS results of two Kapton® films from the leading edge of the LDEF, F9, have been recently reported [58]. The atomic composition of the Kapton® reference sample is 71% carbon, 21% oxygen, 7.4% nitrogen, 0.2% silicon and 0.1% sulfur. The

atomic composition of the reference sample is also in fair agreement with the theoretical composition. Hemminger reported a 12.7% decrease in carbon content, a 33.3% increase in oxygen content and a decrease of 8.1% nitrogen for the Kapton® flight samples. Two percent of inorganic silicon was detected on the flight samples. Small to trace amounts of sodium, sulfur, potassium, fluorine and phosphorus were also detected. Hemminger concluded that the increase observed in the oxygen content was associated with the contaminants as well as polymer oxidation [58].

When comparing the XPS results for both Kapton® films, B9 and F9 (Hemminger's results), located on the leading edge, the change in the overall percent carbon content for both samples is consistent. However, significant differences were observed for the overall change in percent oxygen and nitrogen contents for both samples which are unexplained. Small amounts of inorganic silicon were detected on both flight samples which is a significant result. A greater extent of contamination was detected on the F9 Kapton® flight sample. The sources of this contamination has not been identified.

The basic trends reported by Hemminger, such as decreasing carbon content and increasing oxygen content, are consistent with the XPS results reported here. However, the magnitude of change for the flight samples with respect to the control varies. Further, Hemminger observed a decrease in

nitrogen for the flight sample where an increase in nitrogen was observed in the work presented.

Both Kapton® flight samples showed significant changes in the overall surface composition as a result of the low-Earth orbit environment. The differences observed in the XPS results suggest the effects of the low-Earth orbit environment will not only vary for different types of materials but also among similar materials. The effects of the low-Earth orbit environment on materials located at different position, for example, the leading edge compared to the trailing edge, would be expected. However, materials located on the same row but in different trays would not be expected to show the variations presented here.

b. Curve Fit Analysis

Curve fit analysis was performed to provide information about the type of functionality or chemical environment on the surface. Due to its sensitivity to substituent effects, the carbon 1s peak was the primary photopeak curve-fitted [59]. These substituent effects are observed for the carbon 1s photopeak as a result of changes in electron density around the carbon atom corresponding to shifts in binding energies. The curve fitting procedures were performed utilizing known binding energies. Carbon-oxygen functionality can be interpreted by a shift in binding energy with respect to the

hydrocarbon species (referenced to 285.0 eV) for the number of bonds between carbon and oxygen. For example, carbon singly bonded to oxygen, such as in an alcohol, gives a 1.5 eV shift, whereas, carbon doubly bonded to oxygen, such as in a carbonyl group, shows a 3.0 eV shift.

After known binding energies are accounted for, additional peaks are then assigned to account for the remaining area under the total photopeak. Curve fit peaks contributing less than 3% to the total are considered insignificant. The results of the curve fit analysis are reported as binding energy in eV and percent area under each curve fitted peak. The type of functionality can then be inferred from the binding energies.

The curve fit analysis of the control and flight samples are shown in Table 4.2. The curve fit analysis of the control sample revealed carbon functionality that is consistent with the structure of Kapton® (see Fig. 3.5). However, changes in the overall percent of carbon-hydrogen, carbon-oxygen and carbon-nitrogen functionality was observed for the control compared to the flight sample. A 13% decrease in the C-H functionality (C1 peak) was observed for the flight sample. This decrease is also consistent with the decrease in the total carbon content (see Table 4.1). An increase of 44.5% was observed for the total carbon-oxygen and carbon-nitrogen functionality present on the flight sample. As shown in Table

TABLE 4.2: CARBON 1s CURVE FIT ANALYSIS OF KAPTON® CONTROL AND 10 MONTH FLIGHT SAMPLE.

CONTROL

PEAK	BINDING ENERGY(eV)	% AREA	TYPE OF BOND
C1	285.0	77.4	C-H
C2	286.5	13.5	C-O, C-N
C3	288.0	9.2	C=O

10 MONTH

PEAK	BINDING ENERGY(eV)	% AREA	TYPE OF BOND
C1	285.0	67.2	C-H
C2	286.5	18.7	C-O, C-N
C3	288.0	14.1	C=O

4.2, peak C2 with a binding energy of 286.5 eV, was assigned to carbon-oxygen and/or carbon-nitrogen functionality [60]. The increase observed in the carbon-oxygen and/or carbon-nitrogen functionality is consistent with the observed trends in the atomic composition of oxygen and nitrogen for the flight sample.

Hemminger, using carbon 1s curve-fitting [58], measured only a 5% increase in the oxygen-containing surface functionalities. However, the curve-fitting parameters and, more importantly, the assignment of the oxygen functionality were not identified.

2. Polysulfone

a. Atomic Composition

The XPS atomic concentrations measured for the control and the B9 flight polysulfone films are listed in Table 4.3. The flight sample was located on tray B, row 9 of the LDEF for 10 months. The sample was exposed for the first 10 months of the mission and at which time the experimental bay closed protecting the sample from atomic oxygen and ultraviolet radiation. The theoretical atomic composition of polysulfone, as shown in Figure 3.6, is 84.4% carbon, 14.8% oxygen and 3.7% sulfur.

The XPS analysis of the control sample revealed carbon, oxygen, sulfur in addition to nitrogen and silicon. The

TABLE 4.3: XPS ANALYSIS OF POLYSULFONE CONTROL AND 10 MONTH FLIGHT SAMPLE.

CONTROL

PHOTOPEAK	BINDING ENERGY(eV)	ATOMIC CONC(%)	X/C RATIO
C 1s	285.0	82.1	--
O 1s	532.5	14.2	0.17
N 1s	400.2	1.4	0.02
S 2p	168.7	1.3	0.02
Si 2p	102.4	1.0	0.01

10 MONTH

PHOTOPEAK	BINDING ENERGY(eV)	ATOMIC CONC(%)	X/C RATIO
C 1s	285.0	79.1	--
O 1s	532.4	18.6	0.24
N 1s	399.9	1.7	0.02
S 2p	168.4	0.4	0.00_5

carbon and oxygen contents, 82.1% and 14.2%, respectively, for the control sample are in excellent agreement with the theoretical values. The sulfur concentration is 65% lower than the theoretical value. A small amount of nitrogen was present on the control sample. The binding energy of nitrogen at 400.2 eV corresponds to an O=C-N bond [61]. The reason for the low percent of sulfur content on the control sample is unknown. A small amount of silicon was also present on the control sample. The binding energy of silicon at 102.4 eV, corresponds to organic silicon. The origin of nitrogen and silicon on the control sample is unknown.

The XPS analysis of the 10 month flight sample revealed carbon, oxygen, nitrogen and sulfur. A small 4% decrease in the carbon content and a 31% increase in oxygen content were observed for the flight sample with respect to the control. Further, a 21% increase in nitrogen and a 69% decrease in sulfur contents were observed for the flight sample. The increase in the nitrogen composition is consistent with the low levels of nitrogen contamination detected on most LDEF exposed surfaces [22-30]. The source of this nitrogen contamination is unknown. Webster and Wightman [62] reported for polysulfone films exposed to a low pressure oxygen rf plasma, a change in the sulfur 2p state from organic with a binding energy at 168 eV to inorganic sulfur with a binding energy of 170 eV. However, no change was observed here in the

sulfur state of the polysulfone film after ten months in the low-Earth orbit environment.

Although extensive silicon contamination has been detected on all LDEF materials [22-30], no silicon was detected on the polysulfone flight sample. The fact that silicon was not detected on the flight sample, which was located in the *same* tray as the Kapton® film, suggests that the mechanism of silicon contamination is complex. The results presented here indicate the mechanism of silicon contamination is not a "blanket" type in which all surfaces were covered. Rather, the results suggest the silicon contamination is "patchy" in which surfaces were randomly covered.

Changes in the surface composition of the polysulfone flight sample were observed as a result of the low-Earth orbit environment. The decrease in the carbon and sulfur contents with the subsequent increase in oxygen may be the result of erosion and/or oxidation of the polymer by atomic oxygen.

b. Curve Fit Analysis

The theoretical percents of carbon-carbon, carbon-oxygen and carbon-sulfur bonds from the repeat unit of polysulfone are 81.5%, 11.1% and 7.4% respectively. The results of the curve fit analysis of the carbon 1s region for the control and the ten month flight sample are listed in Table 4.4. As shown

TABLE 4.4: CARBON 1s CURVE FIT ANALYSIS OF POLYSULFONE CONTROL AND 10 MONTH FLIGHT SAMPLE.

CONTROL

PEAK	BINDING ENERGY(eV)	% AREA	TYPE OF BOND
C1	285.0	82.7	C-H
C2	286.6	12.6	C-O
C3	288.9	4.6	O-C=O

10 MONTH

PEAK	BINDING ENERGY(eV)	% AREA	TYPE OF BOND
C1	285.0	21.4	C-H
C2	286.7	64.0	C-O
C3	288.4	10.1	O-C=O
C4	290.2	4.4	π-π^* transition

in Table 4.4, 83% of the control carbon 1s photopeak corresponds to carbon-carbon bonds and 13% carbon-oxygen bonds. Thus, the curve fit analysis for the carbon-carbon and carbon-oxygen functionality are also in good agreement with the theoretical values. The carbon-sulfur bond was not resolved in the curve fit analysis. A 74% decrease in the carbon-carbon functionality and a 330% increase in the carbon-oxygen functionality was observed for the flight sample compared to the control. Four percent of the carbon 1s curve fit region corresponds to a π to π^* transition which is well documented for aromatic polymer systems [63]. The curve fit results support the trend of decreasing carbon content with the subsequent increase in oxygen content (see Table 4.3).

The carbon 1s curve fit results are consistent with the degradation and/or oxidation of the polysulfone flight sample. The curve fit results suggest that exposure for 10 months incorporated oxygen, in particular carbon-oxygen functionality, into the surface.

3. PIPSX-6

a. Atomic Composition

The XPS results for the control and 10-month flight PIPSX-6 samples are shown in Table 4.5. The flight sample was located on tray B, row 9 of the LDEF. PIPSX-6 is a polyimide polysiloxane copolymer synthesized at Virginia Tech [45]. The

TABLE 4.5: XPS ANALYSIS OF PIPSX-6 CONTROL AND 10 MONTH FLIGHT SAMPLE.

CONTROL

PHOTOPEAK	BINDING ENERGY(eV)	ATOMIC CONC(%)	X/C RATIO
C 1s	285.0	57.4	--
O 1s	532.8	23.3	0.41
N 1s	400.1	1.5	0.03
Si 2p	102.5	17.5	0.31

10 MONTH

PHOTOPEAK	BINDING ENERGY(eV)	ATOMIC CONC(%)	X/C RATIO
C 1s	285.0	15.5	--
O 1s	531.0	53.8	3.47
Na 1s	1073.1	2.1	0.13
Cl 2p	200.1	1.5	0.09
Si 2p	103.5	27.1	1.73
N 1s	nsp*	--	--

*nsp-no significant peak

structure of the copolymer is shown in Figure 3.7, where n is equal to 6. A 1:1 ratio is assumed for the x and y segments of the copolymer. The theoretical atomic composition of PIPSX-6 is 71% carbon, 17% oxygen, 4% nitrogen, 1% sulfur, and 6% silicon. XPS analysis of the control sample revealed 57.4% carbon, 23.3% oxygen, 1.5% nitrogen and 17.5% silicon. The atomic concentrations measured for the control sample are not consistent with the theoretical values. This discrepancy is probably the result of the preferential migration of the silicon copolymer to the surface. Enhancement of silicon on the surface is well documented for siloxane-containing polymers [45]. The silicon present on the control sample corresponds to organic silicon with a binding energy of 102.5 eV.

Significant changes in the surface composition of the flight sample were observed. XPS analysis revealed only 15.5% carbon, 53.8% oxygen, 2.1% sodium, 1.5% chlorine and 27.1% silicon. Decreasing carbon content with subsequent increases in both oxygen and silicon were observed for the flight sample. These results are shown in Figure 4.2. The O/C ratio increased 750% and the Si/C ratio increased 450% with respect to the control sample.

Small amounts of sodium and chlorine were detected on the flight sample. The fact that sodium and chlorine were not detected on the control sample suggest the contaminants were

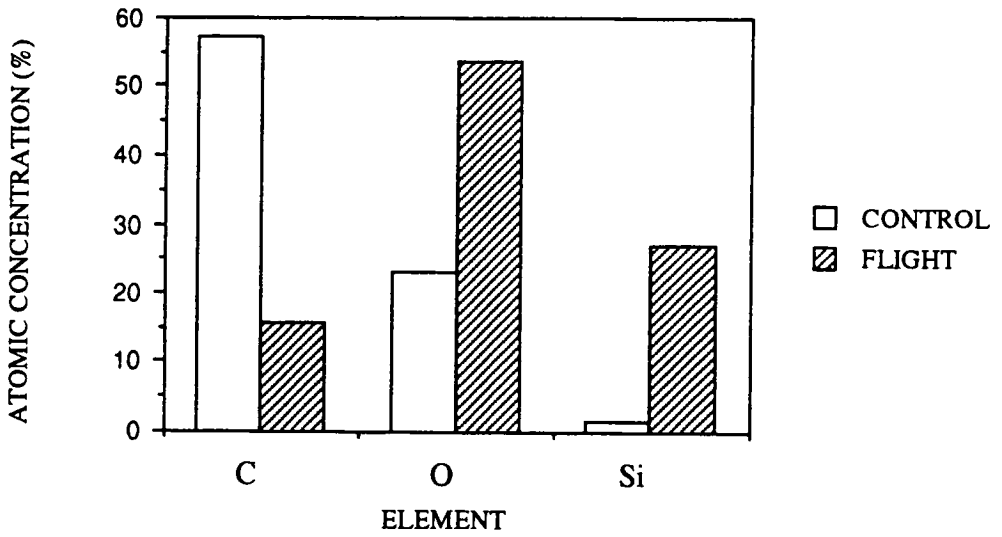

FIGURE 4.2: COMPARISON OF ATOMIC CONCENTRATIONS OF CARBON, OXYGEN, AND SILICON FOR PIPSX-6 CONTROL AND 10 MONTH FLIGHT SAMPLE.

deposited as a result of environmental exposure. The outgassing or degradation of paints flown on the LDEF has been suggested as a possible source of chlorine contamination [22-30].

The flight sample, much like the control, contains a silicon-rich surface. However, the silicon present on the flight sample corresponds to inorganic silicon whereas, the silicon present on the control was organic silicon. The conversion of the organic silicon, present on the control, to inorganic silicon present on the flight, is the direct result of exposure to atomic oxygen. Atomic oxygen has been shown to oxidize silicon materials to silicate-type materials [22-30,64]. The change in the state of silicon is supported by the subsequent shift in binding energy of the silicon and oxygen photopeaks. The shifts in the silicon 2p and oxygen 1s photopeaks noted in Table 4.5 are shown in Figure 4.3.

The increase in the silicon content with respect to the control sample may also be the result of the erosion/degradation of the polyimide segment relative to the siloxane segment of the copolymer. The erosion/degradation of the polyimide segment of the copolymer can also be supported by the absence of nitrogen on the flight sample.

The XPS results suggest that 10 months of exposure to the low-Earth orbit environment, particularly atomic oxygen, significantly changed the overall surface composition of the

C-2

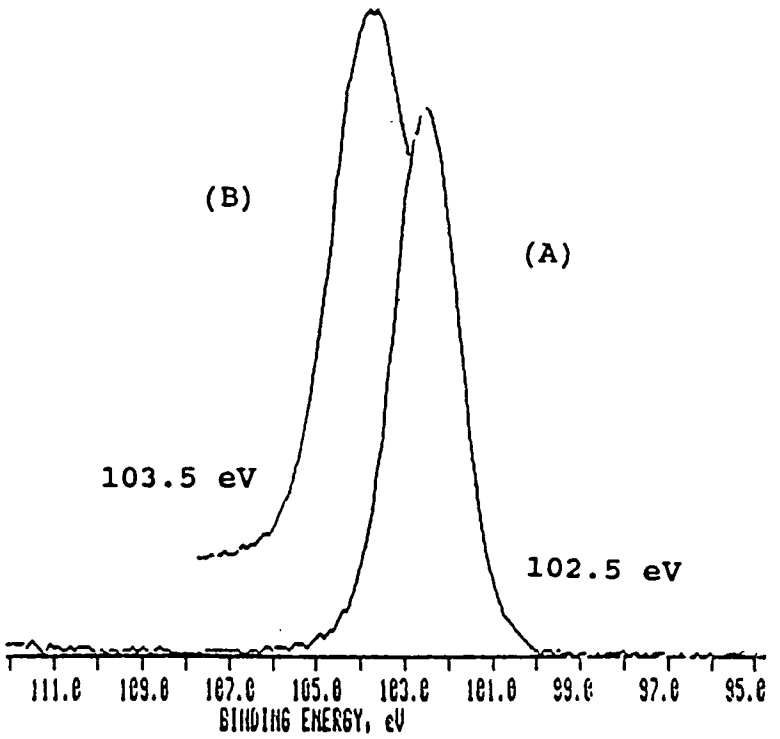

SILICON 2p

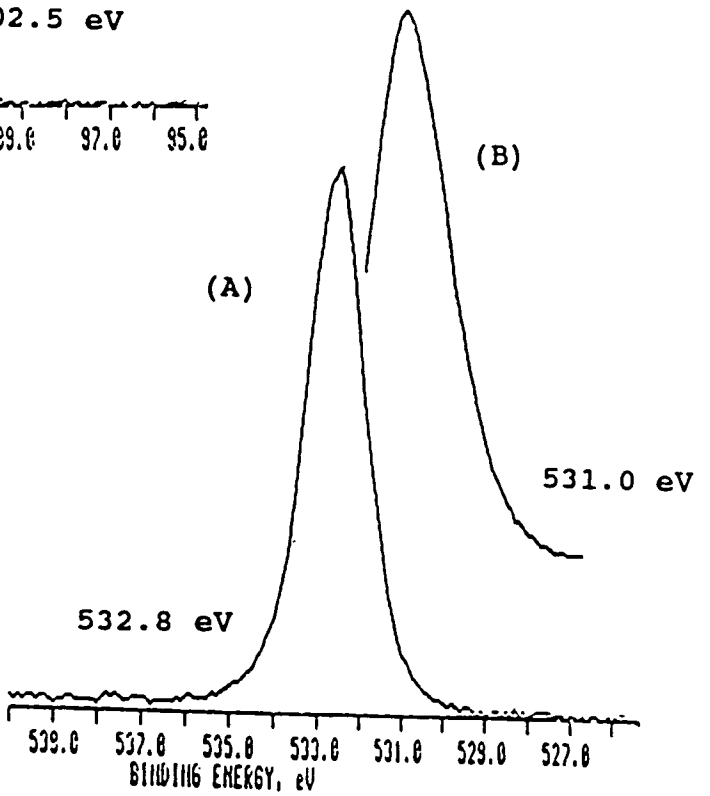

OXYGEN 1s

FIGURE 4.3: COMPARISON OF BINDING ENERGIES OF SILICON 2p AND OXYGEN 1s PHOTOPEAKS OF PIPSX-6 (A) CONTROL (B) 10 MONTH FLIGHT SAMPLE.

copolymer film. The overall surface composition of the control sample can be characterized as an organo-type of surface. By contrast, the overall surface composition of the flight sample can be characterized as an inorgano-type of surface. The enhancement of the silicon content of the flight sample can be attributed to the preferential migration of the silicon copolymer to the surface in conjunction with the erosion/degradation of the polyimide segment of the copolymer.

4. BJPIPSX-11

a. Atomic Composition

The XPS results for the control and flight sample are shown in Table 4.6. The flight sample was exposed for 10 months. BJPIPSX-11 is a polyimide-polysiloxane copolymer synthesized at Virginia Tech [45]. The XPS analysis of the control sample revealed 54.3% carbon, 23.7% oxygen, 0.4% nitrogen and 21.6% silicon. The control sample, like the PIPSX-6 sample, contains a organo-silicon rich surface.

Significant changes in the surface composition of the flight sample were observed. XPS analysis revealed 16.8% carbon, 52.4% oxygen, and 30.8% silicon. A trend of decreasing carbon content and increasing oxygen and silicon contents was observed. As noted in Table 4.6, the flight sample showed a 600% increase in the O/C ratio and a 400% increase in the Si/C ratio. The atomic ratios for the PIPSX-6

TABLE 4.6: XPS ANALYSIS OF BJPIPSX-11 CONTROL AND 10 MONTH FLIGHT SAMPLE.

CONTROL

PHOTOPEAK	BINDING ENERGY(eV)	ATOMIC CONC(%)	X/C RATIO
C 1s	285.0	54.3	--
O 1s	532.8	23.7	0.44
N 1s	400.4	0.4	0.00_7
Si 2p	102.5	21.6	0.40

10 MONTH

PHOTOPEAK	BINDING ENERGY(eV)	ATOMIC CONC(%)	X/C RATIO
C 1s	285.0	16.8	--
O 1s	533.5	52.4	3.12
Si 2p	103.6	30.8	1.83
N 1s	nsp*	--	--

*nsp-no significant peak

sample exposed for 10 months, are similar to the BJPIPSX-11 sample. The flight sample contained an inorgano-silicon rich surface. Nitrogen was not detected on the flight sample.

The XPS results for BJPIPSX-11 samples indicate the low-Earth orbit environment changed the surface chemistry of the copolymer. When comparing the XPS results of the PIPSX-6 copolymer film exposed for only 10 months, to the BJPIPSX-11 copolymer film also exposed for 10 months, the changes observed in both copolymer films are basically the same. The similarity in the surface composition of the two flight samples can be supported by the calculated atomic ratios, particularly O/C and Si/C (see Tables 4.5 and 4.6). The results of the PIPSX-6 copolymer suggest that the inorgano-silicon rich surface, present on both flight samples, formed *within* the first 10 months of exposure. The formation of a protective SiO_x layer on previous materials exposed to the space environment has been reported [35-38,65].

5. Fluorinated Ethylene Propylene

Fluorinated ethylene propylene (FEP) is a light weight thermal control material [42]. FEP samples were housed in several LDEF experimental trays [1]. Therefore, the space environmental effects on FEP can be evaluated as a function of position on the LDEF. Visible changes were observed for the FEP samples during the deintegration of the LDEF. The samples

located on the leading edge of the LDEF possessed a uniform cloudy appearance [42]. On the other hand, the samples located on the trailing edge possessed a nonuniform appearance, with alternating clear to cloudy bands. The visible differences observed in the surface appearance are believed to be the result of varying amount of atomic oxygen fluence accrued during the LDEF mission [42].

Perhaps surprising is the fact that the solar absorptance and infrared emittance measurements of the FEP flight samples were independent of location and were relatively unchanged from the control sample [42]. Scanning electron microscopy revealed two types of surface morphologies depending on the position of the samples [42]. The SEM photomicrographs of the leading edge samples revealed a surface topography with sharp peaks and valleys [42], while, the SEM photomicrographs of the leading edge samples revealed a surface topography analogous to wrinkles [42]. XPS analysis showed significant changes in both the surface composition and surface chemistry for the FEP samples [42]. These differences, much like the surface topography differences, were dependent on location [42].

Previous exposures of FEP films to the low-Earth orbit environment were made during the STS-8 mission and the retrieval of Solar Max [35]. The extent of atomic oxygen interaction with the FEP films was characterized by post-flight analysis. The results for the atomic oxygen

interaction with FEP were inconclusive with respect to the atomic oxygen erosion yield [35-38].

Extensive ground-based laboratory experiments have been conducted to evaluate the effects of atomic oxygen and ultraviolet radiation on FEP films [43,66,67]. Brinza and coworkers [66] have investigated vacuum ultraviolet (VUV) irradiation of FEP films. The VUV radiation produces a damage layer similar to that observed for the trailing edge FEP films [66]. The mechanism of degradation is believed to be an advanced photochemical mechanism [66]. Hill and coworkers [67] have characterized UV and VUV degradation of FEP films by ESR, XPS, and SEM measurements. Stiegman and coworkers [67] have shown similar results for the FEP samples via high energy oxygen atoms and VUV radiation. Stiegman concluded that FEP films located on the trailing edge of the LDEF were subject to degradation and erosion of the carbon backbone [43].

XPS results of FEP films located at four different positions on the LDEF are discussed. The four positions are F2, C5, C8, and B9. Four control samples corresponding to F2, C5, C8 and B9 were also analyzed. An average atomic composition from the four control samples will be used as a reference for the four FEP flight samples.

a. Reference Sample

(i) Atomic Composition

As shown in Table 4.7, the average atomic composition for the reference sample is 35.2% carbon and 64.8% fluorine. The F/C ratio is 1.8. No measurable quantities of oxygen were observed on the four control samples. The carbon and fluorine 1s photopeaks of the F2 control sample were arbitrarily chosen to represent the reference sample. A binding energy of 290.0 eV was chosen for the carbon 1s photopeak and used as a reference for the FEP samples. The average binding energy of the fluorine 1s photopeak was then 688.9 eV.

(ii) Curve Fit Analysis

The structure of FEP shown in Figure 3.4 illustrates three different types of carbon functionality. The three types of carbon functionality correspond to $\underline{C}$-F_3, $\underline{C}$-F_2, and $\underline{C}$-F. The carbon 1s curve fit region of the reference sample is shown in Figure 4.4. The curve fit results are shown in Table 4.8. The curve fit analysis revealed three types of functionality which coincide with the FEP structure.

b. F2 - Flight Sample

(i) Atomic Composition

The XPS atomic composition measured for the F2 flight sample is listed in Table 4.9. The sample was located near

TABLE 4.7: XPS ANALYSIS OF FEP REFERENCE SAMPLE.

PHOTOPEAK	BINDING ENERGY(eV)	ATOMIC CONC(%)
C 1s	290.9	35.2
F 1s	688.9	64.8
O 1s	nsp*	--

*nsp-no significant peak

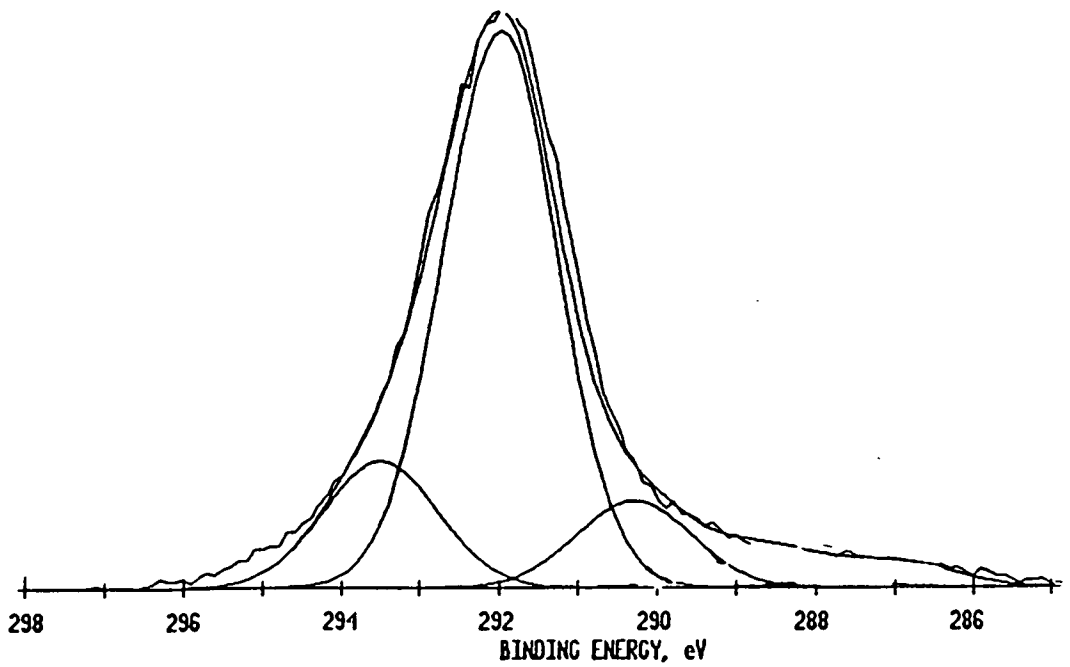

FIGURE 4.4: CARBON 1s CURVE FIT REGION OF FEP REFERENCE SAMPLE.

TABLE 4.8: CARBON 1s CURVE FIT ANALYSIS OF FEP REFERENCE SAMPLE.

PEAK	BINDING ENERGY(eV)	% AREA	BOND
C1	290.3	11.0	$\underline{C}$-F
C2	292.0	72.9	$\underline{C}$-F_2
C3	293.5	16.1	$\underline{C}$-F_3

TABLE 4.9: XPS ANALYSIS OF F2 FEP FLIGHT SAMPLE.

PHOTOPEAK	BINDING ENERGY(eV)	ATOMIC CONC(%)
C 1s	290.9	45.3
F 1s	686.8	45.4
O 1s	531.0	7.7
Si 2p	102.7	1.6

the trailing edge (Row 2) of the LDEF. XPS analysis revealed 45.3% carbon, 45.4% fluorine, 7.7% oxygen, and 1.6% silicon. The first notable difference in the atomic composition of the flight sample compared to the control sample is the appearance of oxygen and silicon on the surface. Both the silicon and oxygen contents were the direct result of exposure of FEP to the low-Earth orbit environment. Hemminger [42] reported similar increases in the oxygen and silicon contents on the surface of FEP samples located on F2 and A2 of the LDEF frame.

The carbon content increased 28.7% and the fluorine content decreased 29.9% compared to the control. The carbon and fluorine contents appeared to increase/decrease in a parallel fashion. The F/C ratio for the F2 flight sample is 1.0 contrasted to 1.8 for the reference sample. Thus, the low-Earth orbit environment significantly changed the surface composition of the polymer. The silicon contamination detected on the flight sample corresponds to the organo-form with silicon 2p binding energy of 102.7 eV.

(ii) Curve Fit Analysis

The carbon 1s curve fit region of the F2 flight sample is shown in Figure 4.5. A significant difference in the carbon 1s photopeak is apparent with respect to the control sample (see Fig. 4.4). Six types of carbon functionality were resolved under the carbon 1s envelope. The curve fit results

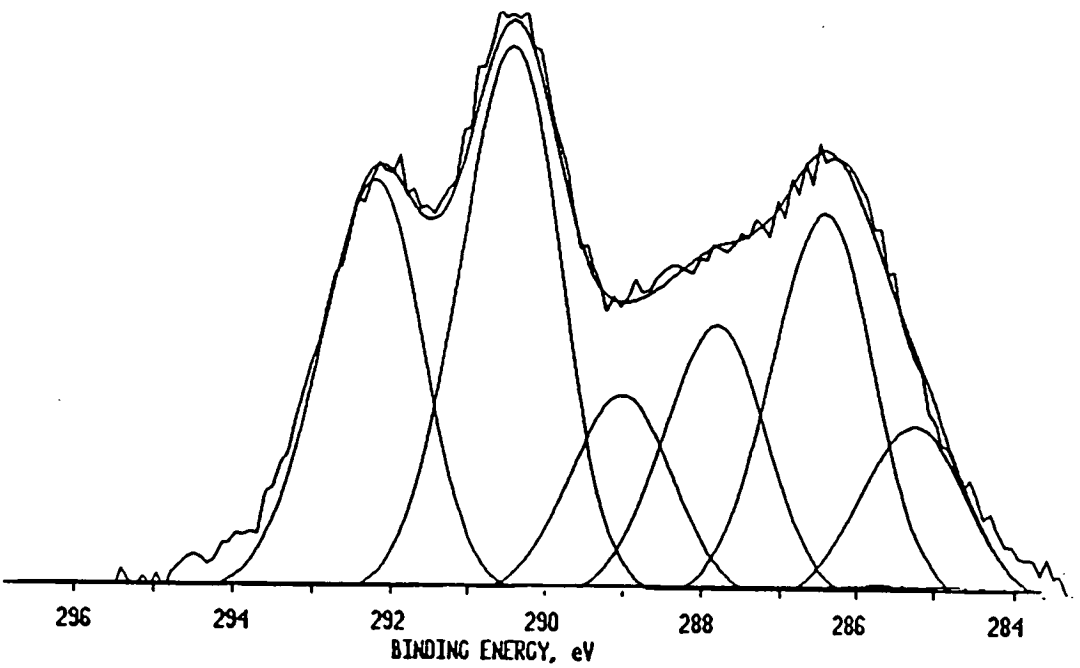

FIGURE 4.5: CARBON 1s CURVE FIT REGION OF F2 FEP FLIGHT SAMPLE.

are shown in Table 4.10. The curve fit carbon 1s photopeak clearly illustrates the low-Earth orbit environment not only significantly changed the surface composition but also the surface chemistry of the FEP polymer system. As shown in Table 4.10, the low-Earth orbit environment modified the type of carbon functionality present on the surface with the addition of 7.2% hydrocarbon functionality, and 43.4% of carbon-oxygen functionality (photopeaks C2-C4).

Photopeak C6 with a binding energy of 293.5 eV corresponds to $C-F_3$ functionality. A 32.2% increase was observed for the $C-F_3$ functionality when compared to the control. Photopeak C5 with a binding energy of approximately 291.3 eV, suggests the peak corresponds to some type of carbon-fluorine functionality [68]. The C5 photopeak was not determined. However, the photopeak may correspond to a carbon-fluorine bond that has undergone double bond rearrangement, chain scission, and cross linking as a result of the low-Earth orbit environment [66,67]. The curve fit analysis also revealed the loss of the C-F functionality, that is, the disappearance of photopeak C1 at 290.8 eV noted for the control.

Brinza and coworkers [66] concluded that photolysis generated by VUV produces an FEP surface that shows a loss of C-F groups. The near trailing edge of the LDEF received a low amount of atomic oxygen fluence and was predominantly

TABLE 4.10: CARBON 1s CURVE FIT ANALYSIS OF F2 FEP FLIGHT SAMPLE.

PEAK	BINDING ENERGY(eV)	% AREA	BOND
C1	285.0	7.2	C-H
C2	286.4	17.6	C-O
C3	287.8	13.5	C=O
C4	289.3	12.3	O-C=O
C5	291.3	28.1	
C6	293.5	21.3	$C-F_3$

subjected to ultraviolet radiation [12-15]. Whereas, the near leading edge of the LDEF was subjected to both atomic oxygen and ultraviolet radiation [12-15]. The resulting surface of the FEP samples may have undergone degradation while in the low-Earth orbit environment.

c. C5 - Flight Sample

(i) Atomic Composition

Three C5 flight samples were analyzed in this study. The position of the C5 flight samples can be considered as half-way between the trailing and leading edge on the LDEF frame. An average atomic composition from the three samples will be used to represent the C5 flight sample. The calculated average atomic composition for the C5 flight sample is shown in Table 4.11. XPS analysis revealed 44.3% carbon, 52.8% fluorine and 2.9% oxygen. Hemminger [42] reported 3% to 5% oxygen and 0.1% silicon on the surface of B5, C5 and D5 flight samples. No detectable quantities of silicon were detected on the three flight samples. The fact that silicon was not detected on the three C5 flight samples reinforces the suggestion (see p.77) that silicon contamination was not a "blanket" mechanism in which all surfaces where contaminated uniformly with silicon.

The carbon content increased 25.8% for the flight sample, whereas, the fluorine content decreased 18.5% compared to the

TABLE 4.11: XPS ANALYSIS OF C5 FEP FLIGHT SAMPLE.

PHOTOPEAK	BINDING ENERGY(eV)	ATOMIC CONC(%)
C 1s	290.7	44.3
F 1s	686.9	52.8
O 1s	531.9	2.9

control. The F/C ratio for the flight sample is 1.2.

The C5 flight sample parallels the F2 flight sample with respect to the observed increase in carbon content and decrease in the fluorine content. The increase observed in the carbon content for F2 and C5 samples was similar. However, a larger decrease in fluorine content was observed for the F2 flight sample. The XPS atomic composition of the C5 flight sample suggests that the surface composition of the polymer system was changed as a result of the low-Earth orbit environment. The components of the low-Earth orbit environment, as discussed in Chapter I, include temperature, pressure, atomic oxygen, and ultraviolet radiation. Further, the observed differences in the atomic composition of the F2 and C5 flight samples suggest the changes induced by the low-Earth orbit environment were position dependent.

(ii) Curve Fit Analysis

The carbon 1s photopeak for the C5 flight sample is shown in Figure 4.6. A significant difference in the carbon 1s photopeak was observed compared to the control. Much like the F2 carbon 1s photopeak (see Fig. 4.5), the C5 photopeaks contain six types of carbon functionality under the carbon 1s envelope.

At first glance the F2 and C5 carbon 1s photopeaks would appear identical. As shown in Table 4.12, the C5 flight

TABLE 4.12: CARBON 1s CURVE FIT ANALYSIS OF C5 FEP FLIGHT SAMPLE.

PEAK	BINDING ENERGY(eV)	% AREA	BOND
C1	285.0	8.7	C-H
C2	286.3	19.3	C-O
C3	287.2	13.7	C=O
C4	289.2	10.1	O-C=O
C5	290.8	27.5	C-F
C6	292.8	20.7	

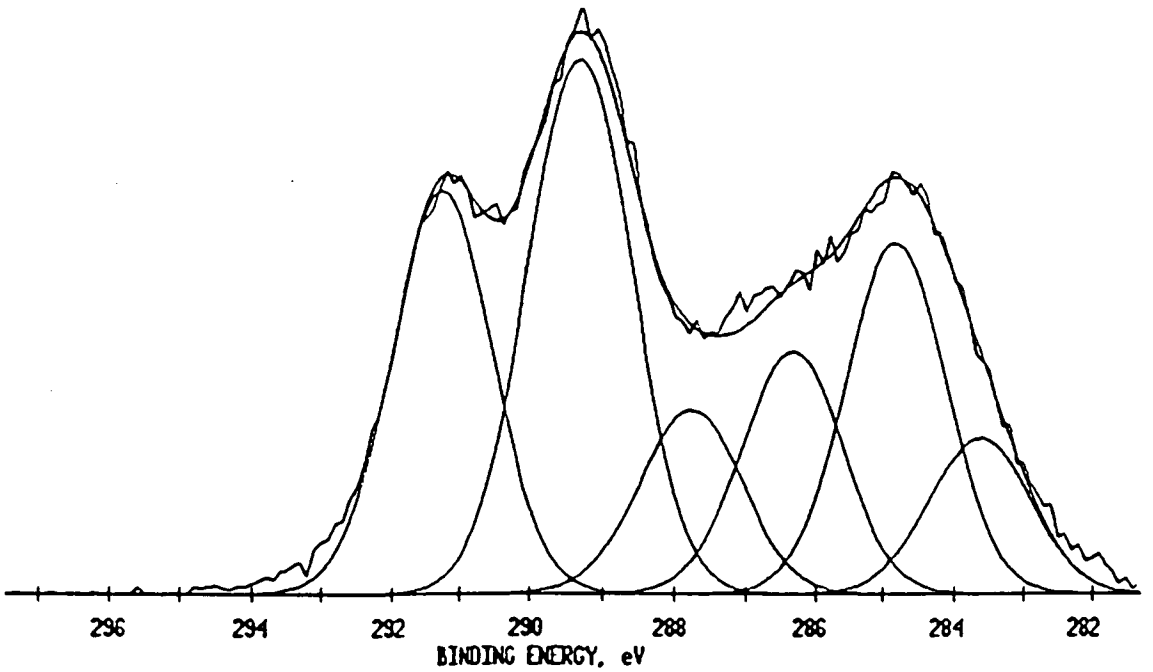

FIGURE 4.6: CARBON 1s CURVE FIT REGION OF C5 FEP FLIGHT SAMPLE.

sample contains both hydrocarbon and carbon-oxygen functionality like the F2 flight sample. However, the type of carbon-fluorine functionality is different. Photopeak C5 corresponds to C-F functionality which was not resolved in the F2 curve fit analysis. Photopeak C6, with a binding energy of 292.8 eV, was resolved in the curve fit analysis but the functionality of this photopeak was not determined. The photopeak may be the result of a radical or crosslinked species [66,67].

The different type of carbon-fluorine functionality observed for the F2 and C5 flight samples suggest the changes in the surface chemistry induced by the low-Earth orbit environment were by different degradation/erosion mechanisms. The different mechanisms may be the result of the varying amounts of atomic oxygen and ultraviolet radiation for Rows 2 and 5 [12-15]. The resolved C-F functionality potentially rules out photolysis degradation for the C5 FEP sample, while photolysis can be supported for the F2 flight sample as a result of the loss of the C-F functionality [66,67].

d. C8 - Flight Sample

(i) Atomic Composition

Three C8 flight samples were analyzed in this study. The position of the C8 flight sample is one row away from the

leading edge of the LDEF. An average atomic composition determined for the three samples will be used to represent the C8 flight sample. The XPS results are shown in Table 4.13. XPS analysis revealed 36.7% carbon and 63.3% fluorine. No measurable quantities of oxygen or silicon were detected on the three flight samples. Hemminger [42] reported <0.1 % oxygen on the surface of FEP samples located at C8. Hemminger [42] also reported 0.6% silicon on the C8 FEP samples. The absence of silicon contamination on the three C8 FEP sample analyzed in this study, in conjunction with Hemminger's findings, further supports the "patches" mechanism of silicon contamination.

The XPS results for the F2 and C5 flight samples clearly demonstrate that the low-Earth orbit environment altered the surface composition and surface chemistry of the FEP films. It could have been predicted that the FEP films located near the leading edge of the LDEF, which received a higher atomic oxygen fluence than F2 or C5, would have shown a greater degree of degradation/erosion. However, the atomic compositions measured for the three C8 flight samples were virtually identical to the reference sample. Minor changes were observed in both the carbon and fluorine contents of the C8 samples. Only a 4.3% increase in the carbon content was observed while a 2.3% decrease was observed for the fluorine content. The F/C ratio for the C8 FEP flight sample is 1.8

TABLE 4.13: XPS ANALYSIS OF C8 FEP FLIGHT SAMPLE.

PHOTOPEAK	BINDING ENERGY(eV)	ATOMIC CONC(%)
C 1s	290.9	36.7
F 1s	688.8	63.3

compared to the control. Thus, the overall surface composition of the C8 flight sample suggest the fluorocarbon polymer was physically and chemically inert to the well documented effects of atomic oxygen and ultraviolet radiation on materials in the low-Earth orbit environment. The XPS results also suggest the FEP polymer was inert to the synergistic effects that are present only in the low-Earth orbit environment.

(ii) Curve Fit Analysis

The C8 carbon 1s curve-fit peaks are shown in Figure 4.7. The photopeak reveals the three types of carbon functionality that are consistent with the reference FEP sample. As shown in Table 4.14, the percent contribution for the three types of carbon-fluorine functionality compare quite closely to the reference sample (see Table 4.8). The carbon 1s curve fit region clearly illustrates that the surface chemistry of the FEP samples located on Row 8 of the LDEF was not changed by the low-Earth orbit environment (atomic oxygen and ultraviolet radiation). The XPS results also reinforce the position dependence of the FEP flight samples with respect to the resistance/nonresistance of the samples to the low-Earth orbit environment.

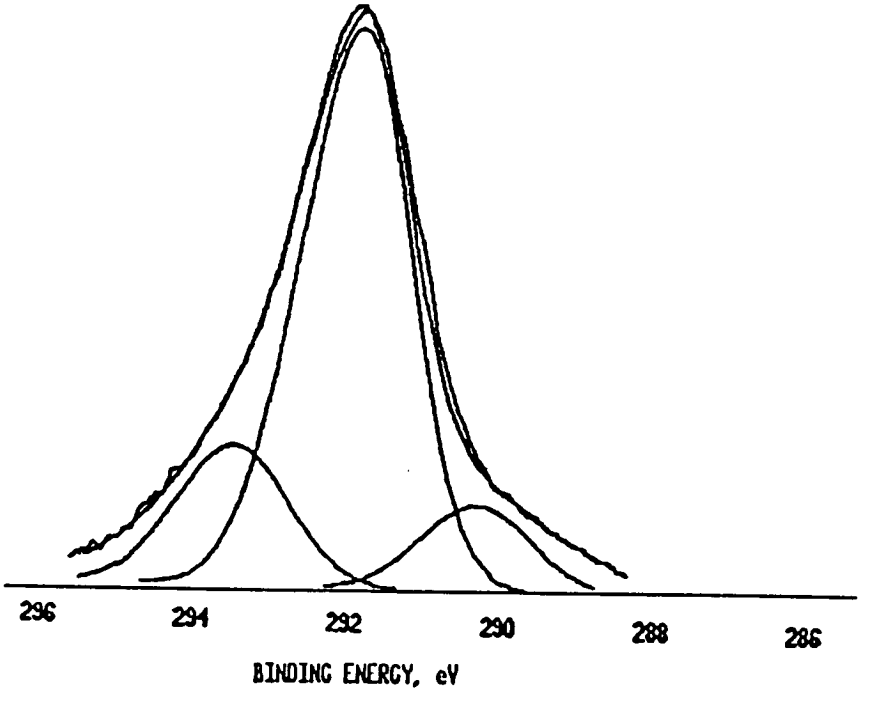

FIGURE 4.7: CARBON 1s CURVE FIT ANALYSIS OF C8 FEP FLIGHT SAMPLE.

TABLE 4.14: CARBON 1s CURVE FIT ANALYSIS OF C8 FEP FLIGHT SAMPLE.

PEAK	BINDING ENERGY(eV)	% AREA	BOND
C1	290.3	17.9	C-F
C2	292.0	71.1	$C-F_2$
C3	293.5	11.0	$C-F_3$

e. B9 - Flight Sample

(i) Atomic Composition

Three B9 flight samples were analyzed in this study. These FEP samples were located on the leading edge of the LDEF frame. An average atomic composition of the three samples will be used to represent the B9 flight sample.

The XPS results for B9 are shown in Table 4.15. The average atomic composition determined for B9 is 41% carbon, 58.8% fluorine and 0.2% oxygen. Hemminger [42] reported 0.1% - 0.8% oxygen on the surface of FEP samples located at D9 and F9. No measurable quantities of silicon were detected on the flight samples, whereas, Hemminger detected 0.8% silicon on the D9 and F9 FEP samples [42].

A 16.5% increase in the carbon content was observed with a 9.2% decrease in the fluorine content compared to the control. The atomic composition of the B9 flight sample then is in fair agreement with both the reference and C8 flight sample. The differences observed in the atomic composition, particularly the 0.2% oxygen content, may be the result of the higher atomic oxygen fluence associated with the leading edge of the LDEF.

The F/C ratio for the B9 flight sample is 1.4. This F/C ratio is 22.2% lower than that determined for the reference sample. The overall surface chemistry of the B9 flight sample is surprisingly similar to the reference sample. The

TABLE 4.15: XPS ANALYSIS OF B9 FEP FLIGHT SAMPLE.

PHOTOPEAK	BINDING ENERGY(eV)	ATOMIC CONC(%)
C 1s	290.9	41.0
F 1s	688.4	58.8
O 1s	532.5	0.2

significant changes in the surface composition that were observed for the near trailing edge FEP samples, F2 and C5, were not observed for the B9 flight sample. The XPS results suggest that the surface chemistry of the FEP located on the leading edge of the LDEF was not influenced by exposure to the low-Earth orbit environment.

(ii) Curve Fit Analysis

The curve fit carbon 1s photopeak of the B9 flight sample is shown in Figure 4.8. The curve fit analysis revealed four types of carbon functionality. As shown in Table 4.16, the four peaks correspond to the three types of carbon-fluorine functionality as well as one type of carbon-oxygen functionality. The curve fit analysis revealed a small decrease in the $C-F_3$ and $C-F_2$ functionality with a small increase in the C-F functionality. However, the overall curve fit analysis is in fair agreement with the reference sample (see Table 4.8). The carbon oxygen functionality corresponds to O-C=O [70].

The curve fit analysis revealed the surface chemistry of the FEP film located on the leading edge of the LDEF was essentially the same as the reference sample. The addition of carbon-oxygen functionality may have resulted from the higher atomic oxygen fluence for the leading edge of the LDEF.

The atomic compositions for the four samples are shown in

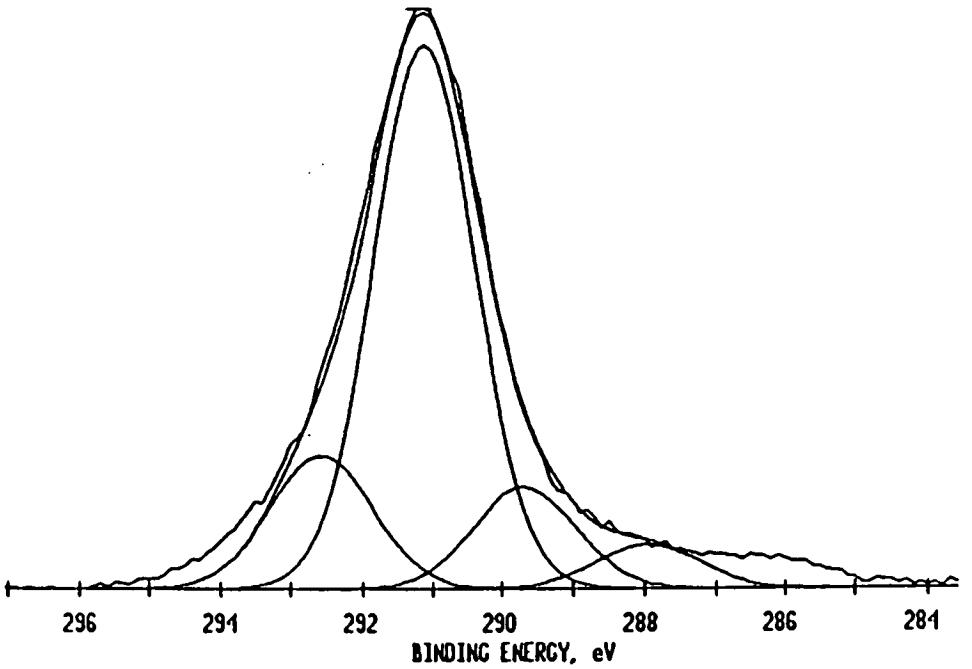

FIGURE 4.8: CARBON 1s CURVE FIT REGION OF B9 FEP FLIGHT SAMPLE.

TABLE 4.16: CARBON 1s CURVE FIT REGION OF B9 FEP FLIGHT SAMPLE.

PEAK	BINDING ENERGY(eV)	% AREA	BOND
C1	288.0	5.7	O-C=O
C2	290.3	11.5	C-F
C3	291.8	63.0	$C-F_2$
C4	293.4	12.4	$C-F_3$

Figure 4.9. These XPS results for the FEP samples located at four different locations clearly demonstrate the position dependence of the FEP films. The carbon 1s curve fit regions of the FEP reference sample, F2, C5, C8 and B9 flight samples are shown in Figure 4.10. Figures 4.9 and 4.10 together illustrate the significant differences observed in both the surface composition and surface chemistry as a result of sample position on the LDEF. The XPS results for the near leading edge and leading edge samples (C8 and B9) compared to the near trailing and trailing edge samples suggest the different low-Earth orbit environments, particularly the amount of atomic oxygen and ultraviolet radiation, generated two different FEP surfaces.

f. Oxygen Plasma Treatment of FEP Samples

The XPS analysis of the C5 and C8 FEP flight samples clearly revealed two different types of polymer surfaces. Several LDEF investigators have attributed the observed difference in the carbon 1s curve fitted region to the varying amounts of atomic oxygen and ultraviolet radiation accrued during the LDEF mission [66,67]. The observed differences for the C5 and C8 flight samples have generated numerous laboratory experiments designed to simulate the type of surface effects induced by the low-Earth orbit environment [66,67].

(A)

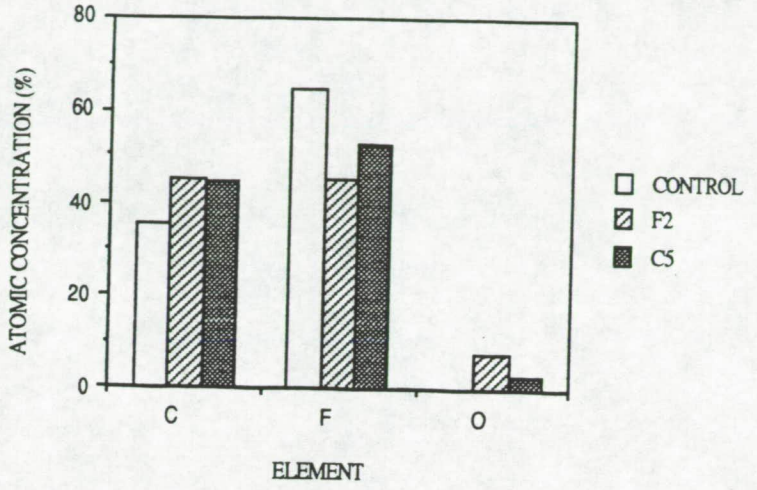

(B)

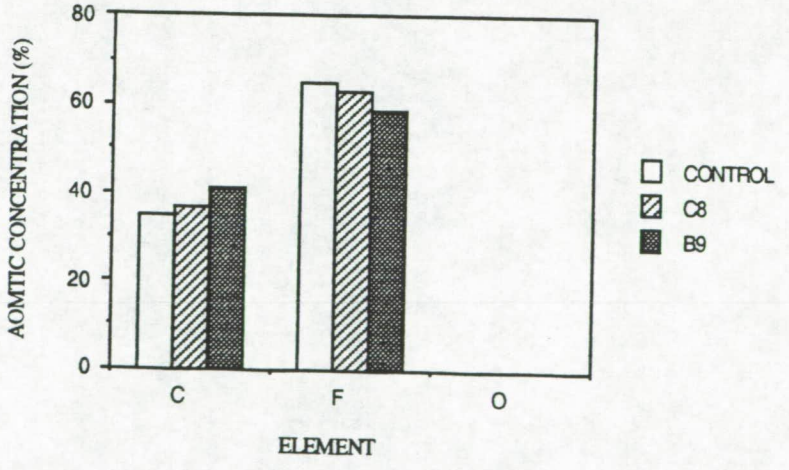

FIGURE 4.9: COMPARISON OF ATOMIC CONCENTRATIONS OF FEP SAMPLES (A) CONTROL, F2, AND C5 (B) CONTROL, C8, AND B9.

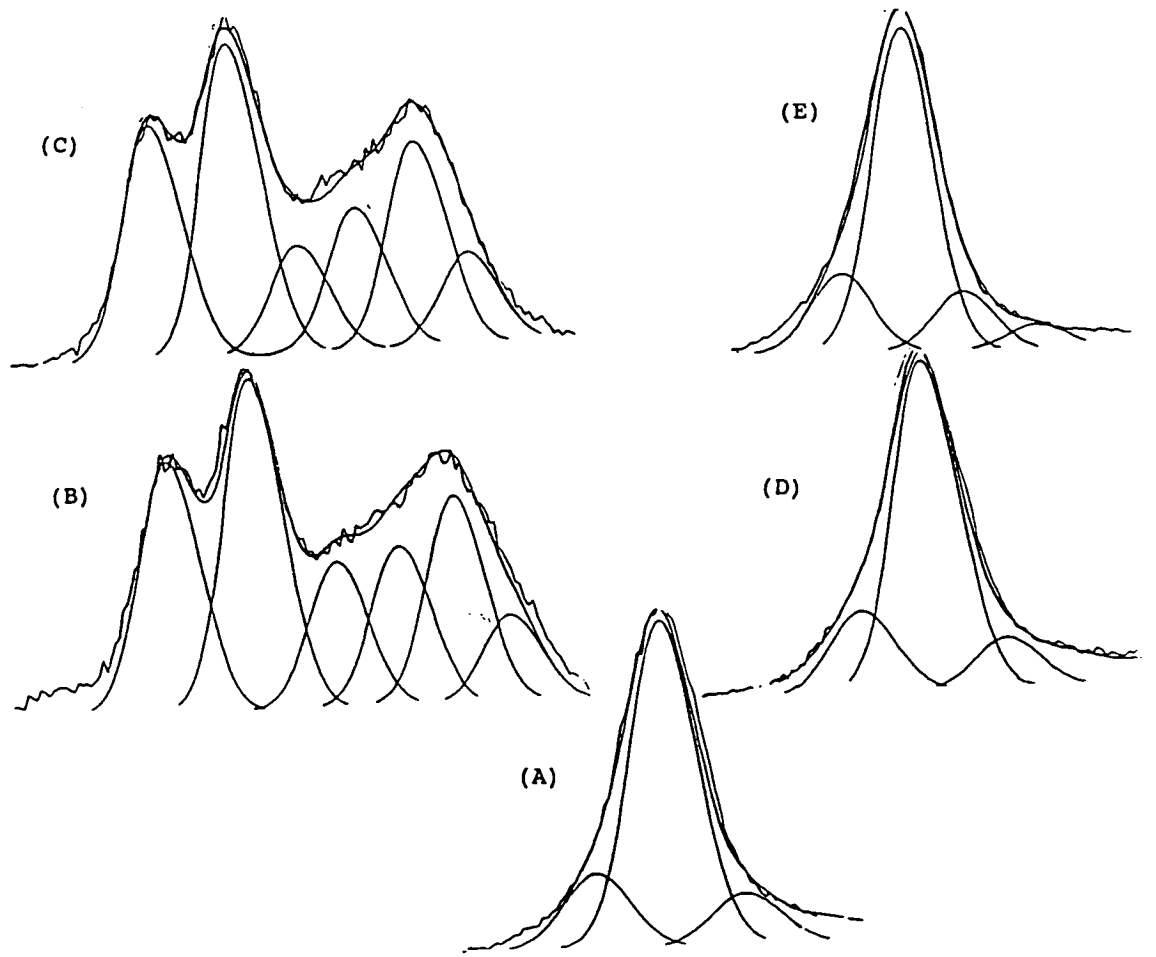

FIGURE 4.10: COMPARISON OF CARBON 1s CURVE FIT REGION OF FEP SAMPLES. (A) CONTROL (B) F2 (C) C5 (D) C8 (E) B9

An in-house experiment was conducted using a low pressure oxygen rf plasma to determine if the changes observed in the carbon 1s region were the result of the low-Earth orbit environment or the result of deposited contamination. A plasma is a spatially neutral ionized gas containing ions, free radicals and extremely energetic vacuum ultraviolet light [71]. Ions create free radicals on the surface which react with the plasma gas to form new chemical species on the surface or react with themselves and crosslink the surface [71]. Researchers have shown that the changes induced via plasma varies for the type of polymer systems. For example, ablation primarily occurs for polymer systems containing hetero-atoms such as oxygen in the backbone, which thus facilitates active sites for chain scission [73]. Fluorocarbon polymers by contrast are typically inert to the plasma treatment with little or no ablation or chain scission occurring. Plasma treatment of polymers, particularly fluoropolymers, where the polymer surface is thought of as inert to the ablation effects, has been shown to be very useful in the removal of low molecular weight organic/inorganic contamination [71,72,73].

Several FEP samples were plasma treated to evaluate changes in both the surface composition as well as surface chemistry. If the differences observed for the carbon 1s region were induced by atomic oxygen and ultraviolet

radiation, the plasma treatment might not change the curve fit region. Whereas, if the differences observed were the result of deposited contamination the plasma treatment may "clean" the surface to expose a contamination-free FEP surface. XPS was the surface tool used to characterize changes observed in the surface composition and surface chemistry of several FEP samples after plasma treatment.

The plasma treated FEP samples consisted of a control and two FEP flight samples. C5 and C8 were the two flight samples chosen as they represented the two extremes observed with respect to the flight samples and the control. The plasma treatment times for the control and two flight samples were 5 and 10 minutes.

(i) Control Sample

The XPS results for the control sample prior to and after plasma treatment are shown in Figure 4.11 The atomic concentrations of the plasma treated sample compared closely to the control. Plasma treatment then did not change the surface composition of the FEP control sample. Figure 4.12 illustrates the carbon 1s curve fit spectra for the control and plasma treated samples. The curve-fit carbon 1s region for the three samples is identical. Figure 4.12 clearly illustrates that the oxygen plasma did not change the surface chemistry of the FEP control sample. The XPS results,

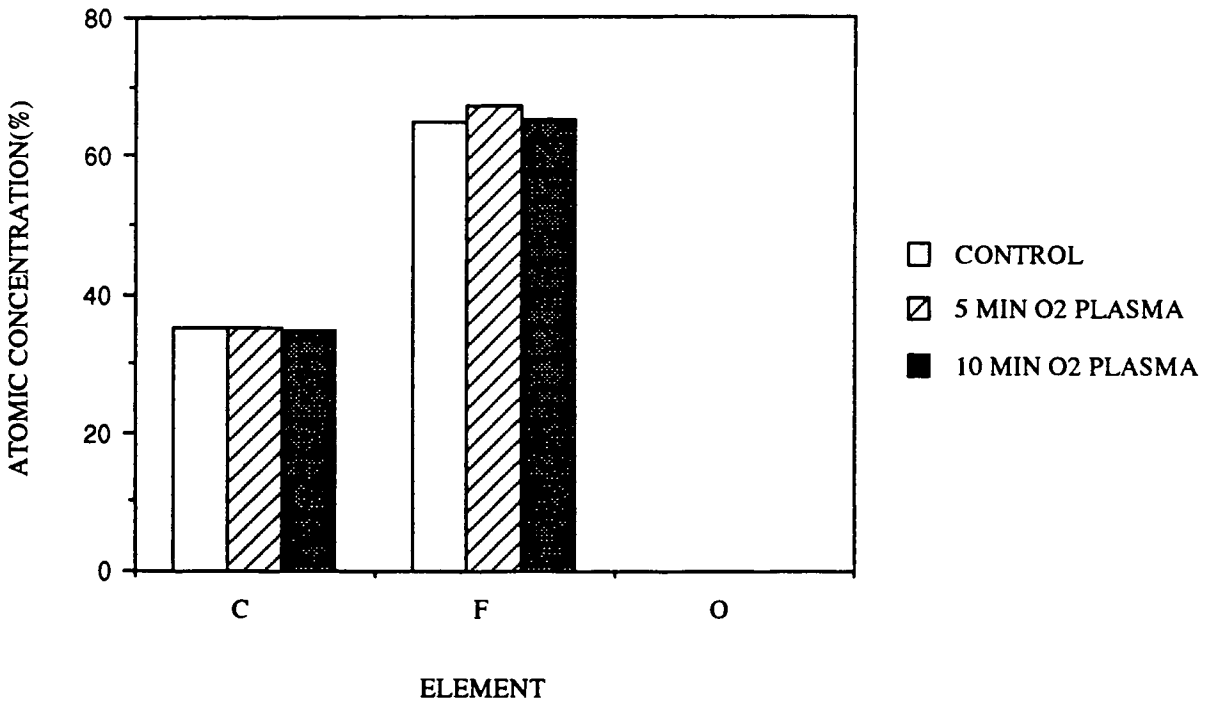

FIGURE 4.11: COMPARISON OF ATOMIC CONCENTRATIONS OF PLASMA TREATED FEP CONTROL SAMPLE.

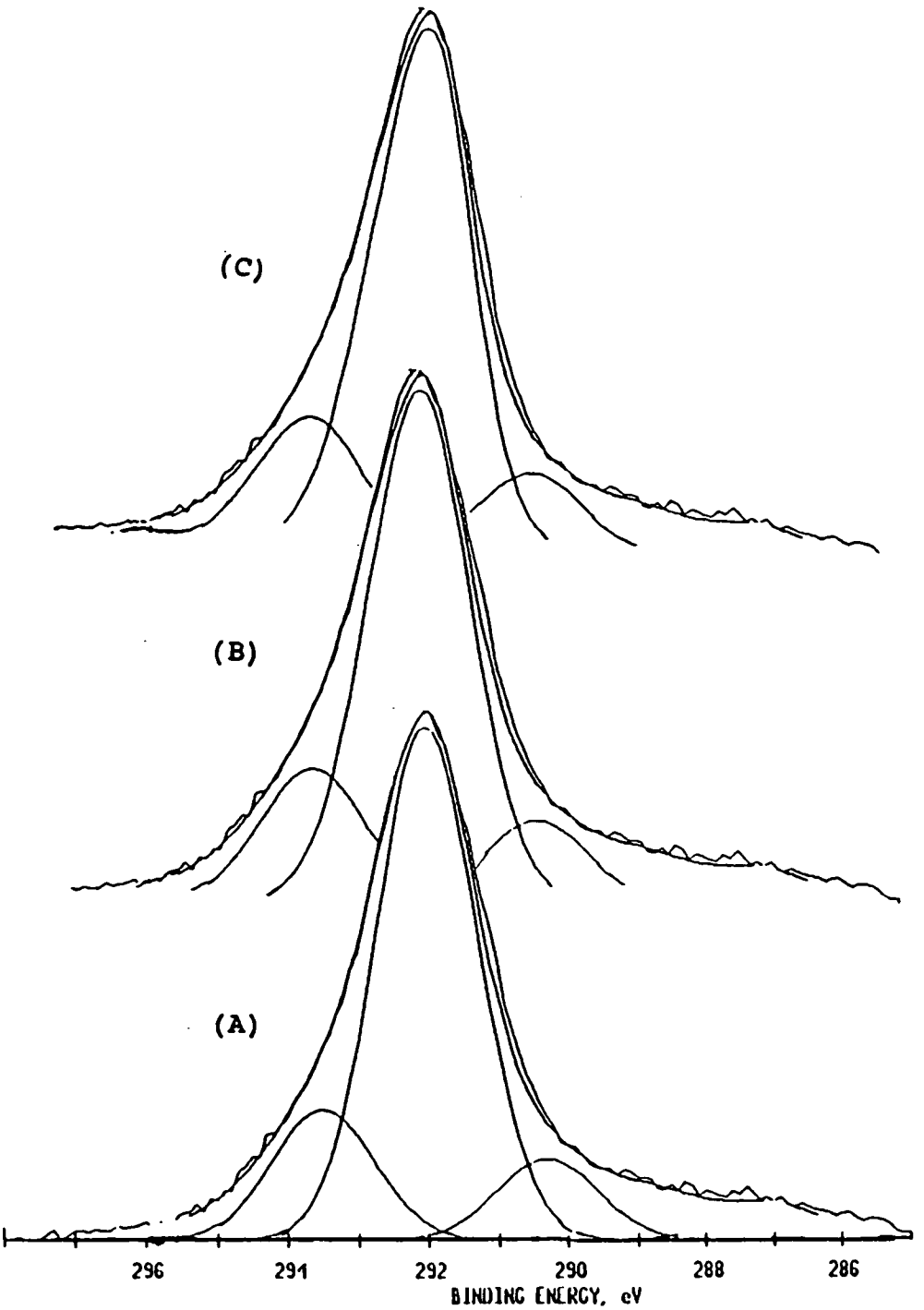

FIGURE 4.12: COMPARISON OF CARBON 1s CURVE FIT REGION OF PLASMA TREATED FEP CONTROL SAMPLE. (A) CONTROL (B) 5 MINUTES OXYGEN PLASMA (C) 10 MINUTES OXYGEN PLASMA

particularly the curve fit analysis of the plasma treated control FEP sample, established that the oxygen plasma did not induce surface changes such as ablation or chain scission.

(ii) C8 - Flight Sample

The XPS results of the plasma treated C8 FEP flight sample are shown in Figure 4.13. The atomic composition of the plasma treated flight sample compares quite closely to the C8 flight sample prior to plasma treatment. The XPS results support the arguments that the oxygen plasma did not change the surface composition of the C8 FEP flight sample. The carbon 1s curve fit regions for the C8 flight sample prior to and after plasma treatment times are shown in Figure 4.14. The curve fits for the three samples are virtually identical indicating that the plasma treatments did not change the surface chemistry of the C8 FEP flight sample as was observed for the control sample.

(iii) C5 Flight Sample

The XPS results of the plasma treated C5 FEP flight sample are shown in Figure 4.15. Significant changes in the surface composition of the C5 sample were observed following plasma treatment. A decrease in the carbon and oxygen contents with a subsequent increase in the fluorine content was observed. The change in the atomic composition of the

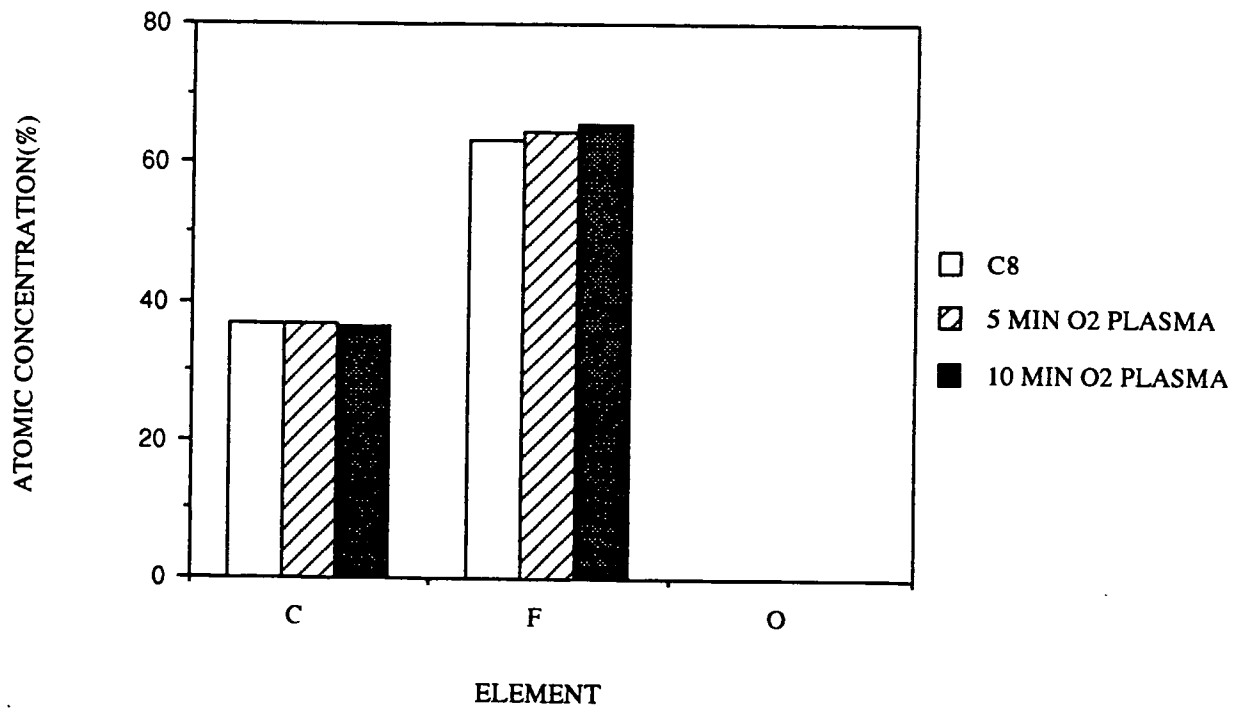

FIGURE 4.13: COMPARISON OF ATOMIC CONCENTRATIONS OF PLASMA TREATED C8 FEP FLIGHT SAMPLE.

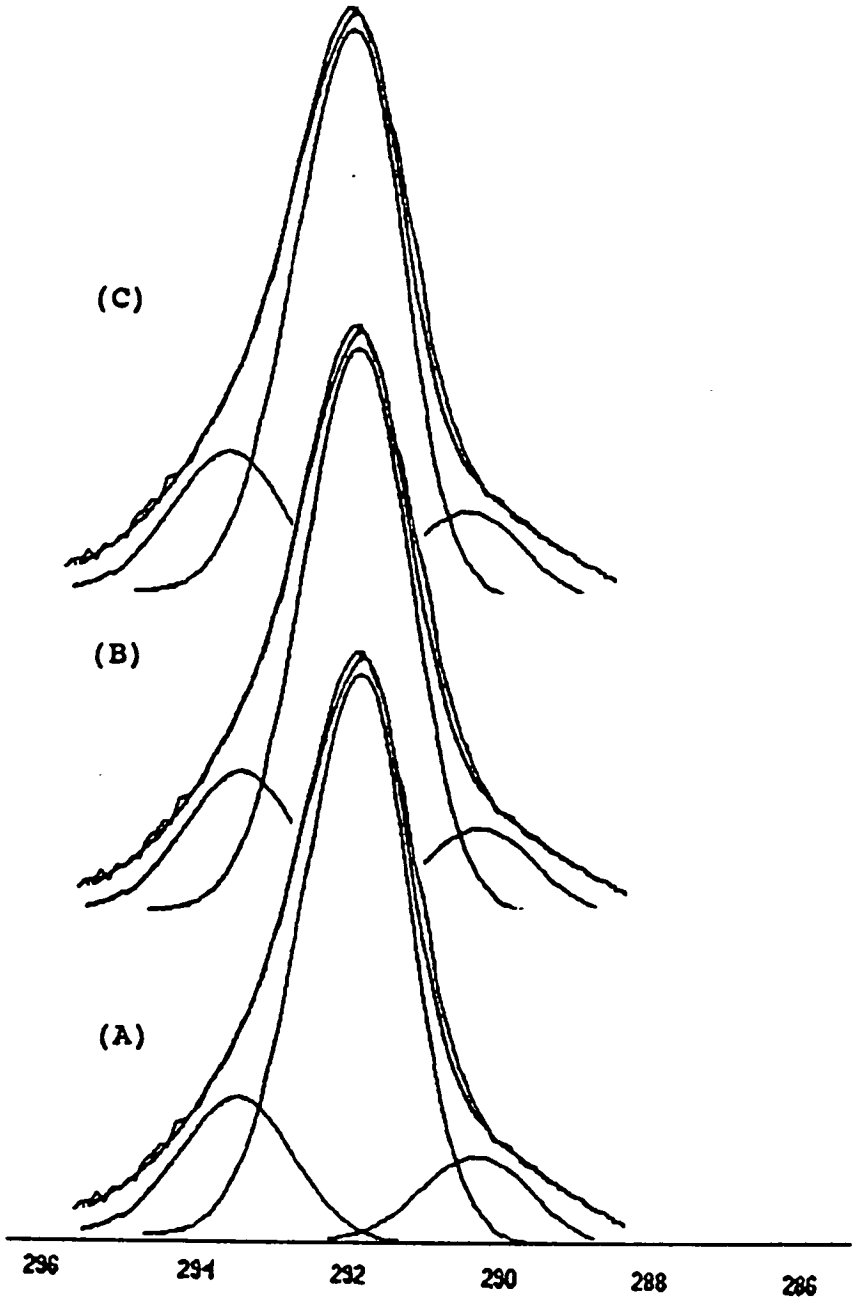

FIGURE 4.14: COMPARISON OF CARBON 1s CURVE FIT REGION OF OXYGEN PLASMA TREATED C8 FEP FLIGHT SAMPLE. (A) C8 FLIGHT SAMPLE (B) 5 MINUTES OXYGEN PLASMA (C) 10 MINUTES OXYGEN PLASMA

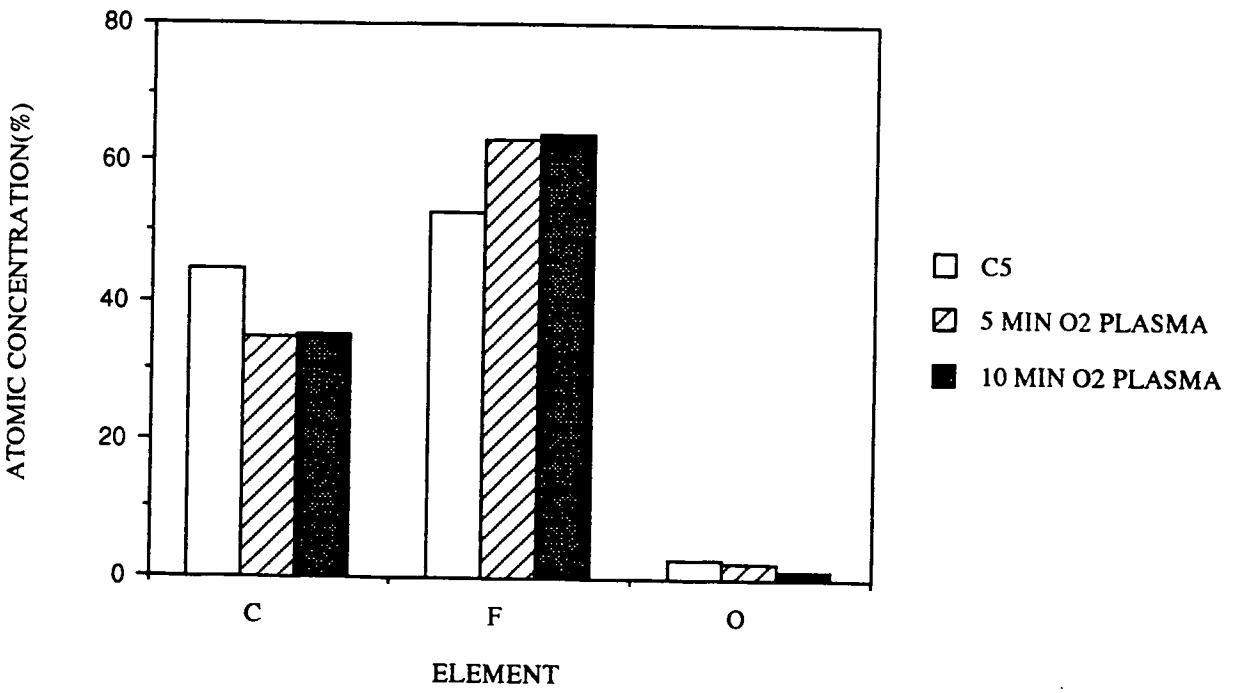

FIGURE 4.15: COMPARISON OF ATOMIC CONCENTRATIONS OF PLASMA TREATED C5 FEP FLIGHT SAMPLE.

flight sample suggest the C5 FEP flight sample was "cleaned" by the oxygen plasma environment. The atomic composition of the 10 minute plasma treated sample compares closely to the control sample.

The carbon 1s curve fit regions of the C5 flight sample prior to and after plasma treatment are shown in Figure 4.16. A significant change in the overall shape of the carbon 1s region was observed after plasma treatment. Figure 4.16 clearly shows the removal of the hydrocarbon and carbon-oxygen functionality as a result of plasma treatment. The overall functionality of the carbon 1s region after 5 minutes of plasma treatment showed a large decrease in the contribution of photopeaks C2, C3, C4 and C6. No hydrocarbon functionality was present after 5 minutes of plasma treatment. The XPS results suggest the five minute oxygen plasma treatment started to remove the contamination present on the surface of the C5 FEP flight sample as evident by the curve fit analysis.

The carbon 1s curve fit region after a plasma treatment time of 10 minutes, revealed a surface analogous to the control and C8 FEP samples. The curve fit results clearly show that the 10 minute oxygen plasma treatment removed photopeaks C1, C2 and C3, associated with the C5 FEP flight sample. The removal of photopeaks C1, C2 and C3, with the subsequent regeneration of an FEP surface clearly establishes that the photopeaks C1, C2 and C3 were weakly attached layers

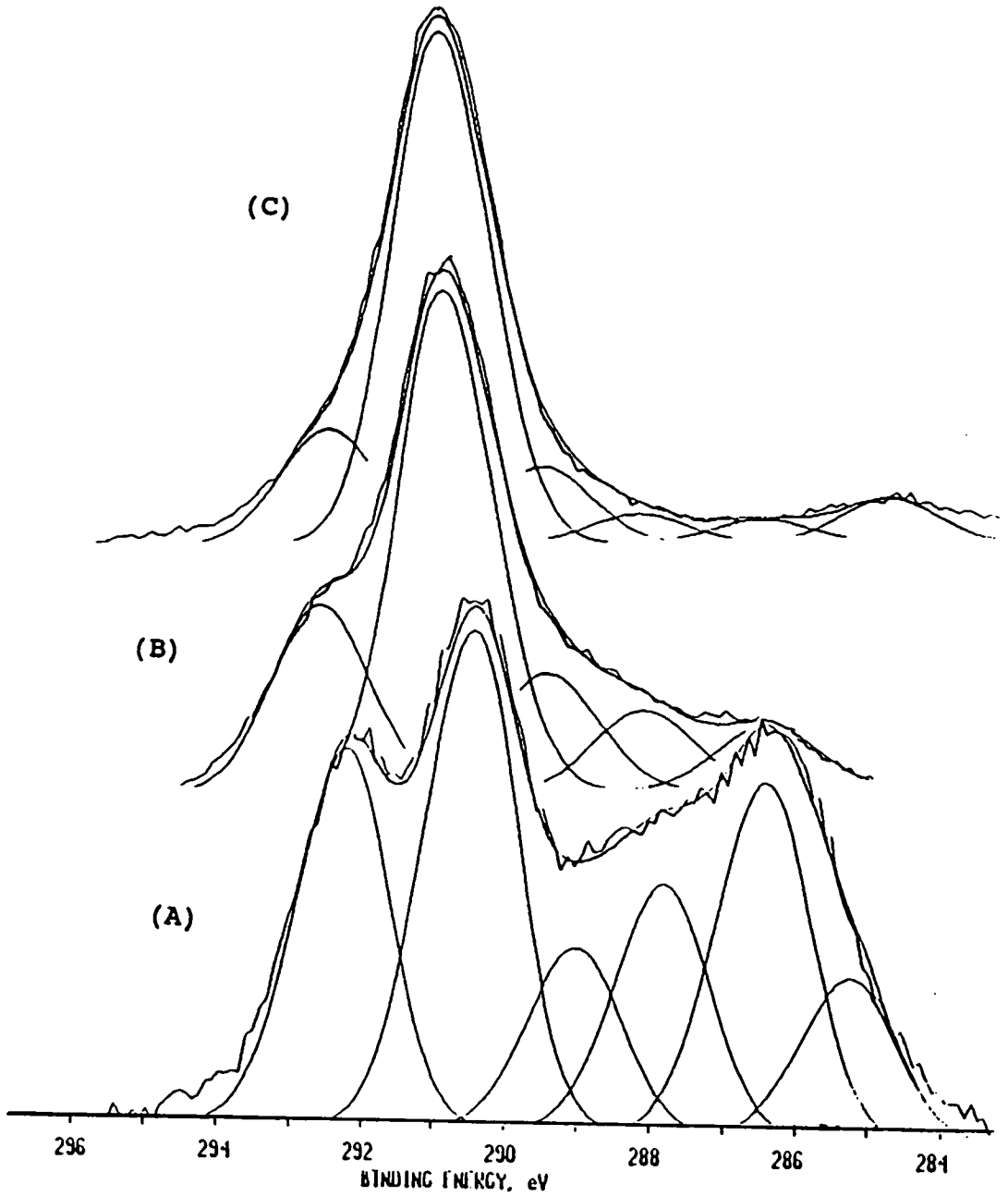

FIGURE 4.16: COMPARISON OF CARBON 1s CURVE FIT REGION OF OXYGEN PLASMA TREATED C5 FEP FLIGHT SAMPLE. (A) C5 FLIGHT (B) 5 MINUTES OXYGEN PLASMA (C) 10 MINUTES OXYGEN PLASMA.

of both organic and inorganic contamination. The XPS results show the oxygen plasma "cleaned" the surface and thus exposing a contamination free FEP surface.

The fact that the control and C8 FEP flight samples were chemically stable to the plasma environment, while the C5 FEP flight sample was not, supports the suggestion that the C5 FEP flight sample contained a weakly attached layer of deposited contamination. The fact that after 10 minutes of plasma treatment a chemically equivalent FEP surface was generated strongly supports that photopeaks, C1, C2 and C3 were the result of deposited contamination.

XPS analysis was performed on the C5 FEP flight sample approximately 69 days after the plasma experiment. The carbon 1s photopeak for the C5 flight sample prior to and 69 days after the plasma experiment are shown in Figure 4.17. The carbon 1s photopeak reveals a surface very similar to the C5 FEP flight sample.

Through this series of experiments, it is proposed that during the LDEF mission contamination, such as Si-containing and C-O containing, was deposited on both C5 and C8 FEP samples, as well as other surfaces. However, the surface of C8 was kept "clean" of Si-containing and C-O containing contamination as a result of the higher atomic oxygen fluence of C8 as opposed to C5.

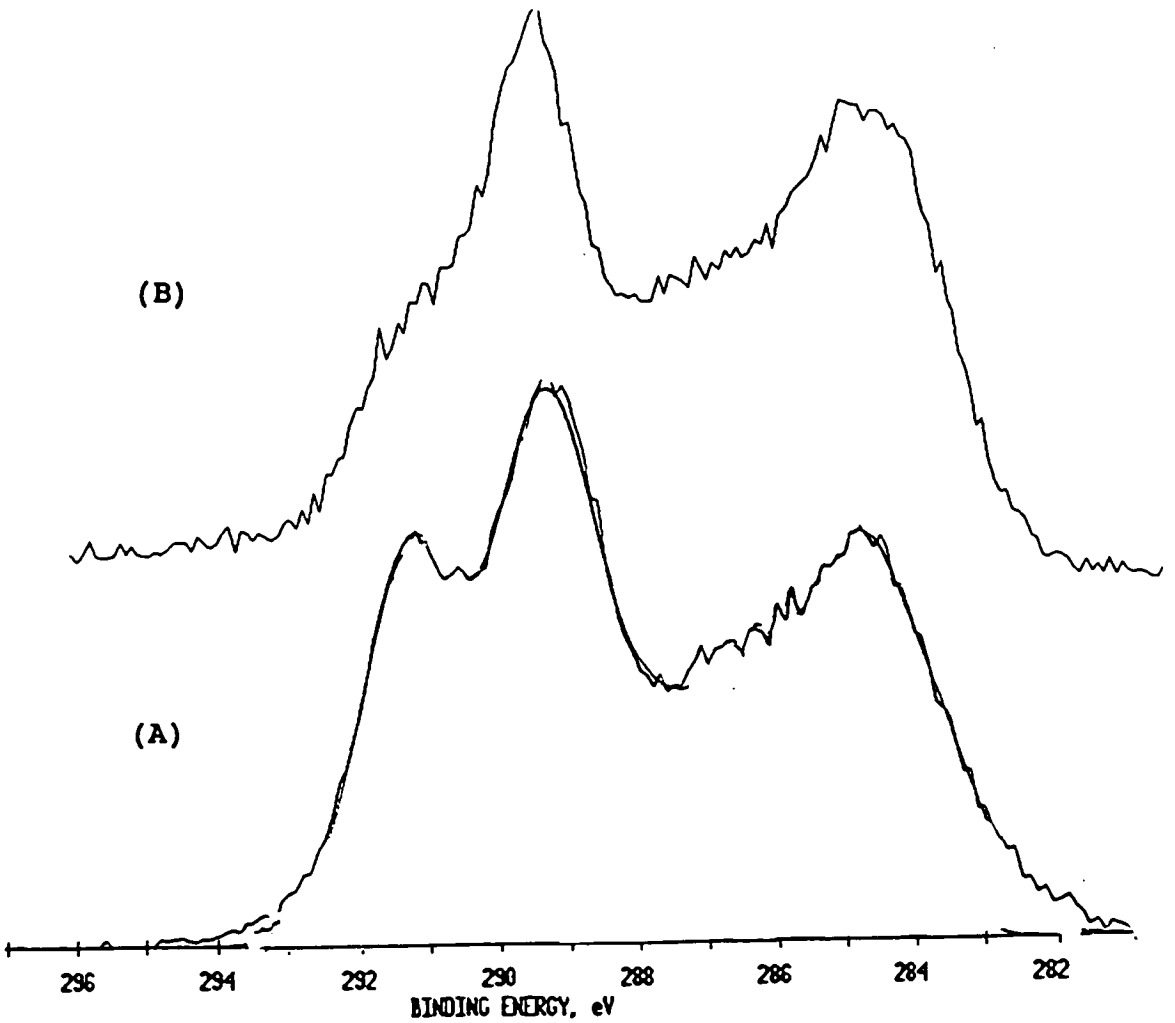

FIGURE 4.17: COMPARISON OF CARBON 1s CURVE FIT REGION OF (A) C5 FEP FLIGHT SAMPLE PRIOR TO PLASMA TREATMENT (B) PLASMA TREATED C5 FEP FLIGHT SAMPLE 69 DAYS AFTER PLASMA TREATMENT.

B. Surface Characterization of Composites

The surface characterization of the composites described in the Experimental chapter is discussed in this section. XPS and SEM were the two surface tools used to characterize the surface chemistry changes induced by the low-Earth orbit environment.

1. 934/T300 Epoxy - Composite

a. Atomic Composition

934/T300 is a carbon fiber reinforced epoxy composite. The XPS results for the control, 10 and 69-month flight samples are shown in Tables 4.17 and 4.18. The atomic composition of the control sample is 68.8% carbon, 18.1% oxygen, 2.0% sodium, 5.5% fluorine, 3.4% nitrogen, 1.1% sulfur and 1.1% silicon. The overall surface composition of the composite sample is complex. Moyer and Wightman [74] reported a 30% fluorine content on the surface of a polyimide/carbon fiber composite. The fluorine present most likely resulted from organo-fluoro release agents used in the fabrication of the composite. Mallon [75] reported the surface composition for a typical release cloth used in the fabrication of carbon/organic matrix composites as 39% carbon, 4% oxygen 56% fluorine and 0.7 % silicon. The major component of the release cloth is organo-fluorine. Transfer of fluorine from the release cloth during the fabrication of the composites is

TABLE 4.17: XPS ANALYSIS OF 934/T300 CONTROL SAMPLE.

PHOTOPEAK	BINDING ENERGY(eV)	ATOMIC CONC(%)	X/C RATIO
C 1s	285.0	68.8	--
O 1s	532.6	18.1	0.26
Na 1s	1072.2	2.0	0.03
F 1s	689.3	5.5	0.08
N 1s	399.9	3.4	0.05
S 2p	168.4	1.1	0.01
Si 2p	103.2	1.1	0.01

TABLE 4.18: XPS ANALYSIS OF 934/T300 10 AND 69 MONTH FLIGHT SAMPLES.

10 MONTH

PHOTOPEAK	BINDING ENERGY(eV)	ATOMIC CONC(%)	X/C RATIO
C 1s	285.0	73.3	--
O 1s	531.9	18.7	0.26
Na 1s	1071.9	0.5	0.00_7
F 1s	688.2	0.2	0.00_3
N 1s	399.6	5.5	0.08
S 2p	168.4	0.8	0.01
Si 2p	103.7	0.8	0.01

69 MONTH

PHOTOPEAK	BINDING ENERGY(eV)	ATOMIC CONC(%)	X/C RATIO
C 1s	285.0	72.0	--
O 1s	533.3	19.6	0.27
N 1s	400.6	0.8	0.01
S 2p	170.0	0.8	0.01
Si 2p	104.0	6.3	0.09
F 1s	nsp*	--	--
Na 1s	nsp	--	--

*nsp-no significant peak

well documented [74].

The silicon detected on the control sample was inorganic silicon, with a binding energy of 103.2 eV. The minor contaminants (sodium, nitrogen, sulfur, and silicon) have been reported for composites [75]. Mallon [75] and Tennyson [76] have reported similar concentrations of contaminants consistent on the surface of carbon fiber/organic matrix composites. However, the origin of this contamination is unknown.

As shown in Tables 4.17 and 4.18, the surface composition of the 10 and 69 month flight samples parallels that of the control. The atomic compositions of the control, 10, and, 69-month flight samples are shown Figure 4.18. Figure 4.18 would suggest the low-Earth orbit had little or no effect on the surface composition of the epoxy composites. Furthermore, the O/C and S/C ratio for the three samples remained constant at a value of 0.26 and 0.01, respectively.

Unlike the polymer samples, trends of decreasing carbon content and increasing oxygen content were not observed for the two flight samples. However, the silicon content for the 69 month flight sample was observed to significantly increase. Inorganic silicon was also detected on both flight samples. Meshinshnek and coworkers [77] reported the effects of atomic oxygen erosion for epoxy-resin-embedded fiber samples on Shuttle Mission STS-8. Forty hours of exposure to the low-

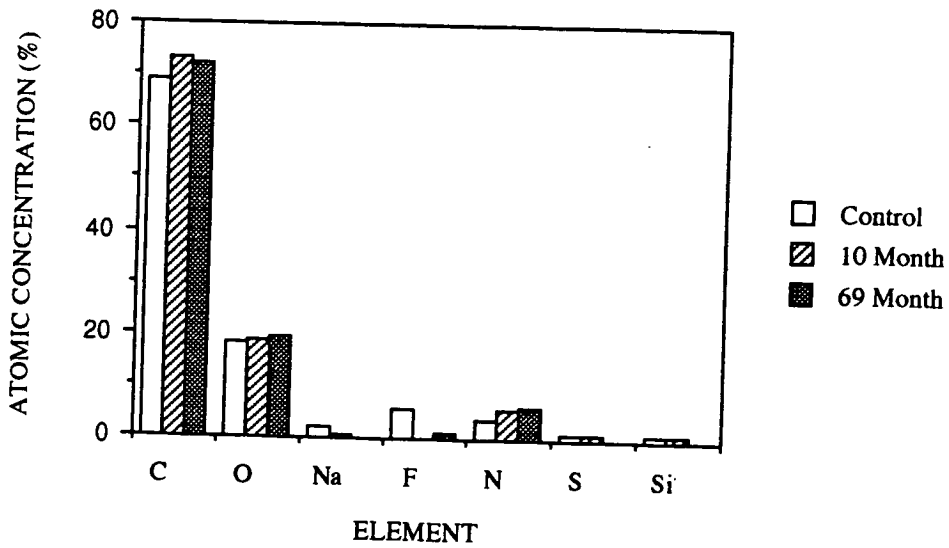

FIGURE 4.18: COMPARISON OF ATOMIC CONCENTRATIONS OF 934/T300 SAMPLES.

Earth orbit environment induced erosion of the epoxy resin at a faster rate than the carbon fibers. The effects of the low-Earth orbit environment were minimal for the carbon fibers. The results from the STS-8 mission would predict preferential erosion of the matrix in contrast to the carbon fibers for a composite sample [77]. The degradation/erosion of polymer matrix composite samples flown on the LDEF, particularly the leading edge, has been discussed previously [78]. Atomic oxygen reaction results in polymer bond breaking and subsequent molecular fragmentation leading to erosion of the materials [78].

b. Curve Fit Analysis

The results of the curve fit analysis for the three samples are summarized in Table 4.19. Figure 4.19 illustrates the carbon 1s curve fit region for the control, 10 and 69 month samples. A significant difference is observed in the carbon 1s curve fit region for the three samples. Figure 4.19 revealed different contributions (percentages) as well as different types of carbon functionality under the carbon 1s envelope. Although the atomic compositions of the three samples were similar, the types of carbon surfaces for each sample are very different. These results reinforce the necessity of curve-fitting photopeaks obtained in XPS measurements. Information obtained from *proper* curve fitting

TABLE 4.19: CARBON 1s CURVE FIT ANALYSIS OF 934/T300 CONTROL, 10, AND 69 MONTH FLIGHT SAMPLES.

CONTROL

PHOTOPEAK	BINDING ENERGY(eV)	% AREA	BOND
C1	285.0	55.7	C-H
C2	286.3	25.0	C-O
C3	287.8	7.8	C=O
C4	289.4	5.2	O-C=O
C5	291.1	3.3	π-π^* transition
C6	293.0	2.7	

10 MONTH

PHOTOPEAK	BINDING ENERGY(eV)	% AREA	BOND
C1	283.6	46.4	graphitic carbon
C2	285.0	30.8	C-H
C3	286.6	11.8	C-O
C4	288.1	7.3	C=O
C5	289.7	3.4	O-C=O

69 MONTH

PHOTOPEAK	BINDING ENERGY(ev)	% AREA	BOND
C1	283.9	49.8	graphitic carbon
C2	285.0	38.9	C-H
C3	286.4	8.6	C-O
C4	288.5	2.9	C=O

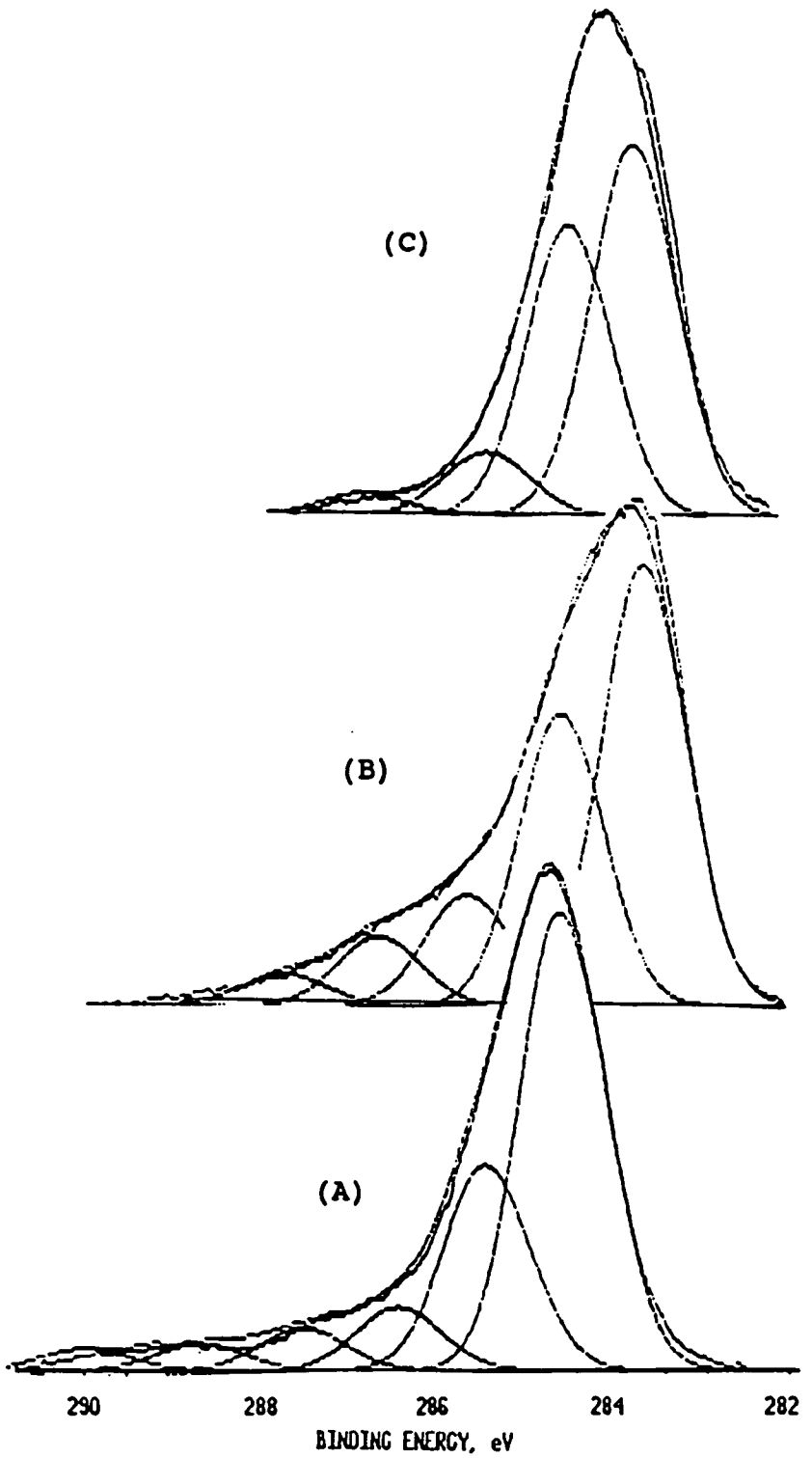

FIGURE 4.19: COMPARISON OF CARBON 1s CURVE FIT REGION OF 934/T300 (A) CONTROL (B) 10 MONTH (C) 69 MONTH SAMPLES.

procedures is useful and critical in describing the surface chemistry of materials.

The carbon 1s photopeak of the control sample revealed a resin rich surface. 55.7% of the total area under the carbon 1s photopeak corresponds to hydrocarbon functionality. The carbon-oxygen functionality corresponds to 38.0% of the area and 3.3% of the photopeak area corresponds to a π to π^* transition. A 41% decrease in the carbon-oxygen functionality, binding energy 286.6 - 289.7 eV was observed for the 10 month flight sample. A lower binding energy peak, at 283.6 eV, was resolved in the curve fit analysis. This lower binding energy peak is assigned to a graphitic type of carbon [79].

The 69 month flight sample showed a further significant decrease in the carbon-oxygen functionality with respect to the control and 10 month flight sample. A lower binding energy peak, at 283.9 eV with respect to the hydrocarbon peak at 285.0 eV, was also resolved in the carbon 1s photopeak for the 69 month flight sample.

An in-house experiment was carried out to determine the carbon-functionality of the lower binding energy peak. Paraffin wax, which is a low molecular weight hydrocarbon, was used to characterize the hydrocarbon species at 285 eV. Hercules ASU4 carbon fibers were ground and used to characterize the graphitic carbon species. The carbon 1s

photopeak was not used as the reference for the paraffin wax and ground carbon fibers when evaluating the two different types of carbon functionality. Therefore, both samples were coated with approximately 5 seconds of gold so that the gold $4f_{5/2}$, $4f_{7/2}$ peaks could serve as the internal reference for both samples.

The carbon 1s photopeak for the paraffin wax and ground carbon fibers is shown in Figure 4.20. Figure 4.20 also includes the gold $4f_{5/2}$, $4f_{7/2}$ photopeaks. As shown in Figure 4.20, the carbon 1s photopeak for paraffin wax is approximately 285.0 eV, whereas, the carbon 1s photopeak for the ground carbon fibers is approximately 283.7 eV. This shift in the carbon 1s photopeak to a lower binding energy corresponds then to a graphitic carbon species. Consequently, the lower binding energy peak present in the carbon 1s photopeak for the 934/T300 composite flight samples was assigned to a graphitic carbon type functionality.

The appearance of the graphitic type carbon is the result of the degradation/erosion of the epoxy matrix to expose the carbon fibers of the composite. The curve fit analysis suggest that the principal ablation of the epoxy matrix occurred *within* the first 10 months of exposure to the low-Earth space environment. A modest 7% increase in the graphitic carbon species was measured for the 69 month flight sample. This suggests further degradation/erosion of the

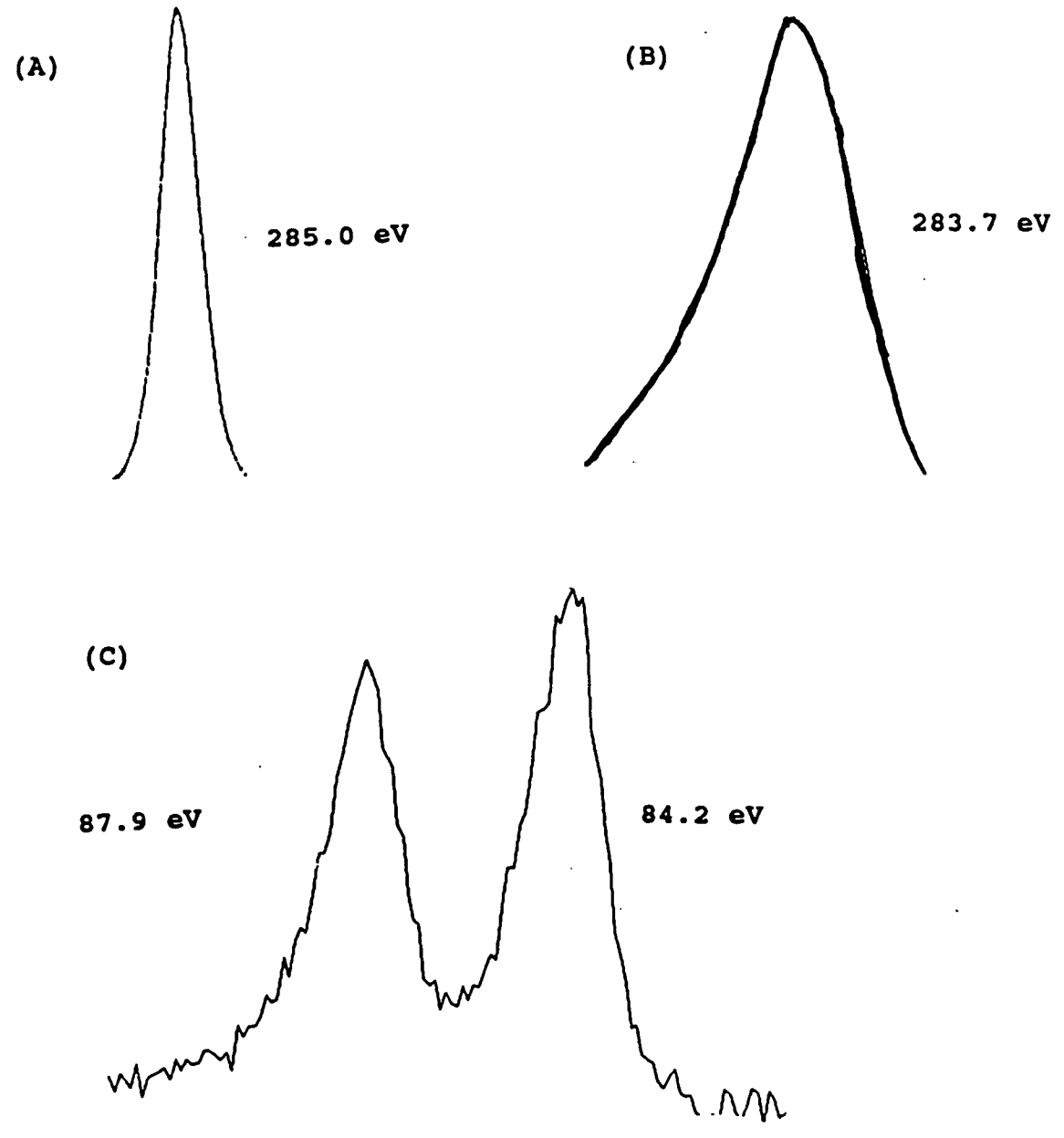

FIGURE 4.20: COMPARISON OF CARBON 1s BINDING ENERGY OF (A) PARAFFIN WAX (B) GROUND CARBON FIBERS REFERENCED TO (C) GOLD $4f_{5/2}$, $4f_{7/2}$ PHOTOPEAKS.

polymer matrix to expose the carbon fibers.

c. SEM Photomicrographs

The SEM photomicrographs of the control, 10, and 69-month flight samples are shown in Figure 4.21. Three very different surface topographies are observed in Figure 4.21 and support the results obtained from the curve fit analysis.

The SEM of the control sample (see Fig. 4.21A) reveals a resin rich surface, thus, supporting the curve fit analysis. The weave pattern present on the control sample is not the weave pattern of the fibers within the composite but rater the impression left from a scrim cloth. Scrim cloths are typically used in the consolidation of composites.

The SEM photomicrograph of the 10-month flight sample (see Fig. 4.21B) revealed both resin and carbon fibers. The curve fit analysis of the 10-month flight sample showed carbon functionality that is consistent with both resin and carbon fiber functionality. The resin functionality corresponds to photopeaks C2 - C5 for the 10-month flight sample. As shown in Figure 4.19, these photopeaks are also observed in the control sample, thus supporting the resin surface. However, the unidirectional fibers are also apparent in the 10-month flight sample. The carbon fiber functionality corresponds to photopeak C1 for the 10-month flight sample.

The SEM photomicrograph of the 69-month flight sample

(A)

(B)

(C)

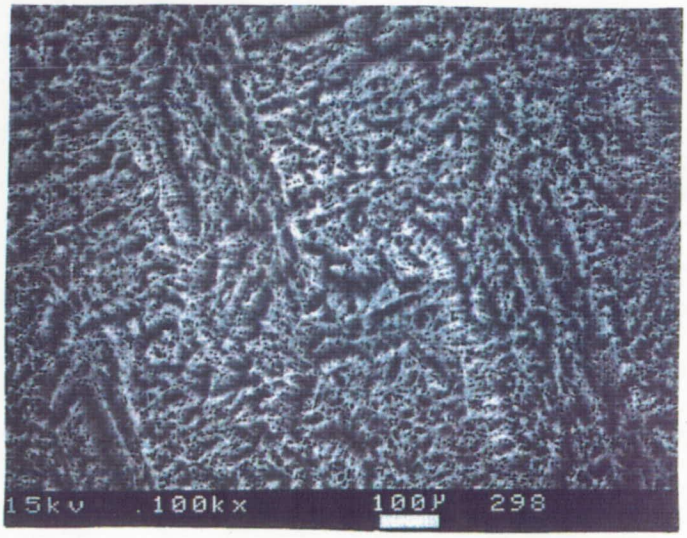

FIGURE 4.21: SEM PHOTOMICROGRAPHS OF 934/T300 COMPOSITE SAMPLES (A) CONTROL (B) 10 MONTH (C) 69 MONTH.

(see Fig. 4.21C) shows significant ablation of the surface with respect to the control and 10-month flight sample. The flight sample exhibits the "carpet" morphology observed for samples exposed to the space environment [35-38]. This "carpet" morphology has also been observed for composite samples from the LDEF [80,81]. The carbon 1s curve fit analysis for the 69-month flight sample infers that the "carpet" morphology observed is a combination of resin and carbon fibers. However, the curve fit results, particularly the contribution of photopeak C1, would suggest the morphology is predominantly due to carbon fibers. The SEM photomicrographs are consistent with the curve fit analysis for the control, 10 and 69-month flight samples. The SEM photomicrographs and the curve fit analysis support the degradation/erosion of the epoxy matrix *within* the first 10 months of the mission as well as further degradation for the remaining 59 months.

Tennyson [82] reported that atomic oxygen fluence on Row 12 was sufficient to erode the epoxy layer and a portion of the reinforcing graphite fibers. The epoxy samples discussed in this study were located on the leading edge of the LDEF where the difference in the atomic oxygen fluence for Row 12 and Row 9 is 7.66×10^{21} atoms/cm^2. Thus, the higher atomic oxygen fluence for Row 9 would facilitate the degradation/erosion of the matrix to expose the carbon fibers

as seen in Figure 4.21. The degradation/erosion of the epoxy matrix to expose more of the carbon fibers within the composite sample can strongly be supported by the curve fit analysis and SEM photomicrographs.

2. P1700/C6000 Polysulfone - Composite

a. Atomic Composition

P1700/C6000 is a carbon fiber reinforced polysulfone composite. The XPS results for the control and two flight samples, exposed for 10 and 69 months, are listed in Tables 4.20 and 4.21. The samples were located on Tray B, Row 9 of the LDEF. The XPS analysis of the control sample revealed 76.9% carbon, 14.5% oxygen, 4.1% fluorine, 1.3% calcium, 0.4% sulfur, 1.2% silicon and 1.6% aluminum. The overall surface composition of this composite, like the 934/T300 composite is complex. The fluorine contamination may have resulted from the use of organo-fluoro release materials in the composite fabrication. The binding energy of sulfur and silicon, 167.9 eV and 102.4 eV respectively, are indicative of the organo-form of both elements. The binding energy of aluminum at 74.7 eV corresponds to aluminum oxide. The source of the minor surface contaminants calcium, silicon and aluminum, are unknown. George and coworkers [78] have reported similar surface contaminants on P1700 polysulfone/T300 composite samples.

TABLE 4.20: XPS ANALYSIS OF P1700/C6000 CONTROL SAMPLE.

PHOTOPEAK	BINDING ENERGY(eV)	ATOMIC CONC(%)	X/C RATIO
C 1s	285.0	76.9	--
O 1s	532.1	14.5	0.19
F 1s	688.9	4.1	0.05
Ca 2p	347.6, 351.1	1.3	0.02
S 2p	167.9	0.4	0.00_5
Si 2p	102.4	1.2	0.02
Al 2p	74.7	1.6	0.02

TABLE 4.21: XPS ANALYSIS OF P1700/C6000 10 AND 69 MONTH FLIGHT SAMPLES.

10 Month

PHOTOPEAK	BINDING ENERGY(eV)	ATOMIC CONC(%)	X/C RATIO
C 1s	285.0	67.0	--
O 1s	532.7	24.5	0.36
Na 1s	1072.8	0.8	0.01
N 1s	399.7	1.1	0.01
S 2p	169.9	2.4	0.03
Si 2p	103.5	2.3	0.03
Al 2p	75.3	1.9	0.09

69 Month

PHOTOPEAK	BINDING ENERGY(eV)	ATOMIC CONC(%)	X/C RATIO
C 1s	285.0	25.0	--
O 1s	533.1	51.9	2.08
N 1s	400.6	1.2	0.05
Ca 2p	348.5, 352.0	0.1	0.04
S 2p	169.6	2.9	0.12
Si 2p	103.7	17.3	0.07

As shown in Table 4.21, the XPS analysis of the 10-month flight sample revealed 67.0% carbon, 24.5% oxygen, 0.8% sodium, 1.1% nitrogen, 2.4% sulfur, 2.3% silicon and 1.9% aluminum. A 13% decrease in carbon content and a 69% increase in oxygen content were observed for the 10 month flight sample compared to the control. George and coworkers [78] also reported trends of decreasing carbon content and increasing oxygen content for the exposed as opposed to the unexposed samples. A 500% and 92% increase were observed for the sulfur and silicon contents respectively. The binding energies of sulfur and silicon, 169.9 eV and 103.5 eV respectively, now correspond to the inorgano form of both elements. In contrast, the organo form of both elements were present on the control sample. The change in state of both elements is the direct result of exposure to atomic oxygen.

Small amounts of sodium and nitrogen contamination were observed for the 10-month flight sample. The fact that sodium and nitrogen were not detected on the control sample suggests the elements were deposited during the mission. Low levels of sodium and nitrogen contamination have been detected on LDEF samples [22-30]. The source of this contamination is unknown.

The fluorine and calcium contents decreased for the 10-month flight sample. A 19% increase in the aluminum content was also observed. The source of the aluminum on the surface of the control and 10-month flight samples is unknown.

XPS analysis of the 69-month flight sample, as shown in Table 4.21, revealed 25% carbon, 51.9% oxygen, 1.2 % nitrogen, 0.1% calcium, 2.9% sulfur and 17.3% silicon. A large decrease in carbon content was observed for the 69-month flight sample with respect to the control and 10-month flight samples. However, large increases in both the oxygen and silicon contents were observed for the 69-month flight sample with respect to the control and 10-month flight sample. This trend of decreasing carbon content and increasing oxygen and silicon contents for the three samples is illustrated in Figure 4.22. George and coworkers [78] also reported an increase in silicon content on the exposed surface of the composite sample. A possible SiO_x contamination layer on the 10 and 69-month flight samples is consistent with the observed increase in oxygen and silicon contents as well as the subsequent shift in binding energy of the silicon 2p photopeak. The inorgano-sulfur content increased 625% with respect to the control sample, whereas, the inorgano- sulfur increased only 21% with respect to the 10-month flight sample. The modest increase in the sulfur content for the 10-month flight sample and, the large increase for the 69-month flight sample coupled with the large decrease in carbon content, supports the degradation/erosion of the polymer matrix while in the low-Earth space environment. Atomic oxygen converted the organo-sulfur to an inorgano-sulfur. The XPS results suggests the

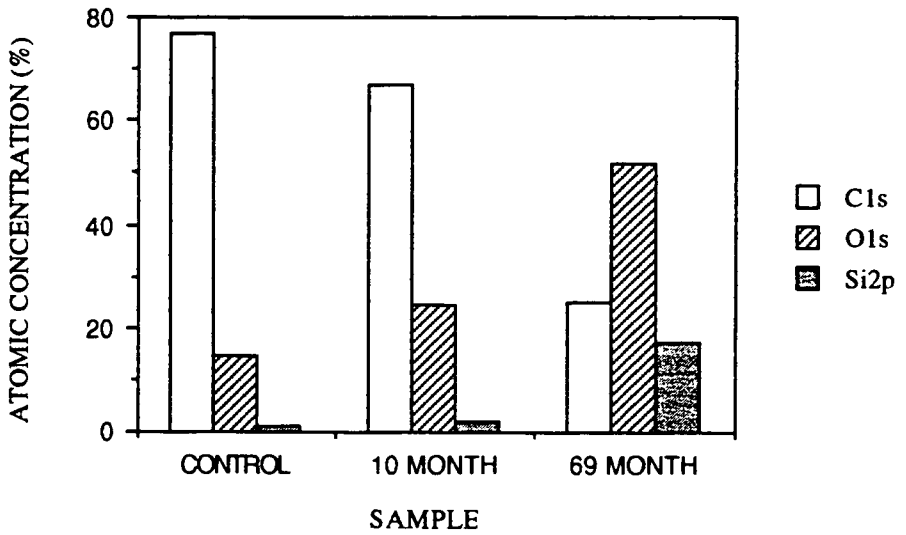

FIGURE 4.22: COMPARISON OF ATOMIC CONCENTRATIONS OF CARBON, OXYGEN, AND SILICON FOR P1700/C6000 SAMPLES.

sulfur was not removed like carbon but rather is concentrated on the surface and thus the S/C ratio increase from the control, 10 and 69 month flight samples.

The XPS results suggest the atomic oxygen present in the low-Earth space environment significantly changed the surface chemistry of the composite samples. The surface of the control sample can be characterized as an organo-type surface. Whereas, the surface of the 10 and 69-month flight samples can be characterized as an inorganic-type of surface. The change in the overall surface chemistry is a direct result of exposure to the atomic oxygen present in the low-Earth orbit space environment.

b. Curve Fit Analysis

The carbon 1s curve fit analysis of the control and two flight samples is shown in Table 4.22. Figure 4.23 illustrates the changes observed in the carbon 1s photopeak. The curve fit analysis of the control sample revealed a resin rich surface. Hydrocarbon functionality corresponds to 90.8% of the total photopeak area. The remaining 11.2% corresponds to carbon-oxygen functionality.

The curve fit analysis of the 10-month flight sample showed a decrease in the hydrocarbon functionality and an increase in carbon-oxygen functionality. The increase in the carbon-oxygen functionality namely, photopeaks C2 -

TABLE 4.22: CARBON 1s CURVE FIT ANALYSIS OF P1700/C6000 CONTROL, 10, AND 69 MONTH FLIGHT SAMPLES.

CONTROL

PEAK	BINDING ENERGY(eV)	% AREA	BOND
C1	285.0	90.8	C-H
C2	286.7	6.3	C-O
C3	288.9	2.8	O-C=O

10 MONTH

PEAK	BINDING ENERGY(eV)	% AREA	BOND
C1	285.0	53.3	C-H
C2	286.5	27.1	C-O
C3	287.6	12.2	C=O
C4	288.9	4.3	O-C=O
C5	290.4	2.7	π-π^* transition

69 MONTHS

PEAK	BINDING ENERGY(eV)	% AREA	BOND
C1	282.0	22.4	
C2	283.4	18.6	graphitic carbon
C3	285.0	33.3	C-H
C4	286.4	12.4	C-O
C5	287.9	4.7	C=O
C6	289.4	3.1	O-C=O
C7	291.0	2.7	π-π^* transition
C8	293.0	2.4	

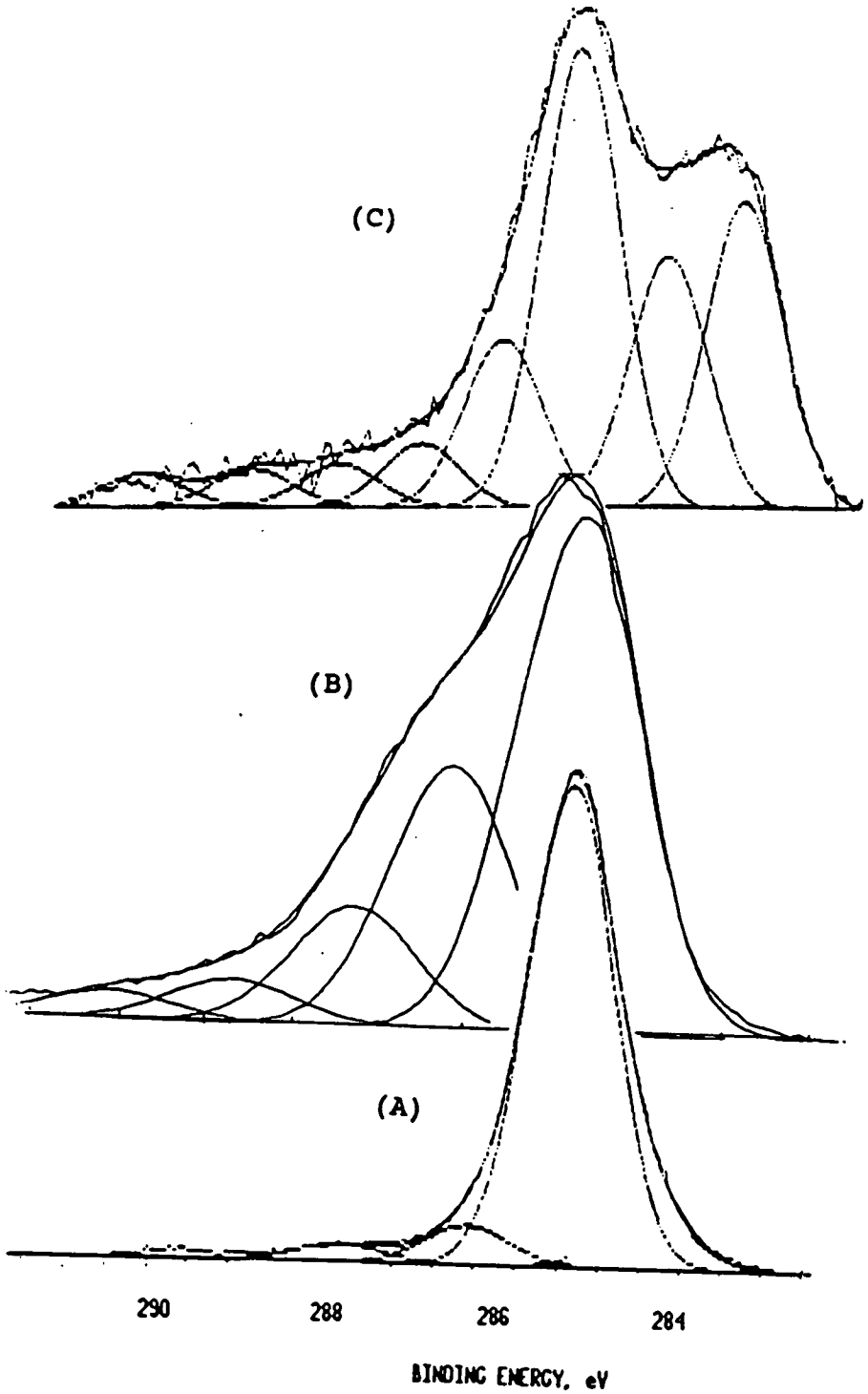

FIGURE 4.23: COMPARISON OF CARBON 1s CURVE FIT REGION OF P1700/C6000 (A) CONTROL (B) 10 MONTH (C) 69 MONTH SAMPLES.

C4,indicated oxidation/erosion of the surface resin.

A significant change in the type of carbon functionality is apparent in the curve fit carbon 1s photopeak for the 69-month flight sample. Two photopeaks, (C1 and C2), with binding energies at, 282 eV and 283.4 eV, were observed for the 69-month flight sample. The 283.4 eV peak corresponds to a graphitic carbon species. This graphitic carbon species, which was not detected on the 10 month sample, suggests that after only 10-months, sufficient ablation of the polysulfone matrix had not occurred to expose the carbon fibers as was the case after 69 months. The lower binding energy peak, 282.0 eV was not identified.

C. Surface Characterization of Aluminum Sample with Impact Crater

A 6061-T6 anodized aluminum sample containing an impact crater is discussed in this section. Figure 4.24 is an optical photograph of the aluminum sample. The impact crater, the pinkish residue region, to the left of the impact crater, and the aluminum surface are the three regions of interest and are shown in Figure 4.24. XPS analysis was performed to determine the surface composition of the residue region. SEM analysis was performed to evaluate the surface topography of the impact crater.

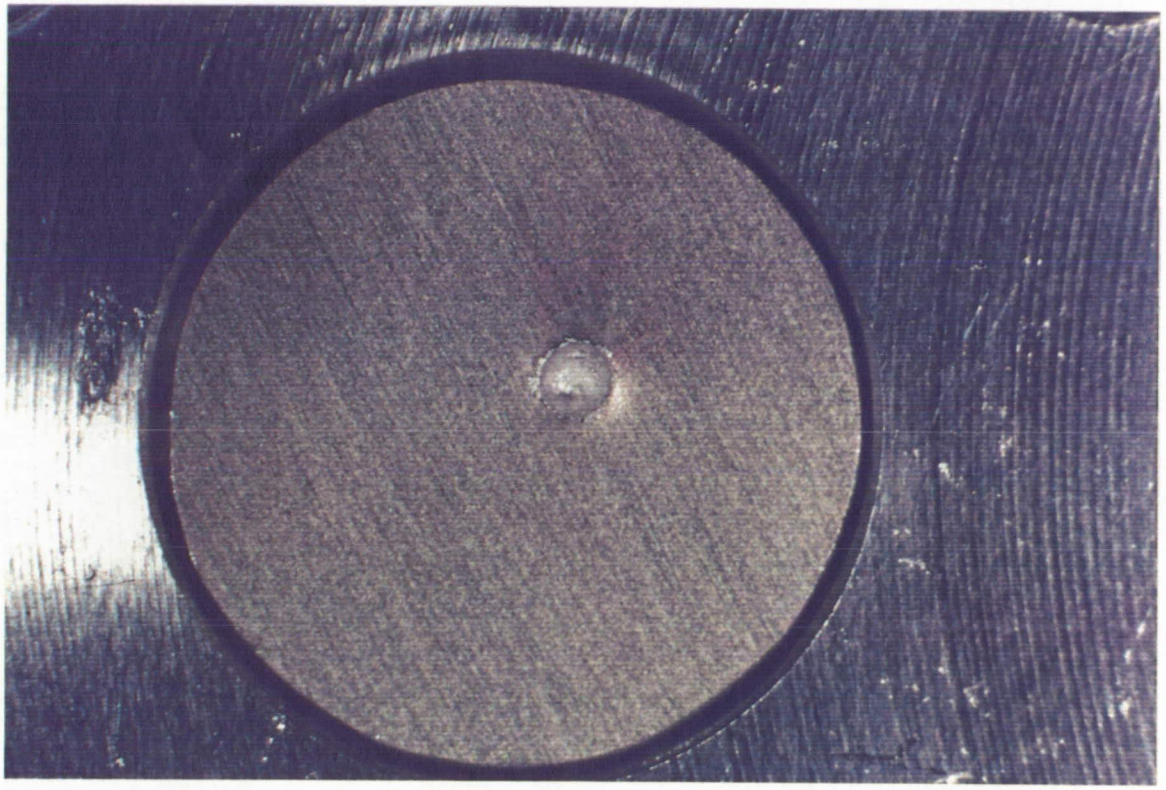

FIGURE 4.24: OPTICAL PHOTOGRAPH OF 6061-T6 ALUMINUM SAMPLE CONTAINING AN IMPACT CRATER.

Impact craters found on the LDEF were very similar to craters produced via hypervelocity accelerators in ground-based laboratories [83]. Typical laboratory impact velocity speeds are approximately 6 km/s (13,422 mi/hr) [84]. The impact craters on the LDEF and ground-based craters have a characteristic petal-like rim of ejecta [84]. Figure 4.25 is an SEM photomicrograph of the impact crater region. The impact crater region is approximately 2 mm in diameter. Researchers have characterized the topography of the crater walls as trapped gas bubbles [84]. This topography is the result of the aluminum becoming momentarily molten upon impact by a micro-meteoroid, with the aluminum subsequently resolidifing [84]. The impact crater region, as shown in Figure 4.25, exhibits these characteristics.

The XPS results of the three regions are shown in Figure 4.26. The carbon, oxygen and aluminum contents of the three regions compare closely to one another. A higher fluorine and silicon contents were detected for the impact crater and aluminum regions, respectively. Magnesium was only detected for the residue region. The overall surface composition of the three regions are very similar with the exception of magnesium.

The Meteoroid & Debris Special Investigation Group has developed compositional classifications and associated criteria for the analysis of LDEF craters utilizing data from

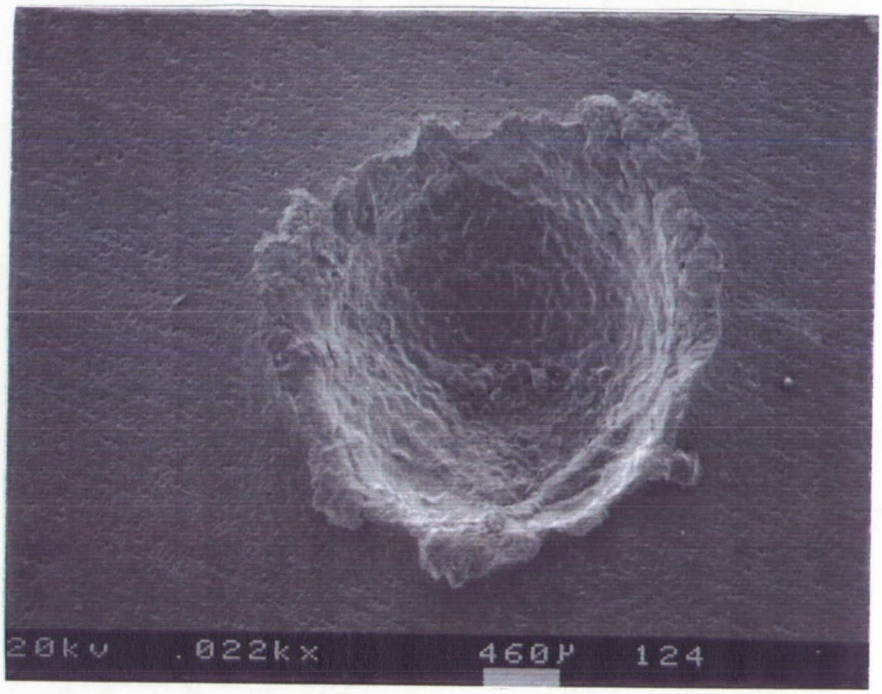

FIGURE 4.25: SEM PHOTOMICROGRAPH OF IMPACT CRATER REGION.

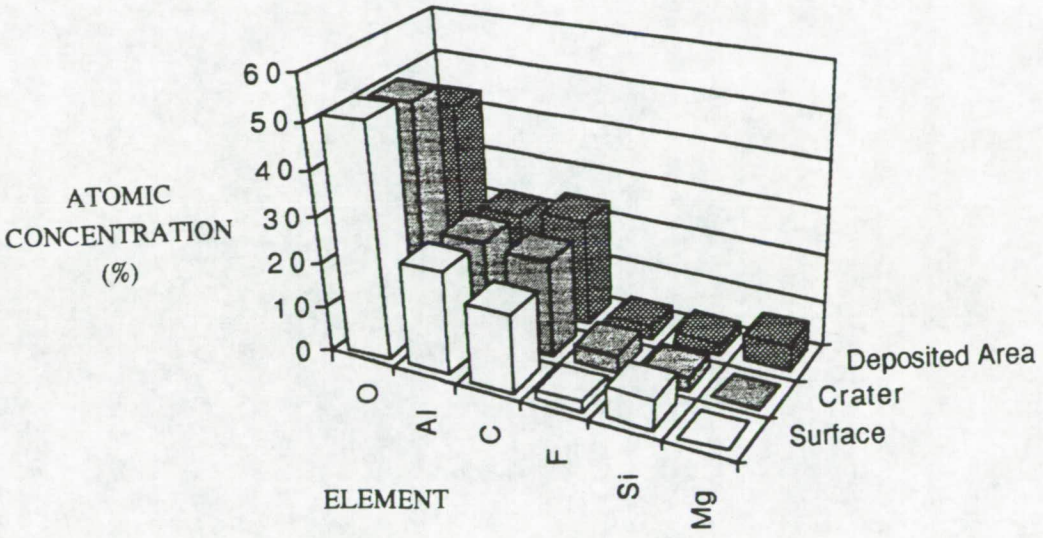

FIGURE 4.26: COMPARISON OF ATOMIC CONCENTRATIONS OF THE THREE REGIONS ON ALUMINUM SAMPLE CONTAINING AN IMPACT CRATER.

the Solar Max surfaces [35]. Natural cosmic particles havebeen divided into three major groups which are in agreement with stratospheric particle populations [85]. Magnesium is a primary component of two out of the three major natural cosmic particle groups. For example, magnesium is present in "chondritic" compositions which are typically fine-grained primitive meteorites.

It is noted that the 6061 aluminum alloy contains 1.00% by weight magnesium. The presence of magnesium only in the residue region in conjunction with the fact that magnesium is a primary component found in meteoroids strongly suggests the magnesium was deposited as a result of a micro-meteoroid impact.

D. Surface Characterization of LDEF Tray Clamps

1. 6061-T6 Aluminum Surface

The surface analysis of the 6061-T6 aluminum portion of 15 tray clamps (fourteen flight and one control) described in the Experimental chapter is discussed in this section. XPS, SEM, Auger depth profiling and contact angle analysis were the four surface tools used in this study. Surface analysis was performed to characterize the changes in both the surface composition and surface chemistry which occurred as a result of exposure to the low-Earth orbit environment.

A detailed study on the integrity of the "anodic thermal

control coating" to the space environment has been reported [86]. Plagemann [86] reported relatively small but statistically significant changes in the optical properties, such as emittance and absorptance, of 228 tray clamps. However, there has been no systematic study reported of the effects of the low-Earth orbit environment on the surface chemistry of these clamps. The surface characterization of these tray clamp provides a unique opportunity in which to evaluate the extent of contamination of fourteen positions on the LDEF, particularly silicon contamination, which has been detected on the majority of LDEF materials [22-30].

a. Auger Depth Profiling

Auger depth profiling was used to determine the thickness of the aluminum oxide layer present on the tray clamps. A representative Auger depth profile of tray clamp B4 is shown in Figure 4.27. The point in the figure at which the aluminum curve - bottom line, crosses the oxygen curve - top line, was arbitrarily defined as the oxide thickness.

Auger depth profiling was performed on both the exposed (top) and protected (bottom) sides of the tray clamps. The exposed/protected profiles were performed for the following reasons: first, to evaluate the uniformity in the thickness of the oxide layer produced by anodization and secondly to evaluate the changes in the oxide thickness as a function of

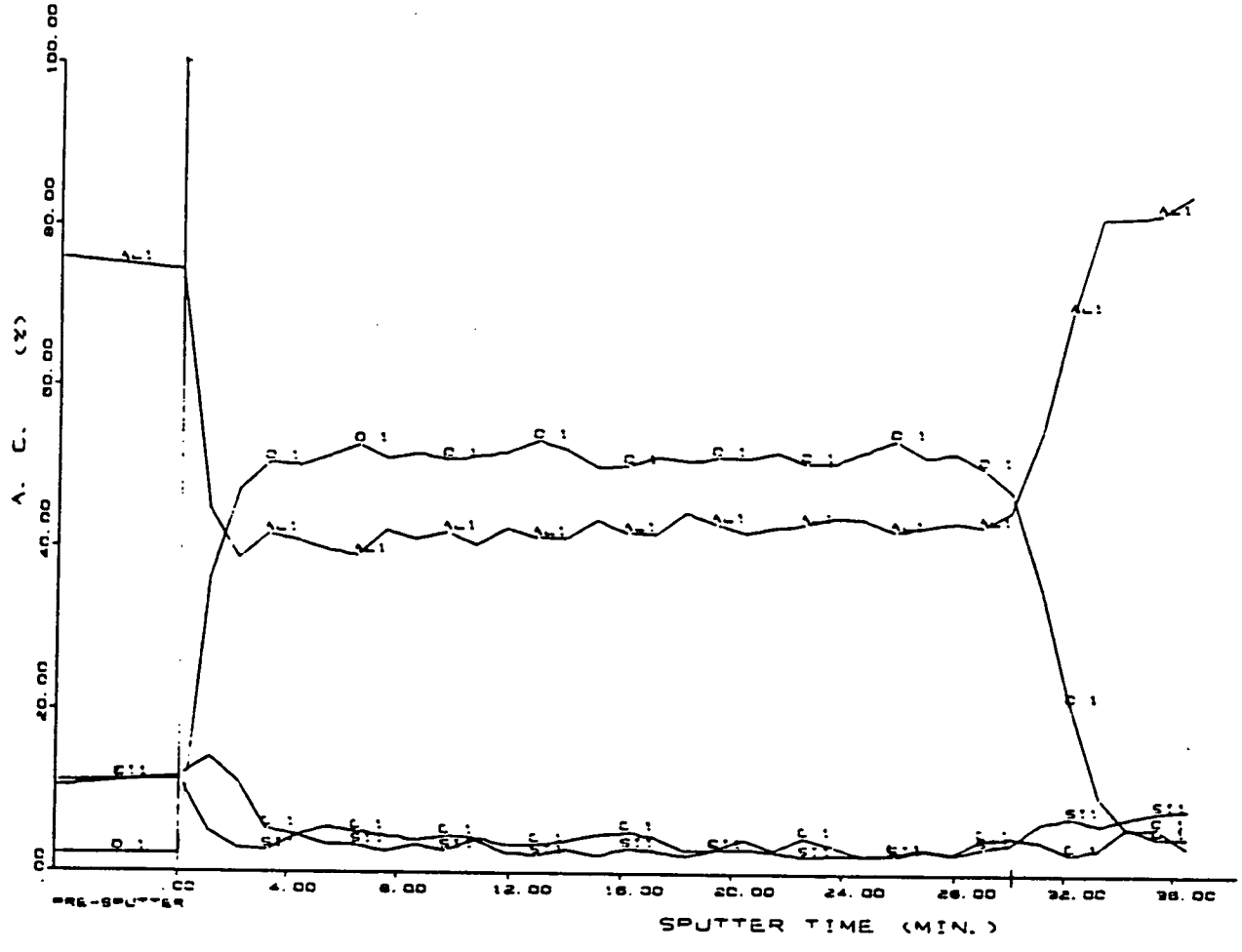

FIGURE 4.27: AUGER DEPTH PROFILE OF TRAY CLAMP B4.

the low-Earth orbit environment and position on the LDEF. Oxide thickness values for the exposed/protected sides are listed in Table 4.23. Considerable variation in oxide thickness values were observed for both exposed and protected surfaces. The average oxide thickness of the exposed sides is 704 Å. These results are consistent with the work of Plagemann [86] who concluded from SEM measurements that the oxide thickness was less than 1 mm. The average oxide thickness of the protected side is 997 Å. But a greater oxide thickness was observed on the protected side for only 53% of the tray clamps. Thus, the observed differences in the oxide thickness values for both the exposed and protected side can not be attributed to the low-Earth orbit environment or position on the LDEF.

As a result of observed variations in the oxide thickness values from sample to sample, Auger depth profiling was performed to evaluate the variation of the oxide thickness present on one tray clamp. Four Auger depth profiles were performed on both the exposed and protected sides of tray clamp D9. Oxide thickness values are shown in Table 4.24. Considerable variation was observed in the oxide thickness on both sides of tray clamp D9. An average oxide thickness for the exposed side is 620 Å, whereas, the average oxide thickness for the protected side is 730 Å. A greater oxide thickness was observed on the protected side of tray clamp D9.

TABLE 4.23: ALUMINUM OXIDE THICKNESS (IN Å) AS DETERMINED BY AES DEPTH PROFILING FOR EXPOSED AND PROTECTED SIDES OF LDEF TRAY CLAMPS.

TRAY CLAMP	EXPOSED (TOP)	PROTECTED (BOTTOM)
Control	785	740
F1	990	810
F2	550	700
E3	1005	450
B4	930	900
B5	270	610
C6	120	900
D7	250	400
A8	645	840
D9	865	1120
A10	720	350
E11	820	900
D12	1140	960
G6	685	3540
H9	785	1080

TABLE 4.24: ALUMINUM OXIDE THICKNESS (IN Å) AS DETERMINED BY AES DEPTH PROFILING FOR EXPOSED AND PROTECTED SIDES OF TRAY CLAMP D9.

REGION	EXPOSED (TOP)	PROTECTED (BOTTOM)
Region 1	900	210
Region 2	530	860
Region 3	350	1230
Region 4	700	620

A greater average oxide thickness was also observed on the protected side for the 15 tray clamp. However, due to the large differences observed particularly for tray clamp D9 and the 15 tray clamps, a correlation of greater oxide thickness on the protected side can not be made. Thus, the discrepancy observed in the oxide thickness values for the tray clamps can be attributed to variations in the anodization process.

b. Contact Angle Analysis

Water contact angles were used to evaluate the wettability of the 6061-T6 aluminum portion of the tray clamps. A clean or contamination-free aluminum oxide surface would give a near zero water contact angle [57]. However, aluminum oxide is a high energy surface which facilitates the adsorption of contaminants, such as carbonaceous (organic) compounds, from the atmosphere [87].

Contact angles of water on the aluminum portion of the tray clamps are shown in Table 4.25. An average water contact angle of 64° was calculated for the 15 samples. The remarkably constant but high water contact angles are representative of a metal oxide surface which is contaminated by adsorption of organic molecules [88]. Alternately stated, the observed high water contact angles are typically characteristic of low energy surfaces such as polymers [89]. As shown in Table 4.25, no change was observed in the

TABLE 4.25: RESULTS OF WATER CONTACT ANGLE ANALYSIS ON LDEF TRAY CLAMPS.

TRAY CLAMP	Θ_w
Control	61°
F1	65°
F2	62°
E3	63°
B4	65°
C5	65°
C6	64°
D7	63°
A8	65°
D9	66°
A10	63°
E11	65°
D12	63°
G6	66°
H9	64°

wettability of the clamps with respect to position on the LDEF. The results clearly illustrate the elements such as pressure and temperature of the low-Earth orbit environment did not change the wettability of the tray clamps. These wettability results are consistent with adsorption of organic compounds commencing immediately on re-exposure of the tray clamps to the laboratory environment.

c. Scanning Electron Microscopy

SEM photomicrographs of the control, leading (D9) and trailing (E3) edge samples are shown in Figure 4.28. The overall surface topography of the three samples is similar. No significant changes in the surface topography were evident for the leading edge compared to the trailing edge samples. A similar surface topography was observed by Crutcher and coworkers [90] for tray clamps located at different positions.

Energy dispersive spectroscopy (EDS) is a near surface/bulk elemental analysis technique. A representative EDS spectrum of the leading edge tray clamp (D9) is shown in Figure 4.29. The EDS results of the control, leading and trailing edge samples are listed in Table 4.26. An average composition of 52 wt% aluminum and 48 wt% oxygen was determined for the three samples. These results are in good agreement with the calculated weight percent of aluminum (53%) and oxygen (47%) for Al_2O_3. As shown in Figure 4.29, aluminum

(A)

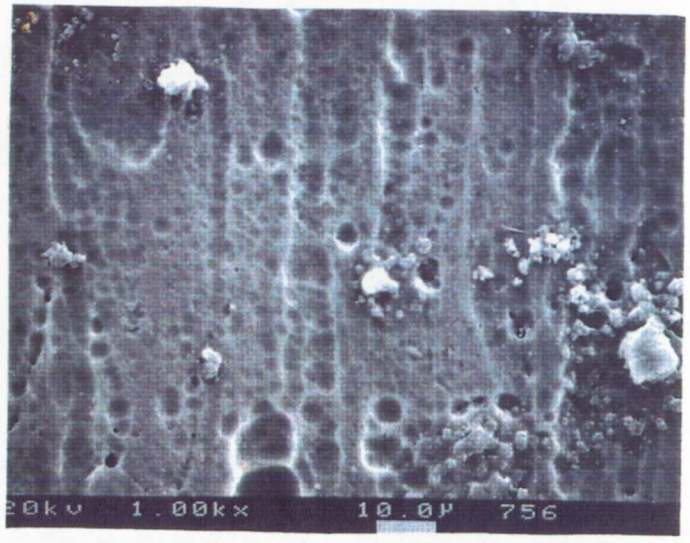

(B)

(C)

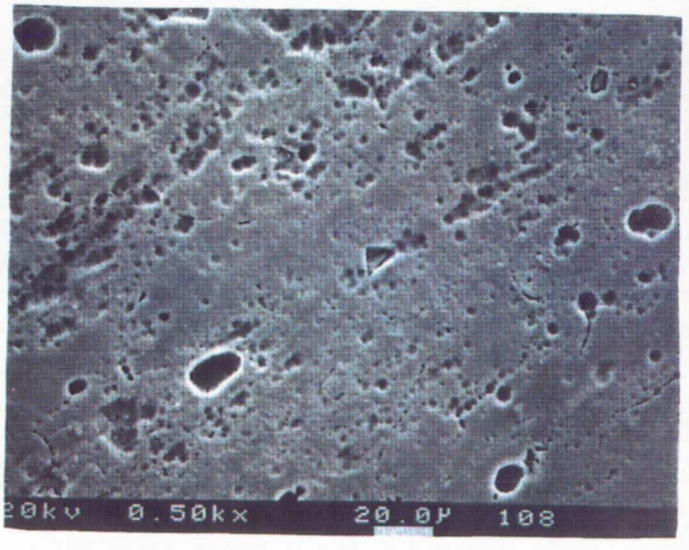

FIGURE 4.28: SEM PHOTOMICROGRAPHS OF 6061-T6 ALUMINUM SURFACE OF (A) CONTROL (B) E3-TRAILING EDGE (C) D9-LEADING EDGE TRAY CLAMPS.

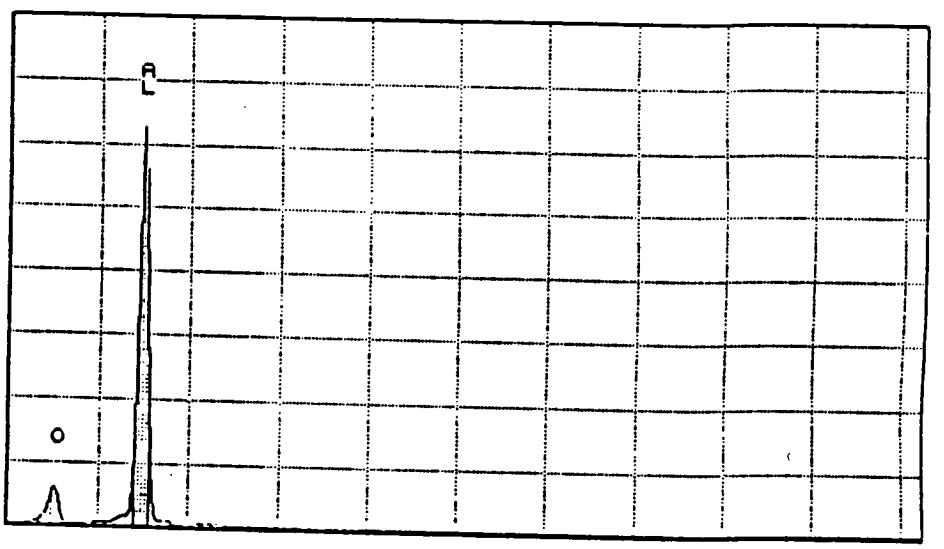

FIGURE 4.29: EDS SPECTRUM OF 6061-T6 ALUMINUM SURFACE OF D9-LEADING EDGE TRAY CLAMP.

TABLE 4.26: ENERGY DISPERSIVE ANALYSIS OF LDEF TRAY CLAMPS.

SAMPLE	ALUMINUM (wt %)	OXYGEN (wt%)
Control	54	46
E3	53	46
D9	49	50

and oxygen were the only elements detected by EDS in the sampling depth of 1-5 microns.

d. X-ray Photoelectron Spectroscopy

The XPS results of the aluminum portion of the tray clamps are shown in Tables 4.27 and 4.28. Tables 4.27 and 4.28 correspond to the XPS analysis of different aluminum pieces cut from the tray clamp. The results listed in Tables 4.27 and 4.28 can be considered to be the first and second XPS runs, respectively. The second XPS run was performed nearly one year after the first XPS run. The second XPS analysis was performed to obtain an "average" atomic composition for the aluminum surface. It is noted that, for a more precise statistical analysis of the atomic composition of the aluminum surface, the number of runs should be between seven and ten.

When comparing the atomic concentrations of the two XPS runs, a higher aluminum content was observed on 10 of the 15 tray clamps for the first XPS run. Conversely, a higher carbon content, as determined by the second XPS run, was observed on 9 of the 15 tray clamps. The fact that a higher carbon content with a subsequent lower aluminum content was observed for the second XPS run suggests additional carbon-containing organic contamination adsorbed onto the surface during the one year period between XPS runs. The adsorption of carbonaceous organic contamination from the atmosphere is

TABLE 4.27: XPS ANALYSIS OF 6061-T6 ALUMINUM PORTION OF LDEF TRAY CLAMPS.

SAMPLE	Al 2p	C 1s	O 1s	Na 1s
Control (eV)	74.7	285.0	532.2	1072.1
(%)	12.1	55.1	28.6	0.4
F1	74.7	285.0	531.9	1072.8
	28.7	15.8	49.0	0.3
F2	74.8	285.0	532.2	1072.5
	17.8	27.8	45.3	0.7
E3	74.6	285.0	532.4	1072.8
	22.2	26.9	41.8	0.5
B4	74.6	285.0	532.5	1072.9
	18.0	28.4	43.7	0.5
B5	74.7	285.0	532.3	1072.4
	12.4	38.1	40.3	1.0
C6	74.6	285.0	531.9	1072.6
	22.2	19.4	50.7	1.1
D7	74.6	285.0	532.5	1072.9
	19.2	16.9	50.0	0.6
A8	74.5	285.0	532.1	1072.5
	18.4	19.3	50.1	3.2
D9	74.8	285.0	532.8	--
	4.9	20.6	51.7	nsp*
A10	74.9	285.0	532.7	1072.5
	6.6	36.6	39.9	1.0
E11	--	285.0	533.2	--
	nsp	9.3	56.7	nsp
D12	74.6	285.0	532.0	1072.5
	19.9	26.9	45.5	0.7
G6	74.8	285.0	532.7	1072.5
	8.2	31.3	42.3	1.4
H9	74.6	285.0	532.5	1073.0
	17.3	17.9	49.4	1.0

*nsp-no significant peak

TABLE 4.27: XPS ANALYSIS OF 6061-T6 ALUMINUM PORTION OF LDEF TRAY CLAMPS.

SAMPLE	F 1s	N 1s	S 2p	Si 2p
Control (eV)	--	399.8	169.1	102.4
(%)	nsp*	1.7	0.5	1.6
F1	685.9	--	169.9	102.7
	1.0	nsp	0.9	4.3
F2	686.1	399.8	169.9	102.8
	2.5	0.9	0.5	4.5
E3	--	400.2	169.7	102.8
	nsp	1.0	0.5	7.1
B4	686.4	400.1	169.6	102.8
	0.5	1.3	0.6	7.0
B5	687.3	399.9	169.5	102.5
	3.4	1.2	0.3	3.3
C6	686.0	399.8	169.9	102.4
	1.2	0.7	0.4	4.3
D7	686.1	--	--	103.3
	1.4	nsp	nsp	11.9
A8	685.8	--	169.3	102.5
	2.1	nsp	0.9	6.0
D9	686.5	--	--	103.5
	0.8	nsp	nsp	22.0
A10	686.2	400.0	--	103.3
	1.5	0.8	nsp	13.6
E11	--	--	--	103.7
	nsp	nsp	nsp	34.0
D12	685.8	--	169.6	102.5
	1.5	nsp	0.5	3.5
G6	688.0	--	--	103.5
	2.7	nsp	nsp	14.1
H9	686.2	--	169.7	103.0
	1.5	nsp	0.9	12.0

*nsp-no significant peak

TABLE 4.28: SECOND XPS ANALYSIS OF 6061-T6 ALUMINUM PORTION OF LDEF TRAY CLAMPS.

SAMPLE	Al 2p	C 1s	O 1s	Na 1s
Control (eV)	74.6	285.0	532.1	--
(%)	15.3	54.5	27.5	nsp*
F1	74.6	285.0	532.2	1072.8
	23.6	18.1	48.7	1.2
F2	74.6	285.0	532.3	1072.8
	16.5	28.3	44.3	0.6
E3	74.6	285.0	532.2	1072.8
	21.6	25.9	42.1	0.8
B4	74.6	285.0	532.4	1072.7
	15.2	28.7	47.4	0.7
B5	74.6	285.0	532.0	1072.9
	21.4	20.9	49.0	1.4
C6	74.6	285.0	532.5	1072.8
	12.3	40.0	39.7	0.8
D7	74.6	285.0	532.4	1072.8
	16.4	20.8	50.2	0.5
A8	74.6	285.0	532.5	1072.7
	18.1	24.3	47.6	2.6
D9	74.8	285.0	533.1	1072.8
	4.7	27.6	45.7	0.6
A10	74.6	285.0	532.6	--
	5.9	28.2	47.4	nsp
E11	74.6	285.0	533.2	--
	10.0	20.5	54.0	nsp
D12	74.6	285.0	532.5	1072.5
	21.0	24.7	47.4	0.8
G6	74.6	285.0	532.8	1072.9
	4.7	52.1	48.8	0.8
H9	74.6	285.0	533.3	--
	11.0	34.4	46.4	nsp

*nsp-no significant peak

TABLE 4.28: SECOND XPS ANALYSIS OF 6061-T6 ALUMINUM PORTION OF LDEF TRAY CLAMPS.

SAMPLE	F 1s	N 1s	S 2p	Si 2p
Control (eV)	--	399.9	--	102.5
(%)	nsp*	1.2	nsp	1.5
F1	686.0	--	--	102.5
	3.4	nsp	nsp	5.0
F2	686.1	--	169.7	102.5
	1.5	nsp	1.0	7.8
E3	--	400.0	169.7	102.5
	nsp	0.6	1.0	8.0
B4	--	400.0	169.6	102.5
	nsp	0.9	0.7	6.3
B5	685.9	399.8	169.5	102.5
	1.4	1.3	0.6	4.0
C6	687.0	400.1	169.4	102.5
	1.9	1.4	0.6	3.3
D7	686.3	--	--	102.5
	1.6	nsp	nsp	10.5
A8	686.2	--	169.5	102.7
	1.4	nsp	0.8	5.2
D9	--	--	--	103.5
	nsp	nsp	nsp	21.4
A10	686.1	--	--	103.5
	2.1	nsp	nsp	16.4
E11	686.1	--	--	103.6
	1.0	nsp	nsp	14.5
D12	686.4	399.9	169.7	102.5
	1.6	1.0	0.8	2.7
G6	687.9	400.1	169.6	103.0
	1.9	2.4	0.7	7.3
H9	687.4	399.8	--	103.1
	1.6	1.2	nsp	9.8

*nsp-no significant peak

well documented for metal oxides [87]. The adsorption of adventitious carbon contamination from the atmosphere is typically due to carbon-oxygen contamination. Thus, an increase in the oxygen content should be observed for the second XPS run. Indeed, an increase in oxygen content was observed for 11 of the 15 tray clamps for the second XPS run.

The difference observed in the atomic concentrations of aluminum, carbon and oxygen from the two XPS runs, is due in part to the fact that two different pieces of aluminum were used. However, the large discrepancy is believed to the result of adsorption of vary amounts of adventitious carbon from the atmosphere. This conclusion can be supported by the decrease in the aluminum content with the subsequent increase in both the carbon and oxygen contents as determined by the second XPS runs.

When comparing the silicon content for the two XPS runs, the trend of higher or lower content is not as clear cut as the trends observed for the aluminum, carbon and oxygen. Nine of the 15 tray clamps contained a higher silicon content as determined by the first XPS run. Although extensive silicon contamination has been reported for LDEF materials [22-30], silicon is not believed to be a continuing contaminant, like carbon-containing organic compounds, which would accumulate since the time of recovery. The atomic concentrations of silicon as determined by the two XPS runs are in good

agreement with one another. The XPS runs clearly demonstrate the amount of silicon present not only varies for different tray clamps but also for different regions on the same clamp. Figure 4.30 is a schematic picture of the 6061-T6 aluminum surface illustrating the types of contamination present. Figure 4.30 also reiterates the "patches" mechanism of silicon contamination which was observed for the Kapton and FEP polymer samples discussed in Section IV A1 and IV A5 above.

Small amounts of sodium, nitrogen and sulfur contamination were present on the majority of the flight samples. The approximate binding energies of the sodium, nitrogen, and sulfur detected on the tray clamps were 1072.6 eV, 400.0 eV and 169.8 eV, respectively. The amount of this contamination was fairly consistent for the two XPS runs but the source of this contamination is unknown. Low-levels of nitrogen have been reported on LDEF materials [22-30]. The source of the nitrogen contamination is unknown.

The fluorine contamination detected on the flight samples, except for B5, G6, and H9, is in the form of inorganic fluorine, (fluoride), with a binding energy of approximately 686 eV. In contrast, the binding energy of fluorine in a fluoropolymer is approximately 689 eV [68]. The fluorine binding energy of tray clamps B5, G6 and H9, is approximately 687.5 eV which is between the values for the organo- and inorgano- states. The functionality of the

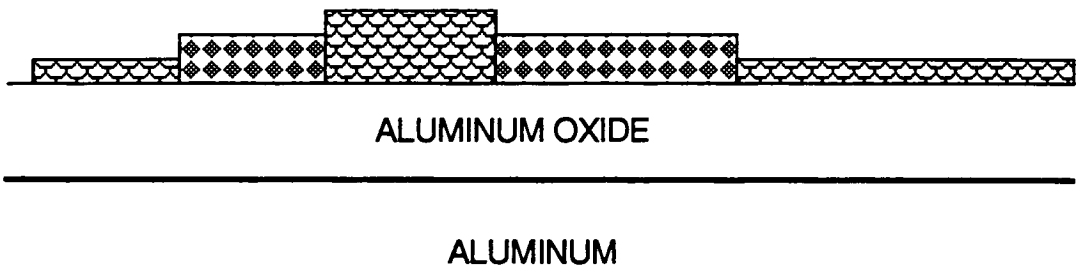

FIGURE 4.30: SCHEMATIC PICTURE OF 6061-T6 ALUMINUM SURFACE.

fluorine detected on theses three flight samples was not determined.

The fact that fluorine contamination was not detected on the control sample suggest the fluorine detected on the flight samples was deposited as a result of environmental exposure. The fluorine contamination present in the ion form may be a result of the degradation effects of ultraviolet radiation on the carbon-fluorine bond of fluoropolymers, such as fluoroethylene propylene, on the backside of the satellite.

The second XPS run provided a an "average" atomic composition for the aluminum surface. Simple comparison of atomic concentrations for separate XPS runs nearly one year apart, demonstrates the need for immediate post-flight analysis to clearly ascertain the effect of the low-Earth orbit environment on materials. It should be noted that most of the carbon-containing contamination present on the tray clamps probably occurred within minutes of exposure of the LDEF to the laboratory environment.

The first XPS run, Table 4.27, will be used to compare and contrast the atomic compositions of the tray clamps with respect to position. The largest amount (55%) of carbon-containing organic contamination was detected on the control sample. However, significant quantities of this same contamination were found on all of the tray clamps, except E11. Figure 4.31 illustrates the higher level of carbon-

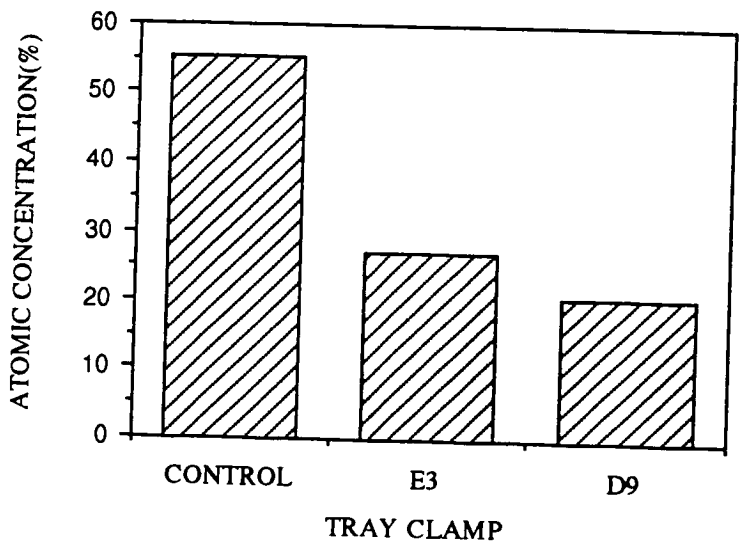

FIGURE 4.31: COMPARISON OF CARBON CONTENT OF 6061-T6 ALUMINUM PORTION ON LDEF TRAY CLAMPS.

containing organic contamination present on the control as compared to the trailing edge and leading edge tray clamps.

The curve-fit carbon 1s photopeaks for the control, trailing edge (E3) and leading edge (D9) tray clamps are shown in Figure 4.32. The curve-fit carbon 1s photopeaks for the three samples are identical. Figure 4.32 is also representative of the other samples. The curve-fit carbon 1s regions exhibit identical hydrocarbon and carbon-oxygen functionality. The similarities in the carbon 1s curve fit region, for the control as well as the flight samples, supports the conclusion that most of the carbon contamination was probably a result of adsorption of adventitious carbon from the atmosphere. As can be seen from Table 4.28, there is no discernible correlation of the surface atomic concentration of carbon with clamp position. The carbon contamination, as determined by XPS, is indicative of a hydrophobic surface and is consistent with the measured high water contact angles.

The binding energy of the aluminum 2p photopeak, 74.6 eV, is characteristic of aluminum oxide. The amount of aluminum content varied from sample to sample. For example, the largest amount of aluminum, (28.7%), was detected on tray clamp F1, while no measurable aluminum signal was obtained for tray clamp E11. The fact that the average atomic concentration of aluminum, for the 14 tray clamps, is only about 20% is prima facie evidence that an ultra-thin

C-3

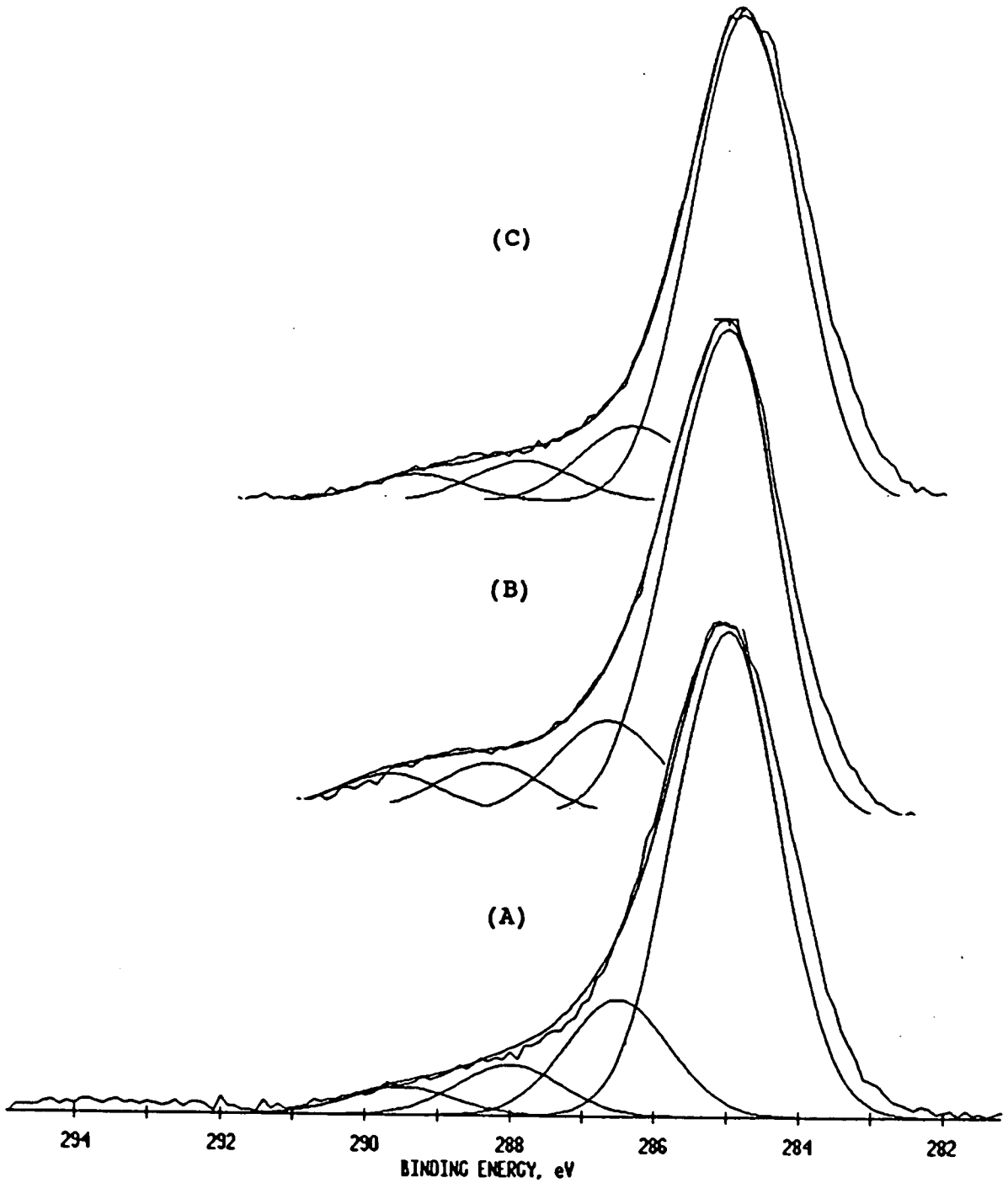

FIGURE 4.32: COMPARISON OF CARBON 1s CURVE FIT REGION OF 6061-T6 ALUMINUM PORTION OF (A) CONTROL (B) E3-TRAILING EDGE (C) D9-LEADING EDGE TRAY CLAMPS.

contamination layer covers the aluminum oxide surface. Except for tray clamp E11, the thickness of the carbon and silicone contamination layer combined cannot be more than 5 nm otherwise no aluminum signal would be detected. Although the amount of aluminum detected varied with location, no correlation of surface atomic concentration with clamp position could be determined.

An increase in oxygen content was observed for all the flight samples with respect to the control. The oxygen content varied from sample to sample. As shown by the carbon 1s curve fit analysis, a portion of the oxygen content is associated with carbon. It is also recognized from the binding energy that some of the oxygen is associated with silicon.

Small amounts of sodium contamination were detected on the control and the majority of the flight samples. The average binding energy of the sodium detected is approximately 1072.8 eV. The binding energy is characteristic of the sodium ion. Although a slightly higher binding energy was observed for the flight samples with respect to the control, the shift is not great enough to ascertain if a change in the state of sodium occurred. The source of this contamination is unknown and is believed to be independent of position.

Fluorine contamination was not detected on the control, E3, or E11. The contamination at first would appear to be

independent of location. The range of fluorine content on the flight samples is 0.8% to 3.4%. Several FEP thermal blankets were housed in experimental trays on the LDEF. Hemminger [42] lists the location of 19 FEP samples on the LDEF. The number of FEP samples varied from row to row. For example, row 1 contained one FEP sample, row 3 contained zero, and row 8 contained three. The rows of the LDEF which housed three FEP samples are 2, 5 and 8. The largest amount of inorganic fluorine contamination, 2.5%, 3.4% and 2.1% was detected on rows 2, 5 and 8, respectively. The tray clamp position for rows 2, 5 and 8 were located on the *same* bays as the FEP thermal blankets. The results suggest that higher levels of fluorine contamination may be observed where fluorine containing materials, particularly FEP, were located nearby.

The largest amount (1.7%) of nitrogen contamination was detected on the control sample. Six out of the 14 flight samples contained nitrogen contamination. With the exception of tray clamp A10, nitrogen contamination was detected on the near trailing and trailing edge tray clamps, rows 2, 3, 4, 5 and 6. The fact that the nitrogen was detected predominately on the near trailing and trailing edge samples would suggest the nitrogen contamination was position dependent but the source of this nitrogen is unknown.

Small amounts of sulfur were detected on the control and 9 of the 14 flight samples. The average binding energy of the

sulfur detected on the control and flight samples is approximately 169.6 eV. The binding energy is indicative of inorganic sulfur. The source of this contamination is unknown and is believed to be independent of position.

Silicon contamination was detected on all flight tray clamps as well as the control. However, the silicon content of all flight samples exceeded that of the control sample from 4 to 16 times. Thus, the silicon contamination detected on the tray clamps further supports the extensive silicon contamination reported already for LDEF materials [22-30]. The average silicon content was 13.6% for the near leading and leading edge tray clamps, D7, A8, D9, A10 and E11. The average silicon content was 5.9% for the near trailing and trailing edge tray clamps, F2, E3, B4, B5 and C6. The increase in the silicon content from the control trailing and leading edge samples are shown in Figure 4.33. The results suggest a higher level of silicon on the near leading and leading edge tray clamps as opposed to the near trailing and trailing edge tray clamps. Several LDEF investigators have reported higher levels of silicon contamination, utilizing XPS and IR measurements, for samples located on the leading edge of the LDEF [22-30]. However, these are the first results which definitely establish a higher level of silicon contamination for materials on the near leading edge and leading edge compared to the near trailing edge and trailing

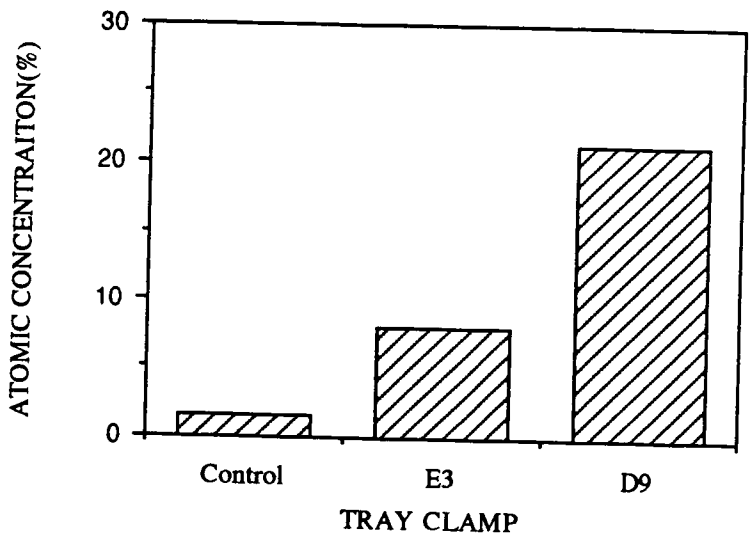

FIGURE 4.33: COMPARISON OF SILICON CONTENT OF 6061-T6 ALUMINUM PORTION ON LDEF TRAY CLAMPS.

edge of the LDEF.

A definitive shift in the binding energy of silicon is observed for tray clamps receiving a higher atomic oxygen fluence compared to tray clamps receiving a lower atomic oxygen fluence. The average silicon 2p binding energy for the near trailing edge tray clamps is approximately 102.5 eV. The average silicon 2p binding energy of the near leading and leading edge tray clamps is approximately 103.5 eV. This definitive shift in binding energy correlates to a change in state of the silicon contamination. The binding energy of the silicon contamination present on the control, near trailing, and trailing edge samples is indicative of organo-silicon. The binding energy of the silicon contamination present on the near leading and leading edge samples by contrast is indicative of inorgano-silicon or a silicate type of material. The XPS results suggest not only a higher content of silicon contamination is present on the near leading and leading edge tray clamps but also the type of silicon contamination is different. These are the first results which revealed that the type of silicon contamination present (organic as opposed to inorganic) was dependent upon position on the LDEF.

Four XPS runs were performed on the aluminum portion of tray clamp D9 to evaluate the consistency in the atomic composition. The XPS runs were performed on a sample with dimensions of 13 mm x 13 mm. The XPS results are shown in

Figure 4.34. Figure 4.34 clearly illustrates the atomic composition of the four regions of tray clamp D9 are fairly consistent with one another. The highest levels of silicon and oxygen contents were determined for region 1. The lowest levels of carbon and aluminum contents were also determined for region 1. Region 4 by contrast the exact opposite trend for the silicon, oxygen, carbon and aluminum contents. The XPS results of the tray clamp D9 suggest that a higher level of silicon is accompanied by a higher level of oxygen but lower levels of carbon and aluminum. The binding energy of silicon for the four regions is 103.5 eV which is characteristic of the inorganic form or an SiO_x type of material and thus further supporting the higher levels of oxygen contents determined for the tray clamps located on the near leading and leading edge of the LDEF. The overall atomic composition of the four runs are also consistent with the previous XPS runs (see Tables 4.27 and 4.28) which were performed on separate pieces of tray clamp D9.

2. A276 Thermal Control Paint - White

The surface characterization of the A276 white thermal control paint described in the Experimental chapter is discussed in this section. XPS was the surface tool used to characterize changes that occurred as a result of exposure to the low-Earth environment. Golden [91] has characterized the

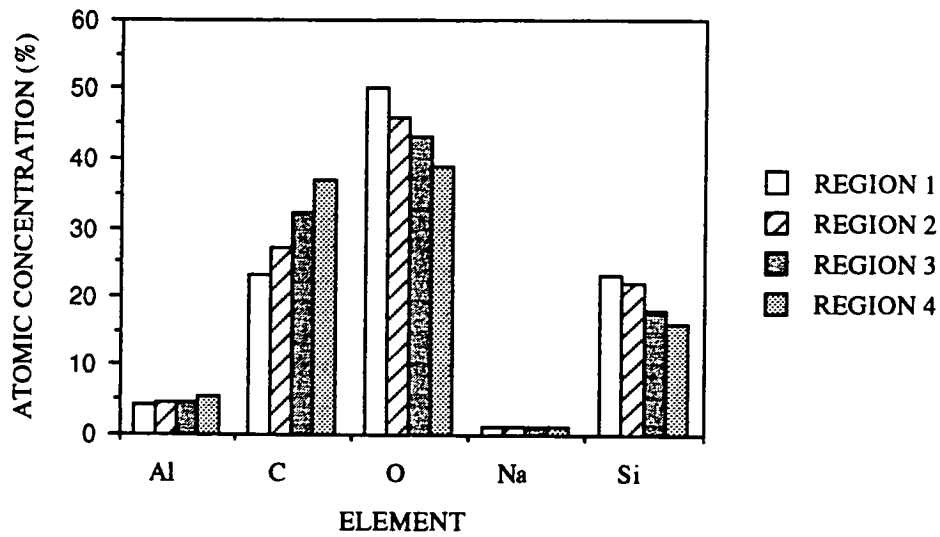

FIGURE 4.34: COMPARISON OF ATOMIC COMPOSITION OF 6061-T6 ALUMINUM PORTION OF LDEF TRAY CLAMP D9.

space environmental effects on the A276 white thermal control paint utilizing XPS, IR, solar and thermal emittance measurements.

The A276 white thermal control paints exhibited degrees of discoloration as a direct result of the LEO environment. The A276 paint on the Earth end, near leading, and leading edge samples remained white. The A276 paint on the space end, near trailing, and trailing edge samples was discolored. Thus, the discoloration observed for the A276 paint is position dependent. Golden [91] concluded the brown discoloration was largely due to the degradation of the top organic layer or surface resin of the paint as a result of ultraviolet radiation exposure. Golden [91] concluded that the polyurethane binder for the near leading and leading edge samples was eroded by atomic oxygen, leaving the titanium dioxide pigment exposed.

The XPS results for the A276 white paint are shown in Table 4.29. The elements detected on the control sample are consistent with the chemical components of a polyurethane based paint. The organic silicon observed on the control sample was expected as silicon is part of the pigment system [91]. Small amounts of aluminum may be the result of aluminum particles used in the formulation of the paint.

The largest amount (67.0%) of carbon was detected on the control sample. All flight samples showed a decrease in

TABLE 4.29: XPS ANALYSIS OF A276 WHITE PORTION OF LDEF TRAY CLAMPS.

SAMPLE	C 1s	O 1s	Na 1s	F 1s	N 1s	Si 2p
Control (eV)	285.0	532.7	--	--	400.0	102.5
(%)	67.0	22.5	nsp*	nsp	2.6	7.1
F1	285.0	532.9	1073.2	--	400.0	103.1
	34.4	44.5	0.2	nsp	1.1	15.8
F2	285.0	533.2	--	--	400.0	103.5
	51.3	35.1	nsp	nsp	1.9	11.0
E3	285.0	532.9	1072.8	689.5	400.4	103.1
	54.7	32.3	0.5	1.0	2.5	8.5
B4	285.0	533.0	1072.8	689.2	400.4	103.2
	48.7	35.5	0.3	0.4	2.0	11.9
B5	285.0	532.8	--	689.1	400.3	103.1
	63.9	27.5	nsp	1.5	1.5	5.0
C6	285.0	533.6	1073.7	686.5	399.8	103.9
	47.4	34.9	0.7	0.8	1.3	11.1
D7	285.0	532.7	1073.0	685.9	400.3	103.5
	15.2	51.8	0.4	1.7	0.7	24.7
A8	285.0	534.3	--	687.5	399.3	104.6
	40.5	40.9	nsp	0.6	14.0	14.0
D9	285.0	533.2	--	--	400.1	103.5
	28.8	46.3	nsp	nsp	1.6	21.7
A10	285.0	532.6	1072.9	686.0	399.9	102.9
	25.5	47.3	0.5	1.7	1.3	18.5
E11	285.0	533.7	--	687.0	399.8	103.9
	45.3	35.1	nsp	1.5	1.8	13.4
D12	285.0	532.9	--	686.1	400.1	103.1
	23.7	49.8	nsp	1.2	1.2	19.2
G6	285.0	532.8	1072.9	--	399.9	103.0
	25.7	48.8	0.8	nsp	1.1	18.7
H9	285.0	533.3	--	--	400.0	103.6
	31.7	46.4	nsp	nsp	1.0	19.4

*nsp-no significant peak

TABLE 4.29: XPS ANALYSIS OF A276 WHITE PAINT PORTION OF LDEF TRAY CLAMPS.

SAMPLE	Al 2p	Sn 3d5	Ti 2p
Control (eV)	74.6	--	--
(%)	0.8	nsp*	nsp
F1	74.9	--	--
	4.0	nsp	nsp
F2	74.6	--	--
	0.7	nsp	nsp
E3	72.6, 74.5	487.4, 495.9	--
	0.4	0.1	nsp
B4	72.2, 74.6	--	--
	0.9	nsp	nsp
B5	74.6	--	--
	0.6	nsp	nsp
C6	73.7, 75.5	488.0, 496.4	--
	3.6	0.2	nsp
D7	74.5	487.2, 495.7	459.2, 464.8
	4.9	0.2	0.4
A8	76.0	--	460.7, 466.1
	2.8	nsp	0.2
D9	74.6	--	--
	1.6	nsp	nsp
A10	74.4	--	459.4, 464.9
	4.8	nsp	0.4
E11	75.6	--	--
	2.9	nsp	nsp
D12	74.6	--	459.2, 465.0
	4.5	nsp	0.4
G6	74.5	487.2, 495.7	459.0, 464.8
	4.5	0.2	0.2
H9	74.8	487.4, 496.0	--
	1.3	0.2	nsp

*nsp-no significant peak

carbon content. Figure 4.35 illustrates the trend of decreasing carbon content for the control, trailing, and leading edge tray clamps. These three samples were chosen as they represent the three extremes of the 15 tray clamps. Figure 4.35 clearly illustrates the position dependence on the surface atomic concentration of carbon for the A276 white paint.

The curve-fit carbon 1s region of the control, trailing and leading edge tray clamps are shown in Figure 4.36. A significant difference is observed in the curve fit analysis. Figure 4.36 shows three different carbon surfaces. The control sample exhibits carbon functionality that is characteristic of the components of a polyurethane based paint. However, the curve-fit carbon 1s curve of the trailing edge tray clamp reveals a modified carbon surface with respect to the control sample. The trailing edge tray clamp contains the same functionality as the control except for the addition of a peak corresponding to carbon doubly bonded to oxygen. The curve fit analysis of the trailing edge tray clamp is consistent with IR spectra which revealed a modified surface [91] thus, supporting the curve fit analysis. The modified surface is believed to be a result of the degradation induced by ultraviolet radiation [91].

The leading edge tray clamp revealed a carbon surface which has been oxidized. The major component under the carbon

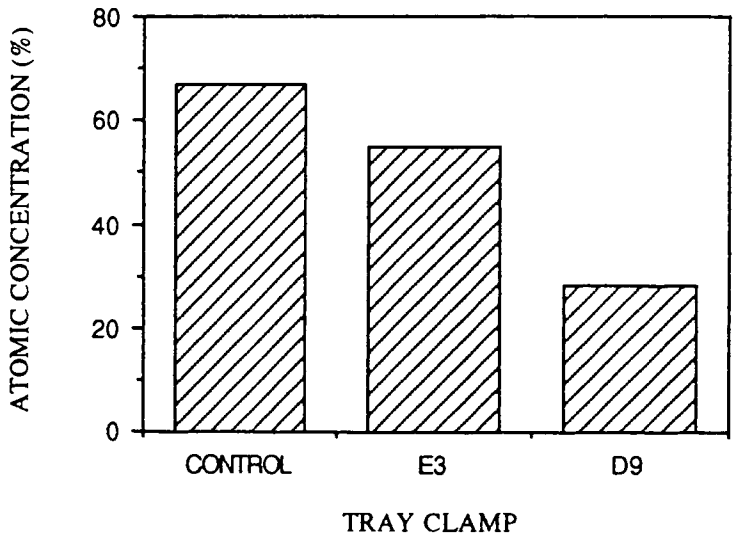

FIGURE 4.35: COMPARISON OF CARBON CONTENT OF A276 WHITE PAINT PORTION OF LDEF TRAY CLAMPS.

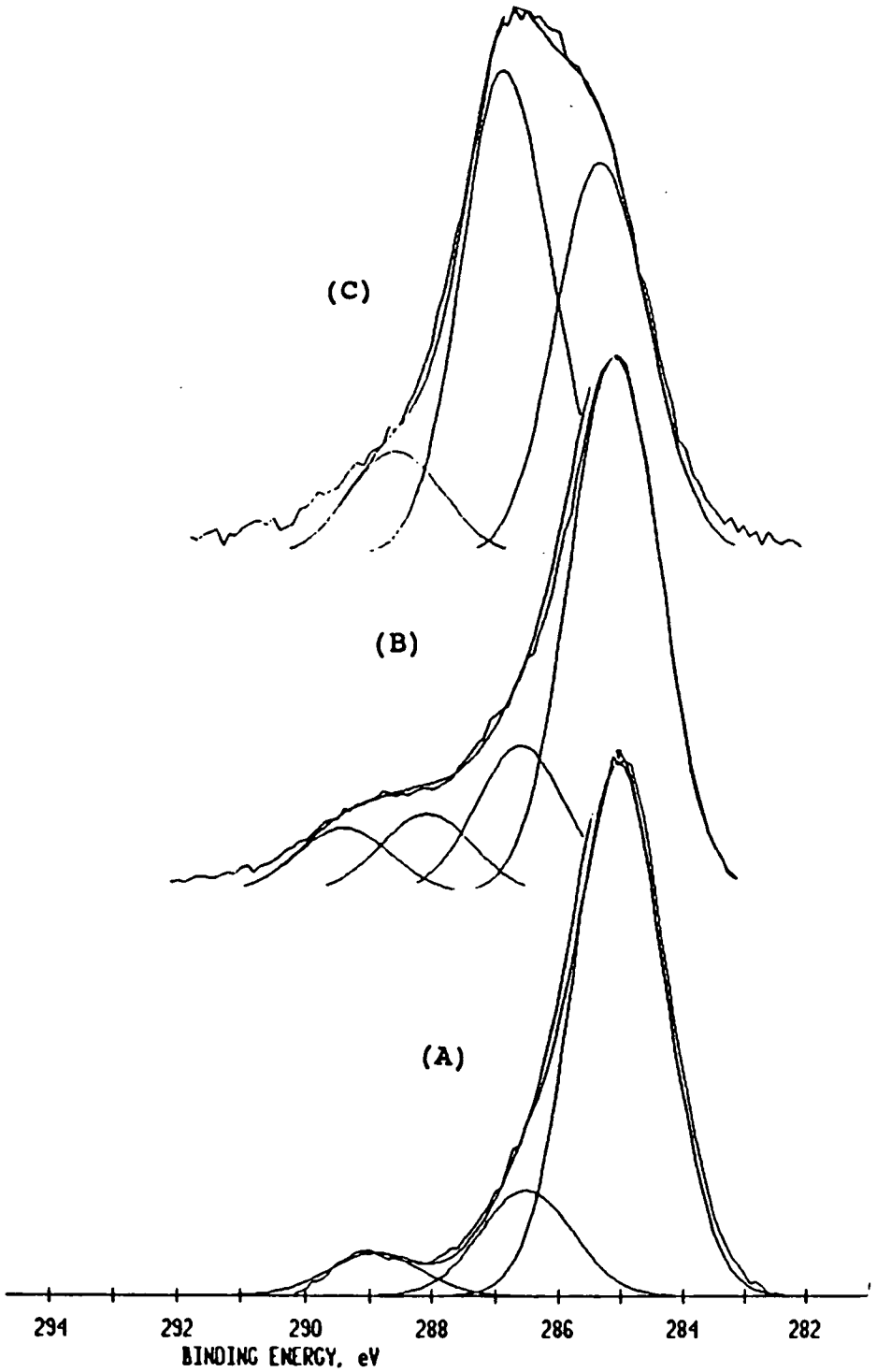

FIGURE 4.36: COMPARISON OF CARBON 1s CURVE FIT REGION OF A276 WHITE PAINT PORTION OF (A) CONTROL (B) E3-TRAILING EDGE (C) D9-LEADING EDGE TRAY CLAMPS.

1s envelope is carbon-oxygen functionality. Unlike the trailing edge sample, the urethane functionality is not present for the leading edge sample. The curve fit analysis of the leading edge tray clamp is consistent with Golden's [91] IR measurements which revealed an oxygen-rich surface. The XPS results suggest that the higher atomic oxygen fluence for the leading edge eroded the surface resin of the paint. Thus the position dependence of the A276 paint was clearly demonstrated by significant changes in the atomic composition as well as the surface chemistry of the carbon content seen in the XPS results.

An increase in oxygen content was observed for all flight samples with respect to the control. Figure 4.37 illustrates the trend of increasing oxygen content for the control, trailing and leading edge samples. The increase in oxygen content is also consistent with the increase in carbon-oxygen functionality as shown in Figure 4.36. The increase in oxygen content is believed to be associated primarily with silicon.

Trace amounts of sodium contamination were detected on half of the flight samples. The average binding energy of the sodium is approximately 1073.0 eV. The binding energy of the sodium is characteristic of the sodium ion. The fact that sodium was not detected on the control sample indicates that sodium may be a result of environmental exposure. However, sodium was detected on the control 6061-T6 aluminum portion of

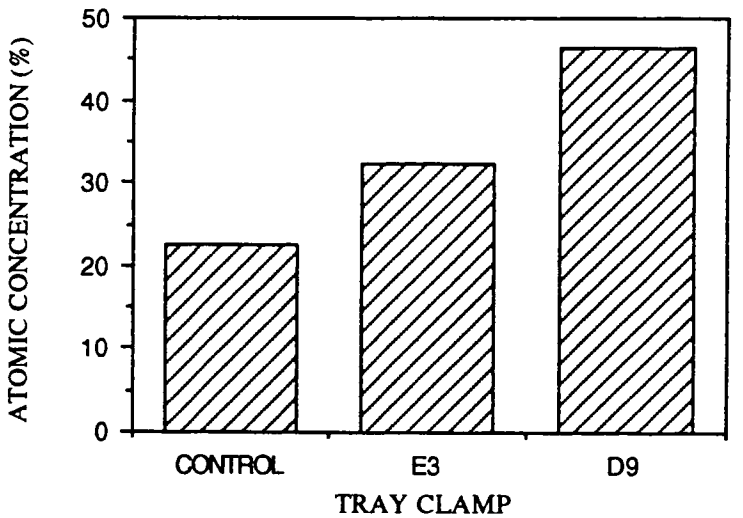

FIGURE 4.37: COMPARISON OF OXYGEN CONTENT OF A276 WHITE PAINT PORTION OF LDEF TRAY CLAMPS.

the tray clamp as well as the majority of the flight samples. The source of the sodium contamination is unknown.

Small quantities of fluorine contamination were detected on 9 of the 15 tray clamps. Fluorine contamination was not detected on the control and, therefore, is believed to be the result of environmental exposure. The average fluorine contamination detected on the flight samples was 1.6%. The binding energies of the near trailing and trailing edge samples, (E3, B4, and B5), are indicative of a carbon-fluorine bond, whereas, the binding energies for the other samples are indicative of the fluorine ion. The XPS results suggest that fluorine contamination detected on the A276 white paint is position dependent with respect to the state or form of the contamination. Fluorine contamination was also detected on the 6061-T6 aluminum surfaces of the tray clamps (see section above). However, the fluorine contamination on the 6061-T6 aluminum surface was predominately the fluoride ion. The largest amount of fluorine contamination for the 6061-T6 surface was detected on rows 2, 5 and 8. However, the largest amount of fluorine contamination for the A276 white paint was detected on rows 5, 7 and 10. The XPS results of the 6061-T6 portions of the tray clamps suggest that higher levels of fluorine may be detected on clamps near where FEP thermal blankets were located. On the other hand, the XPS results of the A276 portion of the clamps suggest the fluorine

contamination was independent of position of the clamp with respect to the FEP thermal blankets. Collectively, the XPS results demonstrate the fluorine contamination was not a direct line of sight mechanism as suggested by Golden [91].

Small amounts of nitrogen were detected on the control and all of the flight samples. Nitrogen is a component of the binder used in the A276 paint. A small decrease in nitrogen content was observed for all the flight samples with respect to the control. The atomic concentration of the nitrogen appears to be independent of position. The nitrogen detected on the flight samples may be part of the binder system or deposited contamination. However, 1.6% nitrogen was detected on tray clamp D9. Thus, the source of the nitrogen content detected on the flight samples is difficult to ascertain whether it is the result of deposited contamination or part of the paint system.

Silicon contamination was detected on all the flight tray clamps as well as the control. Organo-silicon was detected on the control. A mixture of inorgano and organo silicon contamination was detected on the flight samples. Unlike the 6061-T6 aluminum, the binding energy of the silicon is between what is typically characterized as organic as opposed to inorganic. Mallon [75] reported similar binding energies for silicon detected on composite samples. Mallon [75] concluded the silicon detected on the samples was predominately a

mixture of silicone/silicate/silica, based on the measured binding energy for the silicon 2p photopeak. The binding energy of the silicon present on the A276 white paint would like wise suggest the silicon is a mixture of silicone/silicate/silica contamination. Figure 4.38 illustrates the trend of increasing silicon content for the control, trailing and leading edge sample. The average silicon content detected on the near leading and leading edge sample was 18.5%. Only 9.5% was detected on the near trailing and trailing edge samples. The XPS results supports the trend of higher silicon deposition on the near leading and leading edge of the LDEF. This trend of higher silicon contamination of the A276 white paint is consistent with the 6061-T6 aluminum portion of the tray clamps.

Small amounts of aluminum were detected on the control as well as the flight sample. The binding energy for the majority of flight samples as well as the control is characteristic of aluminum oxide. However, as shown in Table 4.29, two binding energies are listed for the aluminum 2p photopeak for tray clamps E3, B4 and C6. The lower binding energy is characteristic of the elemental aluminum [92]. The atomic concentration of aluminum appears to be independent of position. Trace amounts of tin and titanium were detected on several tray clamps. The binding energies are indicative of the metal oxides. Tin and titanium are characterized by two

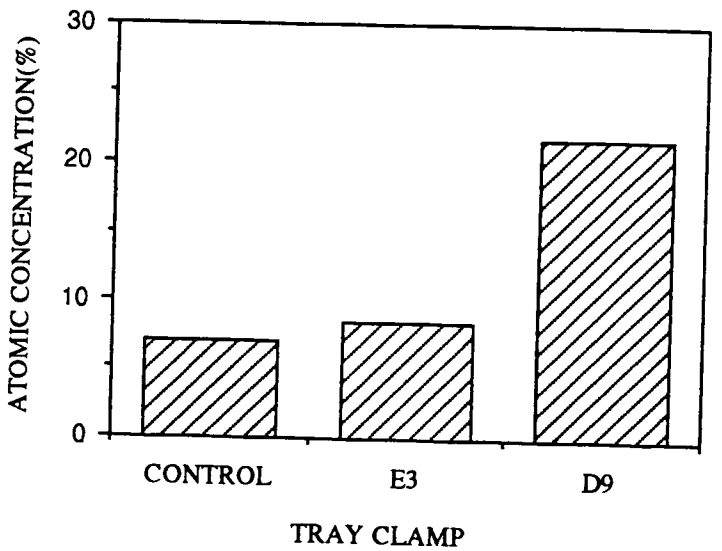

FIGURE 4.38: COMPARISON OF SILICON CONTENT OF A276 WHITE PAINT PORTION OF LDEF TRAY CLAMPS.

photopeaks with a 8.5 eV and 5.7 eV difference between the $3d_{3/2}$, $3d_{5/2}$ and $2p_{1/2}$, $2p_{3/2}$ peaks, respectively. The tin on the flight samples appears to be independent of position. The titanium was predominately on the near leading edge and Earth end samples of the LDEF. Golden [91] utilizing SEM measurements has reported titanium on the leading edge A276 white paint samples. These results support a mechanism of erosion of the binder by atomic oxygen exposing the titanium pigment within the paint. No measurable titanium signal was obtained on the leading edge sample. However, the titanium present may have been covered by the silicon contamination. The fact that titanium was only detected on the near leading edge samples supports Golden's [91] conclusion that the binder was eroded away by atomic oxygen.

3. Z306 Thermal Control Paint - Black

The surface characterization of the Z306 black thermal control paint described in the Experimental chapter is discussed in this section. XPS was the surface tool used to characterize changes that occurred as a result of the low-Earth environment. Golden [93] characterized the changes observed in the Z306 black paint utilizing XPS and IR measurements.

The Z306 black thermal control paint appeared faded as a

direct result of the low-Earth orbit environment. The Z306 black paint on the near leading and leading edge samples were occasionally eroded down to the red primer (see Figure 3.1). The Z306 black paint on the space and Earth end, near trailing and trailing edge samples appeared unaffected. Thus, the discoloration observed for the Z306 paint is position dependent. The XPS results for the Z306 black paint are shown in Table 4.30. The largest amount of carbon (72.9%) was detected on the control sample. All flight samples showed a decrease in carbon content. An average of about 60% carbon was detected on the near trailing and trailing edge samples. By contrast the average carbon content for the near leading and leading edge samples was only 10%. Figure 4.39 illustrates the trend of decreasing carbon content for the control, trailing and leading edge tray clamps. Figure 4.39 clearly illustrates the position dependence on the surface atomic concentration of carbon for the Z306 black paint.

The curve-fit carbon 1s regions of the control, trailing and leading edge tray clamps is shown in Figure 4.40. A significant difference is observed in the curve fit analysis. Figure 4.40 shows three different carbon-containing surfaces. The control sample exhibits carbon functionality that is characteristic of the components of a polyurethane binder. However, the curve-fit carbon 1s curve of the trailing edge tray clamp reveals a modified carbon surface with respect to

TABLE 4.30: XPS ANALYSIS OF Z306 BLACK PAINT PORTION OF LDEF TRAY CLAMPS.

SAMPLE	C 1s	O 1s	F 1s	N 1s	Si 2p
Control (eV)	285.0	532.8	--	400.0	102.5
(%)	72.9	22.7	nsp*	1.7	2.7
F1	285.0	533.1	--	399.9	103.5
	36.3	45.4	nsp	2.1	16.2
F2	285.0	533.2	--	--	103.5
	63.9	25.4	nsp	nsp	10.7
E3	285.0	533.2	689.4	400.0	103.5
	55.8	31.1	0.8	2.4	9.9
B4	285.0	532.9	688.9	400.0	103.5
	52.6	34.7	0.5	2.5	9.6
B5	285.0	533.0	--	--	103.5
	57.6	31.1	nsp	nsp	11.3
C6	285.0	532.8	689.2	400.0	103.5
	63.5	26.3	2.0	3.8	4.4
D7	285.0	533.1	--	--	103.5
	7.2	60.8	nsp	nsp	32.0
A8	285.0	533.1	--	--	103.5
	12.1	57.2	nsp	nsp	30.7
D9	285.0	533.1	--	--	103.5
	8.6	59.1	nsp	nsp	32.3
A10	--	533.1	--	--	103.5
	nsp	55.9	nsp	nsp	32.8
E11	285.0	533.2	--	--	103.5
	9.7	57.0	nsp	nsp	33.3
D12	285.0	533.1	--	--	103.5
	14.9	56.2	nsp	nsp	28.9
G6	285.0	532.9	--	--	103.5
	21.8	37.4	nsp	nsp	26.9
H9	285.0	533.2	--	--	102.3
	35.7	52.8	nsp	nsp	24.2

*nsp-no significant peak

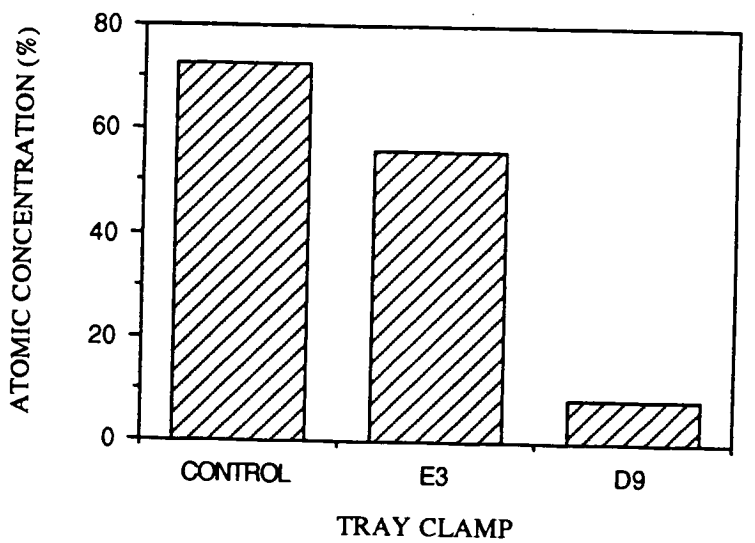

FIGURE 4.39: COMPARISON OF CARBON CONTENT OF Z306 BLACK PAINT PORTION OF LDEF TRAY CLAMPS.

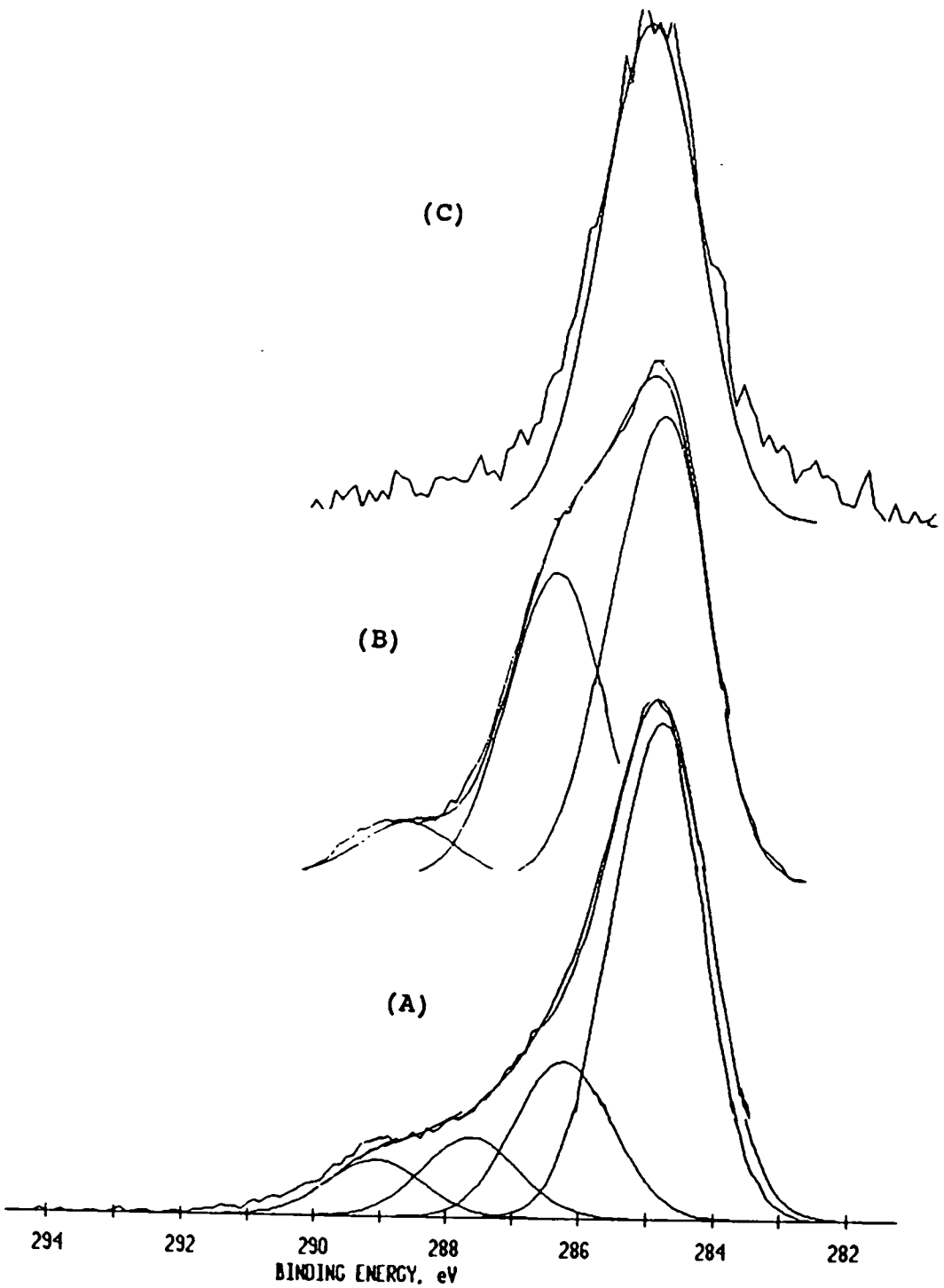

FIGURE 4.40: COMPARISON OF CARBON 1s CURVE FIT REGION OF Z306 BLACK PAINT PORTION OF (A) CONTROL (B) E3-TRAILING EDGE (C) D9-LEADING EDGE TRAY CLAMPS.

the control sample. The curve-fit carbon region of the trailing edge tray clamp (see Fig.4.40B) showed a large increase in the carbon-oxygen functionality.

The curve-fit carbon region of the leading edge tray clamp (see Fig.4.40C) is significantly different than the control as well as the trailing edge sample. The only component under the carbon 1s envelope is assigned to hydrocarbon functionality. Unlike the trailing edge sample, the urethane functionality is not present for the leading edge sample. The XPS result suggests the higher atomic oxygen fluence for the leading edge eroded the black paint to expose the red primer. The XPS results of the Z306 further support the position dependence of the black paint. The position dependence of the Z306 paint was clearly demonstrated by significant changes in the atomic composition as well as the surface chemistry of carbon.

An increase in oxygen content was observed for all flight samples with respect to the control. An average of 30% oxygen was detected on the near trailing and trailing edge samples. An average of 67% oxygen was detected on the near leading and leading edge samples. This trend of increasing oxygen content for the control, trailing and leading edge samples is shown in Figure 4.41. The increase in the oxygen content is believed to be associated with silicon contamination.

Small amounts of nitrogen were detected on the control

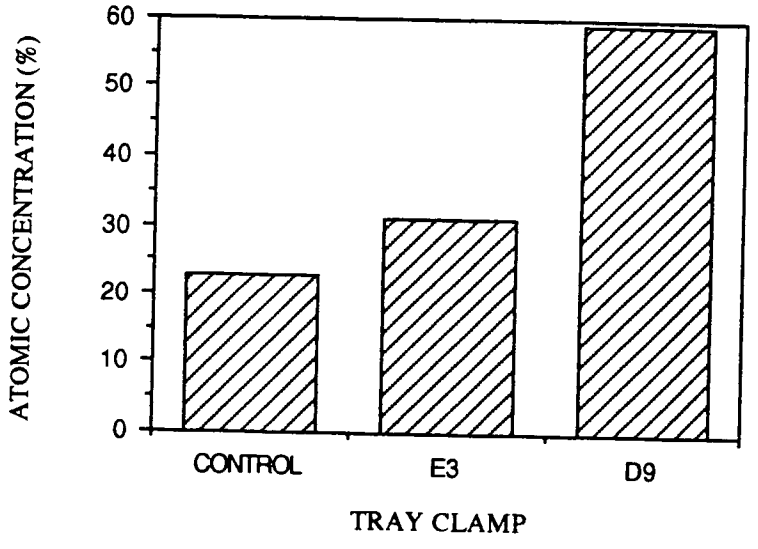

FIGURE 4.41: COMPARISON OF OXYGEN CONTENT OF Z306 BLACK PAINT PORTION OF LDEF TRAY CLAMPS.

and five flight samples. Except for the space end, an increase in the nitrogen content was observed. The nitrogen content appears to be independent of position. The source of the nitrogen detected on the control as well as the flight samples is unknown.

Trace amounts of fluorine were detected on three near trailing edge samples. The binding energy of the fluorine contamination is characteristic of a carbon-fluorine bond. The fact that fluorine was not detected on the control sample suggest the fluorine was deposited as a result of environment exposure. Golden [93] has reported fluorine contamination predominately on samples from the near trailing and trailing edge of the LDEF. The results reported by Golden [93] are consistent with the results present here.

A small amount of organic silicon was detected on the control sample. A significant increase in the silicon content was observed for all flight samples. Unlike the 6061-T6 aluminum and A276 white portion of the tray clamp, all of the silicon contamination detected on the flight samples is inorganic silicon. An average of 9% silicon was detected on the near trailing and trailing edge samples. An average of 32% silicon was detected on the near leading and leading edge samples. The silicon content of the control, trailing and leading edge samples is shown in Figure 4.42. This trend of increasing silicon content is also consistent with the

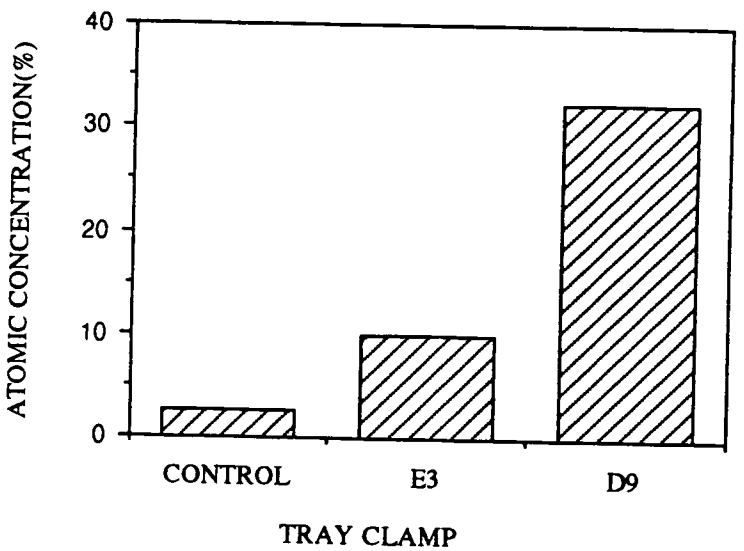

FIGURE 4.42: COMPARISON OF SILICON CONTENT OF Z306 BLACK PAINT PORTION OF LDEF TRAY CLAMPS.

observed increase in the oxygen content. Thus, further supporting the high levels of inorganic silicon contamination detected on the flight samples.

Figures 4.43 through 4.46 are schematic pictures of the possible contamination history of the LDEF tray clamps. The history of the tray clamps were derived from the XPS results (Table 4.27). As shown in Figure 4.43, the 6061-T6 aluminum has a natural oxide on its surface. As a result of the anodic thermal control coating (anodization) a thicker oxide layer was produced. Immediately following the removal of the aluminum from the anodization bath an ultrathin layer of organic contamination adsorbed on the surface. The source of this ultrathin contamination layer is not known. The chemical identity of this contamination is not known. What is known is that it is always found on clean oxide surface and that the thickness does not exceed 5 nm and that the contaminant(s) contain both carbon and oxygen.

Figure 4.44 is the history of the control tray clamp. It is proposed that during the duration of the LDEF flight the control tray clamp continued to facilitate the adsorption of organic contamination from the atmosphere. However, this organic contamination layer did not exceed 5 nm.

Figure 4.45 is the history of the trailing edge tray clamp. During the duration of the LDEF flight predominately organic silicon (Si-C) and carbon (C-O) were the primary

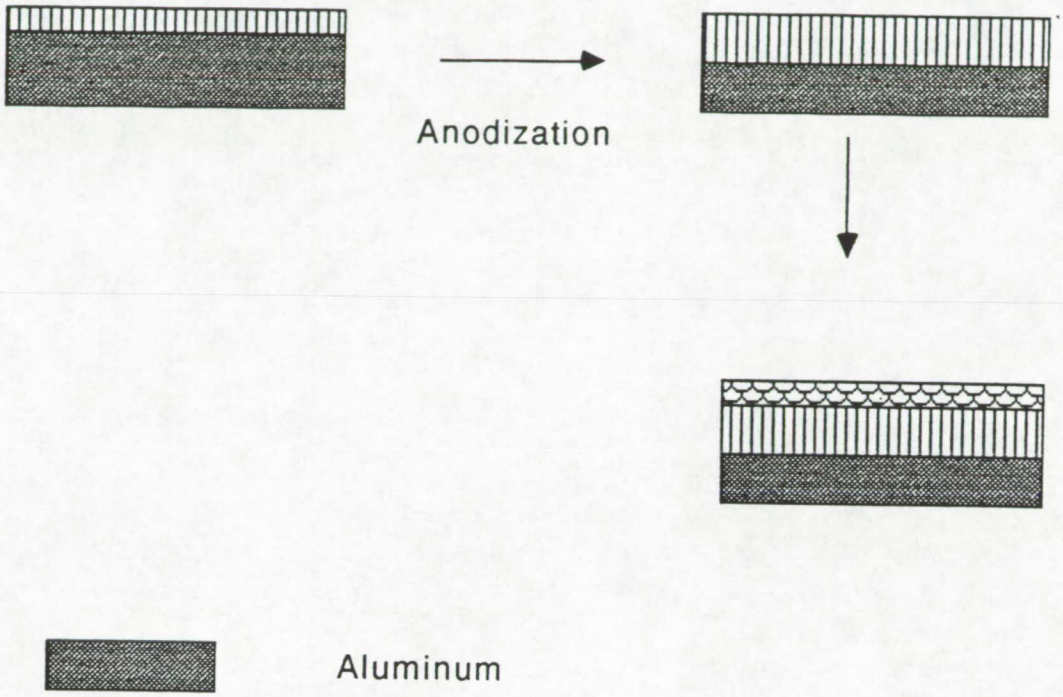

FIGURE 4.43: SCHEMATIC PICTURE OF POSSIBLE CONTAMINATION HISTORY OF LDEF TRAY CLAMPS PRIOR TO LAUNCH.

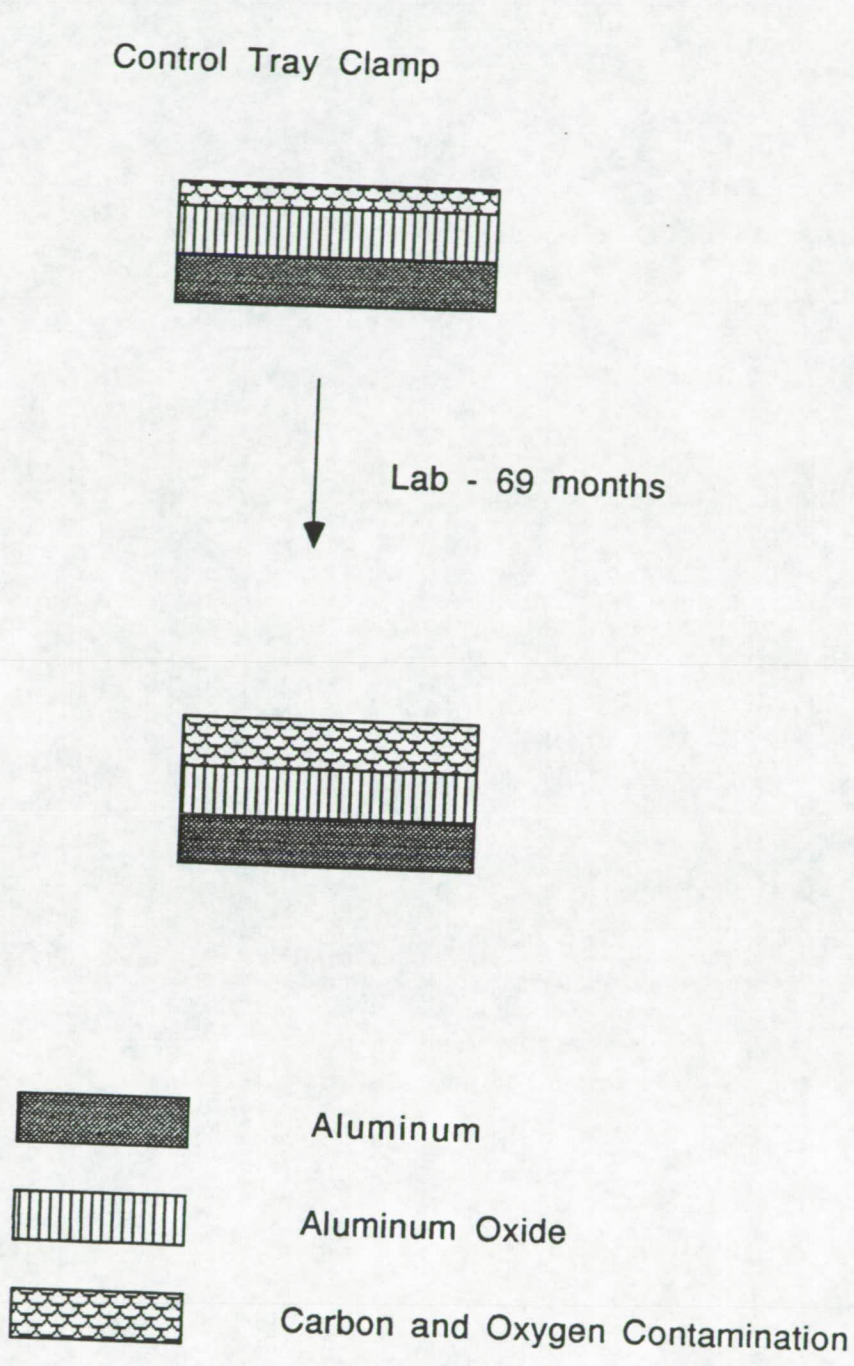

FIGURE 4.44: SCHEMATIC PICTURE OF POSSIBLE CONTAMINATION HISTORY OF CONTROL TRAY CLAMP.

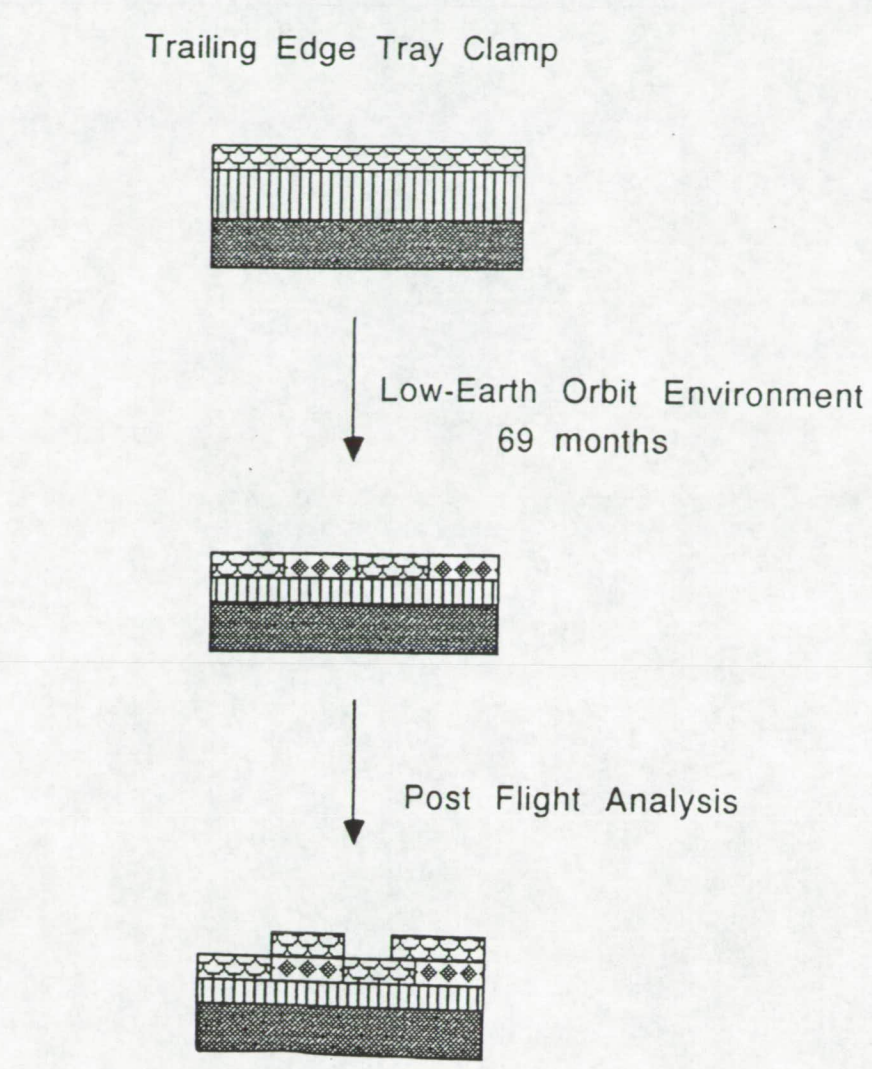

FIGURE 4.45: SCHEMATIC PICTURE OF POSSIBLE CONTAMINATION HISTORY OF E3-TRAILING EDGE TRAY CLAMP.

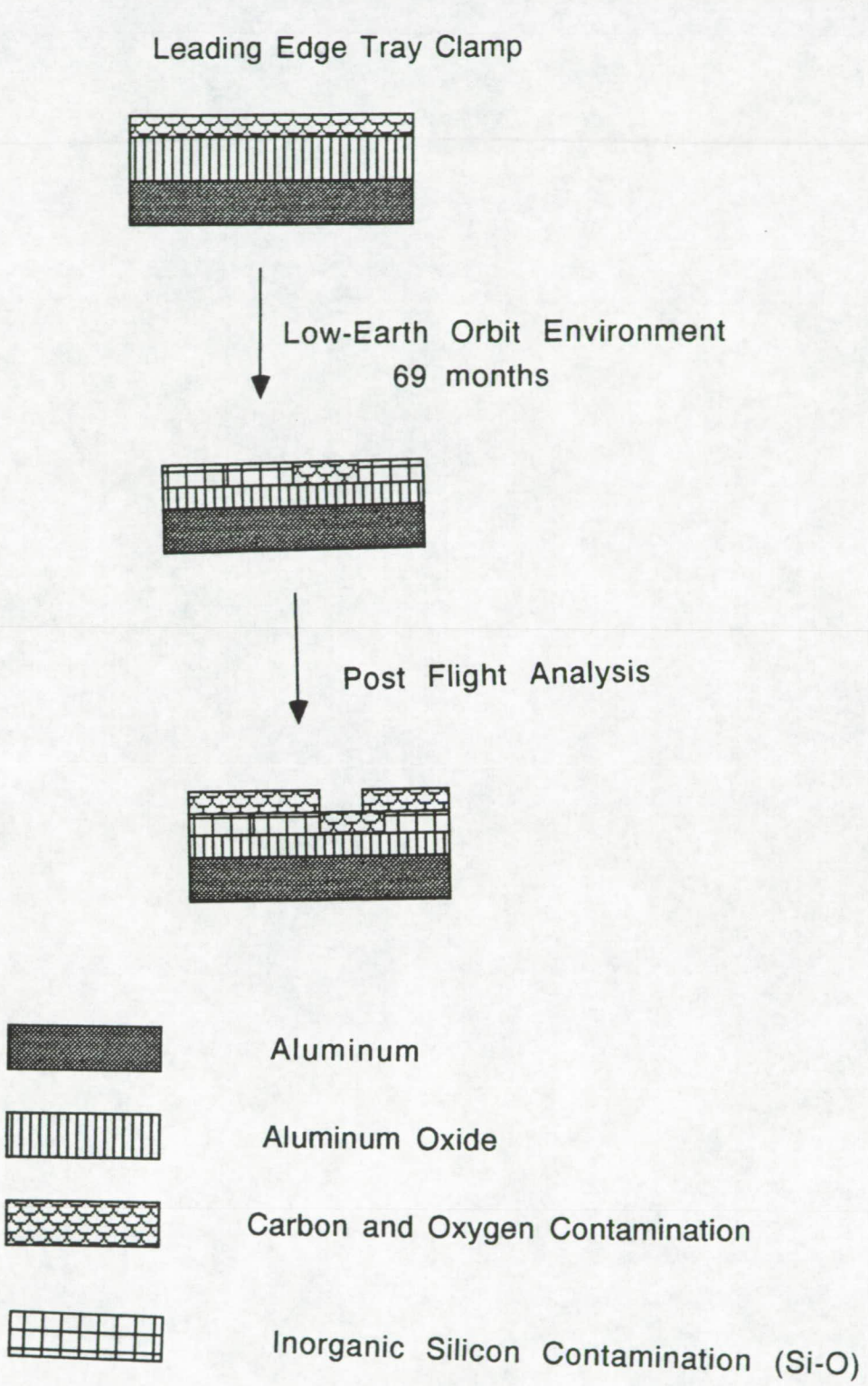

FIGURE 4.46: SCHEMATIC PICTURE OF POSSIBLE CONTAMINATION HISTORY OF D9-LEADING EDGE TRAY CLAMP.

contaminants deposited. Upon retrieval of the LDEF and the time lapse before post flight analysis was performed an ultrathin layer of organic contamination absorbed onto the surface.

Figure 4.46 is the contamination history of the leading edge tray clamp. During the duration of the LDEF flight organic silicon (Si-C) and carbon (C-O) were deposited. The deposited organic silicon (Si-C) contamination was converted to inorganic silicon (Si-O) contamination upon reaction with atomic oxygen. Upon retrieval of the LDEf and the time lapse before post flight analysis was performed an ultrathin layer of organic contamination absorbed onto the surface. The continued absorption of organic contamination for the control, trailing edge, and leading edge tray clamps can be supported by the similarities in the carbon 1s curve fit analysis (see Figure 4.32). Collectively, the XPS results and Figures 4.45 and 4.46 clearly illustrate the position dependence of the LDEF tray clamps.

V. Summary

As stated in the Introduction, the objective of this work was the surface characterization of LDEF materials including polymers, composites, thermal control paints, and aluminum and to correlate the observed changes in the surface composition and surface chemistry of these materials with the low-Earth orbit exposure conditions. Surface-sensitive analytical techniques were utilized to document changes in the surface composition and surface chemistry of these materials.

XPS analysis of the polymer systems, such as Kapton® and the polyimide polysiloxane copolymers, revealed significant changes in both the surface composition and surface chemistry as a direct result of exposure to the low-Earth orbit environment. A common trend among these polymer systems, except for FEP, was an increase in the oxygen and silicon contents with a subsequent decrease in the carbon content. This trend was supported by the carbon 1s curve fit analysis which revealed an increase in the carbon-oxygen functionality and a decrease in hydrocarbon functionality with respect to the control sample. The increase in oxygen content may correspond to surface oxidation of the polymer as a result of exposure to atomic oxygen.

Moderate to high levels of silicon contamination were detected on the majority of polymer systems lending further support to the extensive silicon contamination of LDEF materials reported previously. The state of the silicon contamination, as inferred by the silicon 2p photopeak binding energy, was predominately inorganic silicon or an SiO_x type of contamination for leading edge samples only. The formation of an inorganic silicon contamination or an SiO_x type of material was supported by an increase in both silicon and oxygen contents with subsequent shifts in binding energy of both photopeaks. The state of the silicon contamination, as inferred by the silicon 2p photopeak binding energy, for the near trailing and trailing edge samples was predominately organic silicon.

The FEP polymer samples were unique in that unexpected results with respect to degradation/erosion effects as a function of position on the LDEF, were obtained. Significant changes in the surface composition and surface chemistry were observed for the near trailing edge samples compared to the near leading and leading edge samples. The carbon 1s curve fit analysis clearly illustrated the changes in the surface chemistry as a function of position on the LDEF.

The changes in the carbon 1s region of flight sample C5 were investigated utilizing a low oxygen pressure rf plasma. Oxygen plasma treatment of the control and C8 (near leading

edge) FEP flight samples showed no change in the surface composition or surface chemistry, thus, indicating both systems were chemically stable to the plasma treatments. However, significant changes were observed in both the surface composition and surface chemistry of the C5 (near trailing edge) FEP flight sample. The carbon 1s curve fit region of the C5 FEP flight sample following plasma treatment revealed a "clean" FEP surface analogous to the control and C8 flight samples.

XPS analysis was performed on the plasma treated C5 FEP flight sample approximately 69 days after the initial plasma experiment. The carbon 1s curve fit region revealed a similar carbon surface to the C5 FEP flight sample.

Through this series of experiments, it is proposed that during the LDEF mission contamination, such as Si-containing and C-O containing, was deposited on both C5 and C8 FEP samples, as well as other surfaces. However, the surface of C8 was kept "clean" of Si-containing and C-O containing contamination as a result of the higher atomic oxygen fluence of C8 as opposed to C5.

XPS and SEM analysis of the composite samples revealed significant changes in the surface composition and surface chemistry as a result of exposure to the low-Earth orbit environment. The carbon 1s curve fit XPS analysis in conjunction with the SEM photomicrographs revealed significant

ablation of the polymer matrix resin by atomic oxygen to expose the carbon fibers of the composite samples. This ablation effect on the composites was readily seen after only 10 months in orbit and was even more obvious after 69 months.

Contact angle analysis of the 6061-T6 aluminum portion of the tray clamps revealed an average water contact angle of 64°. The contact angle results clearly illustrate no change was observed in the wettability of the clamps with respect to position on the LDEF. The results also revealed the low-Earth orbit environment did not change the wettability of the tray clamps.

Considerable variation in oxide thickness values, as determined by Auger depth profiling, were observed for the exposed and protected surfaces of the 6061-T6 aluminum portion of the tray clamps. The observed differences in the oxide thickness value for both surface can not be attributed to the low-Earth orbit environment or position on the LDEF. These discrepancies are believed to be the result of variations in the anodization process.

XPS analysis of the 6061-T6 aluminum portion of the tray clamp revealed a contaminated aluminum oxide surface. The majority of the carbon contamination present on the surface is believed to be the result of adsorption of adventitious carbon-containing compounds from the atmosphere. The adsorption of carbonaceous organic contamination from the

atmosphere can be supported by the similarities observed for the carbon 1s curve fit analysis of the control and flight samples. There was no discernible correlation of the surface atomic concentration of carbon with clamp position on the LDEF.

The largest amounts of inorganic fluorine contamination were detected on tray clamps F2, B5 and A8. FEP thermal blankets were also housed in experimental bays F2, B5 and A8. These XPS results revealed that higher levels of fluorine contamination may be observed when fluorine containing materials, particularly FEP, were located nearby.

Extensive silicon contamination was detected on the 6061-T6 aluminum surface. The XPS results clearly demonstrate that the amount and state of silicon contamination was position dependent. These are the first results which definitely establish that a higher silicon content would be expected for materials on the near leading and leading edge compared to the near trailing and trailing edge of the LDEF. The XPS result also definitely revealed that an inorganic silicon contamination was present on the near leading and leading edge samples, whereas organic silicon contamination was present on the near trailing and trailing edge samples.

XPS results of the A276 white paint portion of the tray clamps revealed the discoloration of the white paint corresponded to significant changes in the atomic

concentration. The carbon 1s curve fit analysis revealed three different carbon surfaces.

The fluorine contamination detected on the A276 white paint was independent of position with respect to the FEP thermal blankets. However the state of the fluorine contamination was dependent with respect to tray clamp position on the LDEF. The fluorine contamination present on the near trailing and trailing edge samples was indicative of a carbon-fluorine bond, whereas the fluorine contamination present on the near leading and leading edge of the LDEF was indicative of the fluorine ion. Collectively, the XPS results, for the A276 white and 6061-T6 aluminum portion of the tray clamps, demonstrate the fluorine contamination was not a direct line of sight mechanism.

An analogous trend of higher silicon content for the near leading and leading edge samples as compared to the near trailing and trailing edge samples was also observed for the A276 white portion of the tray clamps. However, the definitive shift in binding energy of the silicon from approximately 102.5 eV to 103.5 eV, for the trailing to leading edge samples, that was observed for the 6061-T6 aluminum portion of the tray clamp was not observed for the A276 white paint. The binding energy of the silicon, for the A276 white paint, was predominately a mixture of silicon/silicate/silica contamination.

The XPS results of the Z306 black paint portion of the tray clamp revealed significant changes in the surface atomic concentration as well as surface chemistry of the carbon content. These results reinforce the position dependence of the Z306 black paint. A higher silicon content was detected on the near leading and leading edge samples as compared to the near trailing and trailing edge samples. However, the state of the silicon contamination on all flight samples was inorganic.

In conclusion, the XPS results, for the three portions of the tray clamps, have established the following trends with respect to position on the LDEF:

- a higher content of silicon contamination was found for materials on the near leading and leading edge of the LDEF;
- a lower content of silicon contamination was found for materials on the near trailing and trailing edge of the LDEF;
- predominately inorganic silicon or an SiO_x type of material was found for materials on the near leading and leading edge of the LDEF;
- predominately organic silicon or a silicone type of materials was found for materials on the near trailing and trailing edge of the LDEF;
- a lower carbon content was found for materials on the near leading and leading edge of the LDEF and
- a higher carbon content was found for materials on the

near trailing and trailing edge of the LDEF.

These trends can be used to ascertain the extent of contamination of other materials aboard the LDEF.

VI. References

1. L.G. Clark, W.H. Kinard, D.J. Carter, J.L. Jones, *The Long Duration Exposure Facility Mission 1 Experiments,* NASA SP-473, NASA, Washington (1984).
2. H.W. Dursch, W.S. Spear, E.A. Miller, G.L. Bohnhoff-Hlavacek, J. Edelman, *Analysis of Systems Hardware Flown on LDEF - Results of the Systems Special Investigaion Group,* NAS1-19247, NASA, Washington (1992).
3. P.R. Young and W.S. Slemp, *NASA Technical Memorandum 104096,* December 1991.
4. T.F. Tascione, *Introduction to the Space Environment,* (Orbit Book Company, Malabar, 1988).
5. J.T. Durcanin and D.R. Chalmer, *The Definition of Low Earth Orbital Environment and Its Effects on Thermal Control Materials,* AIAA-87-1599 (June 1987).
6. J.T. Vesentine, *Environmental Definition of the Earth's Neutral Atmosphere.* NASA/SDIO Space Environmental Effects on Materials Workshop, NASA CP 3035, Part 1, p. 179, NASA, Washington (1988).
7. S.B. Gabriel and H.B. Garrett, *An Overview of Charging Environment.* NASA/SDIO Space Environmental Effects on Materials Workshop, NASA CP 3035, Part 2, p. 505, NASA,

Washington (1988).

8. L.J. Leger, *Oxygen Atom Reaction With Shuttle Materials at Orbital Altitudes,* NASA TM-58246 (May 1982).

9. R.H. Liang and A. Gupta, *Mechanistic Studies of Interaction of Materials With Energetic Oxygen Atoms in Low Earth Orbit,* AIAA 85-0422 (1985).

10. J.T. Visentine and L.J. Leger, *Material Interaction With the Low Earth Orbit Environment: Accurate Reaction Rate Measurements,* AIAA 85-7019 (1985).

11. A.F. Whitaker, R.R. Kamenetzky, M.M. Finckenor, J.K. Norwood, *Atomic Oxygen Effects on LDEF Experiment A0171.* LDEF 69 Months in Space Second Post-Retrieval Symposium, NASA CP 3194, Part 3, p. 1125, NASA, Washington (1992).

12. R.J. Bourassa and J.R. Gillis, K.W. Rousslang, *Atomic Oxygen and Ultraviolet Radiation Mission Total Exposure For LDEF Experiments.* LDEF 69 Months in Space First Post-Retrieval Symposium, NASA CP 3134, Part 2, p. 643, NASA, Washington (1991).

13. R.J. Bourassa and J.R. Gillis, *Atomic Oxygen Exposure of LDEF Experiment Trays,* NAS1-19247, NASA, Washington (1992).

14. A.S. Jursa, Editor, *Handbook of Geophysics and Space Environment,* p. 4, Air Force Geophysical Laboratory (1985).

15. R.J. Bourassa and J.R. Gillis, *Solar Exposure of Long Duration Exposure Facility Experiment Trays,* NAS1-18224, NASA, Washington, (1990).

16. Smith, G. Louis, D. Rutan, T. Bess, *Atal of Albedo and Absorbed Solar Radiation Dervived From Nimbus 7 Earth Radiation Budget Data Set,* NASA Refernce Publication 1231, NASA, Washington (1990).

17. W.M. Berrios and T. Sampair, *Long Duration Exposure Facility Solar Illumination Data Package,* Orbital Environmental Data Group, NASA LaRC (1991).

18. W.M. Berrios, *Use of LDEF's Thermal Measurement Systems for the Verification of Thermal Models.* LDEF 69 Months in Space First Post-Retrieval Symposium, NASA CP 3134, Part 1, p. 69, NASA, Washington (1991).

19. F. Horz, R. Bernhard, J. Warren, T.See, D. Brownlee, M. Laurance, S. Messenger, R. Peterson, *Preliminary Analysis of LDEF Instrument A0187-1 "Chemistry of Micrometeroroids Experiment".* LDEF 69 Months in Space First Post-Retrieval Symposium, NASA CP 3134, Part 1, p. 487, NASA, Washington (1991).

20. Kessler, R.C. Reynolds, P.D. Anz-Meador, *NASA Technical Memorandum* 100471 (1989).

21. D.J. Kessler, *J. Spacecraft,* **28(3)**, 347 (1991).

22. E.R. Crutcher, L.S. Nishimura, K.J. Warner, W.W. Wascher, *Qanification of Contaminations Associated with LDEF*. LDEF 69 Months in Space First Post-Retrieval Symposium, NASA CP 3134, Part 1, p. 101, NASA, Washington (1991).

23. E.R. Crutcher and K.J. Warner, *Molecular Films Associated with LDEF*. LDEF 69 Months in Space First Post-Retrieval Symposium, NASA CP 3134, Part 1, p. 155, NASA, Washington (1991).

24. G. Harvey, *Organic Contamination on LDEF*. LDEF 69 Months in Space First Post-Retrieval Symposium, NASA CP 3134, Part 1, p. 179, NASA, Washington (1991).

25. G.A. Harvey, *Sources and Transports on Silicone NVR*. LDEF Materials Workshop'91, NASA CP 3162, Part 1, p. 175, NASA, Washington (1991).

26. R. Crutcher, *Materials SIG Quantification and Characterization of Surface Contaminants*. LDEF Materials Workshop'91, NASA CP 3162, Part 1, p. 95, NASA, Washington (1991).

27. J.L. Golden, *Z306 Molecular Contamination Ad Hoc Committee Results*. LDEF Materials Workshop'91, NASA CP 3162, Part 1, p. 115, NASA, Washington (1991).

28. T. Gordon and R. Rantanen, *Long Duration Exposure Facility (LDEF) Contamination Modeling.* LDEF Materials Workshop'91, NASA CP 3162, Part 1, p. 141, NASA, Washington (1991).

29. G. Pippin and R. Crutcher, *Contamination on LDEF: Sources, Distribution, and History.* LDEF 69 Months in Space Second Post-Retrieval Symposium, NASA CP 3194, Part 3, p. 1023, NASA, Washington (1992).

30. E.R. Crutcher, L.S. Nishimura, K.J. Warner, W.W. Wascher, *Migration and Generation of Contaminants From Launch Through Recovery: LDEF Case History.* LDEF 69 Months in Space First Post-Retrieval Symposium, NASA CP 3134, Part 1, p. 121, NASA, Washington (1991).

31. B.A. Stein, *NASA Technical Memorandum 107664*, December 1992.

32. T.A. Parnell, *Summary of Ionizing Radiation Analysis on the Long Duration Exposure Facility.* LDEF 69 Months in Space First Post-Retrieval Symposium, NASA CP 3134, Part 1, p. 199, NASA, Washington (1991).

33. J.B. Mason, H. Dursch, J. Edelman, *Systems Special Investigation Group Overview.* LDEF 69 Months in Space First Post-Retrieval Symposium, NASA CP 3134, Part 3, p. 1217, NASA, Washington (1991).

34. B.A. Stein, *LDEF Materials: An Overview of the Interim Findings*. LDEF Materials Workshop'91, NASA CP 3162, Part 1, p. 1, NASA, Washington (1991).

35. S.L. Koontz, *Atomic Oxygen Effects on Spacecraft Materials the State of the Art of Our Knowledge,* NASA/SDIO Space Environmental Effects on Materials Workshop, NASA CP 3035, Part 1, p. 241, NASA, Washington (1988).

36. J.L. Leger, *STS Flight 5 LDO Effects Experiment - Background Description and Thin Film Results*, AIA 83-2631, Washington (1983).

37. K. Smith, *Evaluation of Oxygen Interaction with Materials (EIOM) - STS-8 Atomic Oxgyen Effects,* AIAA 85-7021, Houston (1985).

38. D.G. Zimcik, C.R. Maag, *Results of Apparent Atomic Oxygen Reactions with Spacecraft Materials During Shuttle Flight STS41-G,* AIAA 85-7020, Houston (1985).

39. J.E. Hatch, Editor, *Aluminum: Properties and Physical Metallurgy,* (ASTM, Ohio, 1984).

40. R.J. Duckett and C.S. Gilland, *Variable Anodic Thermal Control Coating on Aluminum,* AIAA (1983).

41. P.R. Young, W.S. Slemp, C.R. Gautreaux, *Characterization of Selected LDEF-Exposed Polymeric Films,* Presented at the 37th International SAMPLE Symposium and Exhibition (1992).

42. C.S. Hemminger, W.K. Stuckey, J.C. Uht, *Space Environmental Effects on Silvered Teflon Thermal Control Surfaces,* Aerospace Report No. TR-0091(6935-03)-1 (1991).

43. A.E. Stiegman, *An Investigation of the Degradation of Fluorinated Ethylene Propylene (FEP) Copolymer Thermal Blanketing Materials Aboard the LDEF and in the Laboratory.* Jet Propulsion Laboratory 91-10 (1991).

44. P.R. Young, W.S. Slemp, E.J. Siochi, J.R.J. Davis, *Analysis of a Space-Exposed Thermoplastic Resin,* Presented at the 24th International SAMPE Technical Conference (1992).

45. J.D. Summers et al., *Inorganic and Organometallic Polymers.* ACS Symposium Series 360 (ACS, Washington, DC 1988), p. 180.

46. A. Dilks, in *Electron Spectroscopy-Theory, Techniques and Applications,* C.R. Brundle and A.D. Baker eds., Vol 4 (Academic Press, London, 1981).

47. D. Briggs and C.R. Kendall, *Polymer,* **20**, 1053 (1979).

48. W.M. Riggs and D.W. Dwight, *J. Electron Spectrosc.,* **5**, 447 (1979).

49. D. Briggs in *Practical Surface Analysis by Auger and X-ray Photoelectron Spectroscopy,* D. Briggs and M.P. Seah eds., p. 359, (John Wiley and Sons, New York, 1983).

50. A. W. Czanderna, ed., *Methods of Surface Analysis* (Elsevier, New York, 1975).

51. D.T. Clark, *Handbook of X-ray and Ultraviolet Photoelectron Spectroscopy,* (Heyden and Sons, London 1977).

52. D.T. Clark, *Characterization of Metal and Polymer Surfaces,* (Academic Press, New York, 1977).

53. D.M. Brewis and D.J. Briggs, *Polymer,* **22**, 7 (1981).

54. C. Jones and E. Samman, *Carbon*, **28(4)**, 509 (1990).

55. D.T. Clark, C.B. Adams, A. Peeling H.R. Thomas, *J. Electron Spectrosc,* **8**, 51 (1976).

56. D.A. Skoog, *Principles of Instrumental Analysis*, 3rd ed. (Saunders College Publishing, Philadelphia, 1985).

57. W.C. Wake, *Adhesion and the Formulation of Adhesives* (Applied Science Publishers, New York, 1982) p. 52.

58. C.S. Hemminger, *Surface Contamination on LDEF Exposed Materials*. LDEF Materials Workshop'91, NASA CP 3162, Part 1, p. 159, NASA, Washington (1991).

59. R. Holm and S. Storp, *Surf. Interface Anal.,* **2(3)**, 96 (1980).

60. J.F. Rabolt, M. Jurich and J.D. Swalen, *Appl. Spectrosc.,* **39(2)**, 269 (1985).

61. B.J. Lindberg, *J. Electron Spectrosc.,* **5**, 149 (1974).

62. H.F. Webster, II, *Characterization of Thin Silicon Films Formed by Migration Across Defined Polymer Substrates*, Virginia Tech, Master's Thesis, 1985.

63. D.M. Brewis and D. Briggs, *Polymer*, **22**, 7 (1981).

64. G.A. Harvey, *Silizane to Silica.* LDEF 69 Months in Space Second Post-Retrieval Symposium, NASA CP 3194, Part 3, p. 797, NASA, Washington (1992).

65. L.J. Leger, *Oxygen Atom Reaction With Shuttle Materials at Orbital Altitudes,* NASA TM-58246 (1982).

66. D.E. Brinza, A.E. Stiegman, P.R. Staszak, *Vacuum Ultraviolet (VUV) Radiation- Induced Degradation of FEP Teflon Aboard the Long Duration Exposure Facility (LDEF).* LDEF 69 Months in Space First Post-Retrieval Symposium, NASA CP 3134, Part 2, p. 817, NASA, Washington (1991).

67. D.J.T. Hill, G.A. George, J.H. O'Donnell, P.J. Pomery, F.A. Rasoul, *A Study of the UV and VUV Degradation of FEP.* LDEF 69 Months in Space Second Post-Retrieval Symposium, NASA CP 3194, Part 2, p. 817, NASA, Washington (1992).

68. A.R. Blythe, D. Briggs, C.R. Kendall, D.G. Rance V.J.I. Zicky, *Polymer,* **19**, 1273 (1978).

69. M. Lee, W. Rooney, J. Whiteside, *An XPS Study of Space-Exposed Polyimide Film.* LDEF 69 Months in Space Second Post-Retrieval Symposium, NASA CP 3194, Part 3, p. 975, NASA, Washington (1992).

70. D.K. Owens, *J. Appl. Polym Sci.*, **19**, 265 (1975).

71. H.V. Boeing, *Plasma Science and Technology* (Cornell University Press, Ithaca, 1982).

72. A.T. Bell and J.R. Hollahan, *Techniques and Applications of Plasma Chemistry* (John Wiley and Sons, New York, 1974).

73. E.M. Liston, *J. Ashes.*, **30**, 199 (1989).

74. D.J.D. Moyer and J.P. Wightman, *Surf. Interface Anal.*, **14**, 496 (1989).

75. J.J. Mallon, J.C. Uht, C.S. Hemminger, *Surface Analysis of Composites Exposed to the Space Environment on LDEF.* LDEF 69 Months in Space Second Post-Retrieval Symposium, NASA CP 3194, Part 3, p. 963, NASA, Washington (1992).

76. R.C. Tennyson and R. Mathews, *Outgassing and Dimensional Changes of Polymer Matrix Composites in Space.* LDEF 69 Months in Space Second Post-Retrieval Symposium, NASA CP 3194, Part 3, p. 877, NASA, Washington (1992).

77. M.J. Meshishnek, W.K. Stuckey, J.S. Evangelides, L.A. Feldman, R.V. Peterson, G.S. Arnold, D.R. Peplinski, *Effects on Advanced Materials: Results of the STS-8 EOIM Experiment*, TR-0086(6935-05)-2, (1987).

78. P.E. George, H.S. Dursch, S.G. Hill, *Space Environmental Effects on LDEF Composites: A Leading Edge Coated Graphite Epoxy Panel.* LDEF 69 Months in Space Second Post-Retrieval Symposium, NASA CP 3194, Part 3, p. 923, NASA, Washington (1992).

79. Surface Science Laboratories Analytical Service Report. SSX-100 ESCA Analysis Report No. 7008-0586.

80. P. George, *Space Environmental Effects on LDEF Low Earth Orbit Exposed Graphite Reinforced Polymer Matrix Composites*. LDEF Materials Workshop'91, NASA CP 3162, Part 2, p. 543, NASA, Washington (1991).

81. G.L. Steckel, T. Cookson, C. Blair, *Polymer Matrix Composites on LDEF Experiments M0003-9 and 10*. LDEF Materials Workshop'91, NASA CP 3162, Part 2, p. 515, NASA, Washington (1991).

82. R.C. Tennyson, *Additional Results on Space Environmental Effects on Polymer Matrix Composites-Experiment AO180*. LDEF Materials Workshop'91, NASA CP 3162, Part 2, p. 515, NASA, Washington (1991).

83. D.H. Humes, *Large Craters on the Meteoroid and Space Debris Impact Experiment*. LDEF 69 Months in Space First Post-Retrieval Symposium, NASA CP 3134, Part 1, p. 399, NASA, Washington (1991).

84. L.E. Murr and W.H. Kinard, *American Scientist,* **81**, 152 (1993).

85. M.E. Zolensky, H.A. Zook, F. Horz, D.R. Atkinson, C.R. Coombs, A.J. Watts, C. Dardano, T.H. See, C. Simon, W.H. Kinard, *Interim Report of the Meteoroid and Debris Special Investigaion Group*. LDEF 69 Months in Space Second Post-Retrieval Symposium, NASA CP 3194, Part 2, p. 277, NASA, Washington (1992).

86. W.L. Plagemann, *Space Environmental Effects on the Integrity of Chromic Acid Anodized Coatings.* LDEF 69 Months in Space First Post-Retrieval Symposium, NASA CP 3134, Part 2, p. 1023, NASA, Washington (1991).

87. P. Swift, *Surf. Interface Anal.* **4**, 47 (1982).

88. A.W. Adamson, *Physical Chemistry of Surface*, 5th ed. (John Wiley and Sons, New York, 1990).

89. M Yekta-Fard and A.B. Ponter, *J. Adhesion Sci. Technol.*, 6, 253 (1992).

90. E.R. Crutcher and W.W. Wascher, *Particle Types and sources Associated with LDEF.* LDEF 69 Months in Space First Post-Retrieval Symposium, NASA CP 3134, Part 1, p. 101, NASA, Washington (1991).

91. J.L. Golden, *Results of Examination of the A276 White and Z306 Black Thermal Control Paint Disks Flown on LDEF.* LDEF 69 Months in Space First Post-Retrieval Symposium, NASA CP 3134, Part 2, p. 975, NASA, Washington (1991).

92. D.T. Clark and R.J. Meier, *J. Electron Spectrosc. Relat. Phenom.* **43**, 131 (1987).

93. J.L. Golden, *Selected Results for LDEF Thermal Control Coatings,* LDEF 69 Months in Space Second Post-Retrieval Symposium, NASA CP 3194, Part 3, p. 1099, NASA, Washington (1992).